

**REDACTOR-ŞEF: Prof. A. NEGUCIOIU**

**REDACTORI-ŞEFI ADJUNCȚI: Prof. A. PĂL, conf. N. EDROIU, conf. L. GHERGARI**

**COMITETUL DE REDACȚIE CHIMIE: Prof. E. CHIFU, prof. I. HAIDUC (redactor responsabil),  
prof. L. KÉKEDY, prof. GH. MARCU, prof. L. ONICIU, conf. S. MAGER,  
conf. E. VARGHA (secretar de redacție)**

**TEHNOREDACTOR: C. Tomoaia-COTIȘEL**

h91180

Anul XXXIII

1988

STUDIA  
UNIVERSITATIS BABEŞ BOLYAI

CHEMIA

1

Redacția: 3400 CLUJ-NAPOCA, str. M. Kogălniceanu, 1 • Telefon 16101

SUMAR — CONTENTS — SOMMAIRE — INHALT

I. MUREŞAN, L. ZADOR, Micellar Dispersion-Ionic Solution Transitions for Polyacrylates	3
V. NEAGU, M. NEAGU, Calculation of Fukui Superdelocalizability Indices $S^R$ for Bipyridine Molecules in Connection with Their Surfactant Properties . . . . .	10
R. ŞERBAN, E. POROJAN, The Best Parameters of Adjustment of Coating Obtained from Aqueous Suspensions Using Anodic Electrodeposition Technology . . . . .	14
I. BRADESCU, C. DANIELIU, G. MACOVESCU, G. ZĂINESCU, J. BRANDSCH, A. CHIFOR, L. DUMITRESCU, Collagen Polypeptides and Reactive Butadiene and Acrylic Co-Polymers in a Disperse System—A Composite Material for Filling and Strengthening Loose Grain Leathers . . . . .	20
ŞT. KISS, M. DRĂGAN-BULARDA, D. PASCA, Activity and Stability of Enzyme Molecules Following Their Contact with Clay Mineral Surfaces . . . . .	27
M. RUSU, AI. BOTAR, GH. MARCU, The Thermal Behaviour and the Molecular Oxygen Absorption Properties of Co(Salen) and Co(BrSalen) Complexes . . . . .	31
D. CEAUŞESCU, M. ELIU-CEAUŞESCU, Rationalisierung und Vereinfachung Einiger Analytisch-Chemischen Berechnungen @ Rationalisation and Simplification of Some Analytical-Chemical Calculations . . . . .	36
AI. BOTAR, D. ITUL, GH. MARCU, The Study of the Formation of Heteropolyanions of Type $ML_2$ , Where $M=Co^{2+}$ and $V^{3+}$ , Respectively, $L=PW_{11}Mo_{10}O_{40}^{4-}$ and $P_2W_{18}Mo_{61}O_{101}^{4-}$ , Respectively, Using Paper Electrophoresis . . . . .	42
S. MAGER, I. GROSU, $^1H$ -NMR Spectra and Stereochemistry of Some 2-Aryl-5,5-Substituted 1,3-Dioxanes . . . . .	47
R. POPESCU, I. OPREAN, N. PALIBORDA, Z. MOLDOVAN, Étude en spectrométrie de masse des arylsulphonamides thiophosphororganiques. I. Arylsulphonamides de	

419/1988

L'acide diéthylthiophosphinique • Mass Spectra of the Arylsulphonamides of the Diethylthiophosphinic Acid . . . . .	54
I. VODNÁR, I. DEMETER-VODNÁR, Studierea reacțiilor chimice și a operațiilor de absorbtie și de extracție în aparate cu serpentina de peliculizare-barbotare. I. Absorbția dioxidului de carbon în soluții apoase de hidroxid de potasiu • The Study of the Chemical Reactions and of Operations as Absorption and Extraction . . . . .	63
F. MÁNOK, CS. VÁRHELYI, H. SZAKÁCS, On the Dioximine Complexes of Transition Metals. LXX. Polarographic Study of Some Rhodium(III)-Chelates with $\alpha$ -Dioximes . . . . .	68
F. A. GOTTHARD, Efficiency Requirements in Today Research, Design and Development of Large Scale Separation Processes by Rectification and Extraction . . . . .	74
M. RUSU, AL. BOTĂR, GH. MARCU, The Gravimetric Determination of Tungsten and Molybdenum . . . . .	82
J. ZSAKÓ, F. MAKKAY, Linearization of Potentiometric Titration Curves. IV. Redox Titrations . . . . .	85
I. A. SILBERG, I. MARIAN, Structural Considerations and Their Correlation with Possible Conduction Mechanisms in Organic Free Radicals of the Highly Halogenated Phenothiazines Series . . . . .	93
GH. MARCU, CS. VÁRHELYI, J. FÜLÖP, D. ITUL, Neue Kobalt(III)-Amin-Komplexbasen mit Heptoxim • New Cobalt(III)-Amine Complex Bases with Heptoxime . . . . .	97
 Recenzii — Book Reviews Comptes Rendus Buchbesprechungen	
Surface and Colloid Science in Computer Technologhy (K. L. Mittal, Ed.) (M. TOMOIA - COTIȘEL) . . . . .	103

## MICELLAR DISPERSION-IONIC SOLUTION TRANSITIONS FOR POLYACRYLATES<sup>1</sup>

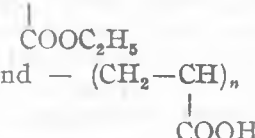
IUDITA MUREŞAN\* and LUCIA ZADOR\*

Received: September 8, 1986

The main results concerning the transitions between ionic solutions and micellar dispersions of polyacrylates, in both directions, are reported. The transitions were brought about by modification of the composition of the water-ethanol solvent mixture, as well as that of the degree of ionization. Viscosimetric, conductometric, potentiometric, optic and rheologic measurements were carried out. The investigations put into evidence a transition range with unusual rheologic properties and unknown conformational changes. The results obtained are reported as level surfaces in ionization degree-solvent composition plots. The discovered conformational transition provides, with a good understanding, the phenomena of "thickening" of polyacrylate latexes, largely employed in leather industry for spreading and coating operations.

Key-words: conformational transition, polyacrylates, polyelectrolytes

The aqueous solutions of the investigated polyacrylates enter the category of polyelectrolytes having the structure given in Fig. 1. The electrically uncharged parts of the chain, symbolised as  are  $-(CH_2-CH)_n-$  in the case of

ethylacrylate-acrylic acid copolymers P(EA-AA); and  $-(CH_2-CH)_n-$  for 

polyacrylic acid (PAA). For the total degree of ionization  $\alpha = 1$ ,  $n = 0$ .

Though, to the theory of polyelectrolytes a great volume of investigations was dedicated [1-7], the complexity of the phenomena did not allow the elaboration of a generally valid unique theory. The numerous theories describe different models and are in agreement with experiments only for given systems in certain conditions. Most of them admit high ionic strength at which the charge of polyions is screened. Therefore, the investigations of polyelectrolytes were carried out mainly in the presence of big amounts of salts.

On the other hand, technologists are using for different purposes saltless polyelectrolytes under conditions where the properties determined by the electric charge of the chains are most spectacular. So, the application of the polyelectrolytes in different fields is rather empirical, frequently without any reference to the ionic character of the used dispersion.

Initially, the presently reported work was undertaken in order to explain such an empirically used phenomenon. It has for a long time been known in

\* University of Cluj-Napoca, Faculty of Chemical Technology, 3400 Cluj-Napoca, Romania

<sup>1</sup> Paper presented in the Symposium on Colloid and Surface Chemistry, Cluj-Napoca, September 8-10, 1986.

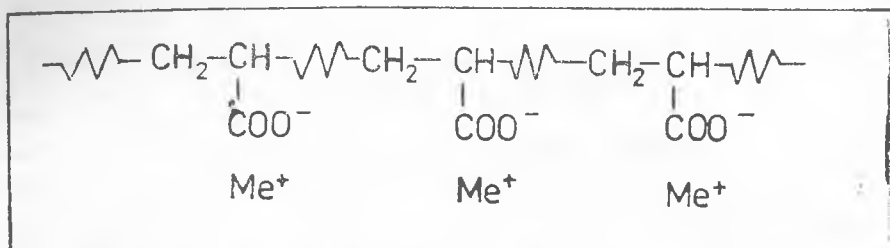


Fig. 1. The structure of partially neutralized polyacrylic acid (PAA) and of ethylacrylate-acrylic acid copolymers P(EA-AA) entirely neutralized.

leather industry [8] that P(EA-AA) latexes may be transformed by alkalination and ethanol addition into transparent and highly viscous systems, suitable for coating and spreading operations. This phenomenon was termed "thickening".

**Latex-solution transition for P(EA-AA).** By emulsion copolymerization P(EA-AA) latexes were obtained, with different content of acrylic acid. Samples with constant polymer concentration (0.13 mol monomer unit/l) and different water-ethanol ratio were prepared from each of them. It was observed that turbidity disappears at an as lower EtOH concentration (15–45 w% EtOH) as the AA content of copolymer, *i.e.*  $\alpha$ , is greater. In parallel with the turbidity decrease, an abrupt viscosity increase occurs. The conclusion could be drawn that thickening has to be attributed to the transition of ultramicro-heterogeneous micellar systems into homogeneous ionic solutions [9,10]. The solubility of the copolymer in the water-ethanol mixture is conditioned by the fact that the first liquid is a good solvent for the ionized carboxylic groups, while the second for the esteric ones. Therefore, the EtOH concentration needed for solubility diminishes with the increase of acrylic acid content.

Though it was ascertained that after reaching a maximum the apparent viscosity  $\eta_{ap}$  abruptly decreases (Fig. 2), meanwhile the phenomenon of rheopexy (dilatancy) appears. For deformation stresses  $\dot{\rho} = 40$ –140 g/cm<sup>2</sup>, the  $\dot{\rho}$ - $v$  rheological curves ( $v$  = deformation speed), could be described for all the systems by the relation

$$v = k\dot{\rho}^m \quad (1)$$

But, while the initial (rich in water) as well as the final (rich in alcohol) samples are pseudoplastical, having  $m > 1$ , in the range of abrupt decrease of  $\eta_{ap}$ , rheopexy appears. Here,  $m < 1$ , *i.e.* viscosity increases with the deformation stress, as illustrated in Fig. 3.

These findings suggested that the latex-solution transition is followed by a conformational one towards a less unsymmetrical shape of the chains. The explanation of dilatancy could be the partial straightening of the contracted coils by the deformation energy, in conditions (EtOH content) where the symmetrical conformation is more stable.

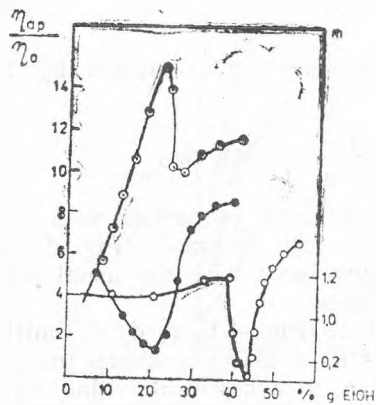


Fig. 2. The dependence of  $\eta_{ap}$  and  $m$  from EtOH % for P(EA-AA). (○)  $\eta_{ap}$  for  $\alpha = 0.3$ ; (○)  $m$  for  $\alpha = 0.2$ ; (●)  $m$  for  $\alpha = 0.3$ .  $\eta_{ap}$  — the apparent viscosity measured at  $p = 100$  g/cm<sup>2</sup>,  $\eta_0$  — the apparent viscosity for the initial latex at the same  $p$ .

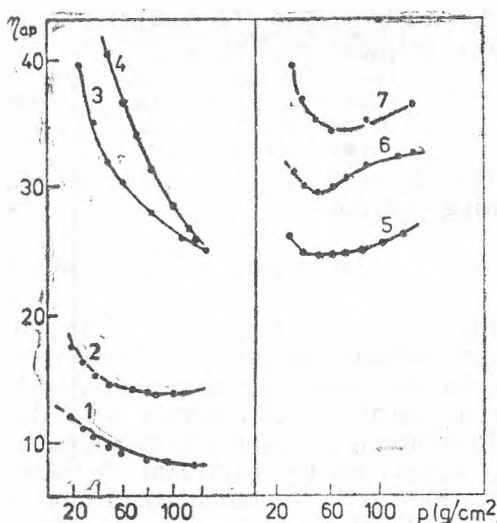


Fig. 3. The influence of deformation stress on  $\eta_{ap}$  for samples having  $\alpha = 0.1$  and different EtOH %.  
1) 5%; 2) 13%; 3) 26%; 4) 31.5%; 5) 18%;  
6) 21%; 7) 22.5%.

This possibility seemed more interesting as for polymethacrylic acid there were observed conformational transitions, *i.e.* sudden modifications of average shape in a narrow range of the degree of ionization [11,12] which could not be found in aqueous PAA solutions. Our results indicated a conformational transition for polyacrylates under the influence not only of  $\alpha$  but also of a second decisive parameter: the EtOH content of the solvent.

**Conformational and solution-micellar dispersion transitions for PAA.** In order to eliminate the insolubility of the uncharged parts of the chain and especially to ensure any possible value for the two parameters  $\alpha$  and EtOH %, we passed to polyacrylic acid. From PAA obtained by polymerization in benzene solution and subsequent purification, samples were prepared by solving in a medium of the wanted composition and neutralization to the wanted degree by a solution of KOH in the same mixture. The constancy of PAA concentration in samples ( $1 \cdot 10^{-2}$  or  $9 \cdot 10^{-2}$  mol monomer units/l) was respected.

Table 1  
The X properties studied by different methods

$X = X(\alpha, \% \text{EtOH})$	Method
Expansion coefficient $A$	Viscosimetric
Acidity exponent $pK$	Potentiometric
Conductivity $\lambda$	Conductometric
Optical density $D_\lambda$	Optical
Rheological parameters $m, k$	Rheologic

Different properties (termed as X) [13-15] in function of the two decisive parameters were studied by methods given in Table 1. The expansion coefficient

*A* is defined by relation (2) accepting as reference state that of the non ionized polymer in acid medium

$$A = \frac{(\eta_{sp}/c)^{1/3}}{(\eta_{sp}/c)_{HCl\ 0.2\ N}^{1/3}} \quad (2)$$

The exponent of acidity constant  $pK_a$  was defined and calculated by the following relation

$$pK_a = pK_0 + \frac{0.43}{RT} \Delta G = pH + \log \frac{1 - \alpha}{\alpha} + \log c_{H_2O} \quad (3)$$

Fig. 4 illustrates the dependence of the first three properties with  $\alpha$  at different solvent compositions. In solvent mixtures rich in water (Fig. 4a) all properties are changing monotonously with  $\alpha$  in agreement with the usual behaviour of linear polyelectrolytes with flexible chain.

In solutions containing large amounts of ethanol (Fig. 4 b, c, d, e) limiting points appear on the curves at the same values of  $\alpha$ . After a sharp increase (up to 200%) the expansion coefficient falls down to a constant value ( $A = 0.65$ ) indicating a more compact shape of coils than for completely uncharged PAA in aqueous solution. The curves of  $pK_a$  and  $\lambda$  up to 70 w% EtOH have two ascending sections corresponding to the ionization of PAA in two distinct states. They are separated by a transition range marked by a descendant portion of the curves.

Thus the observed phenomena requires the admittance of a conformational transition from expanded coils to compact globules brought about in water ethanol solutions by increasing  $\alpha$  or EtOH%, according to the schematic representation given in Fig. 5.

Such transition is similar to that suggested by the rheological study of latex-solution transition for P(EA-AA) and opposed to that found for aqueous polymethacrylic acid.

The chain structure of PAA makes it possible that the energetically unfavourable interaction between the ionized carboxylic groups and EtOH molecules do not lead to the loss of the chain's solubility, but to a change of its shape. The new compact, symmetrical conformation may ensure a lower free energy by "hiding" a higher fraction of ionized groups from the solvent medium, than is able to do the open unsymmetrical swollen conformation. In this way the descendant part of  $\lambda$  and  $pK_a$  curves in the transition range may also be explained.

In order to describe in two dimensions the variation of the investigated properties with the two variables  $\alpha$  and EtOH%, level surfaces were built. Figs. 6, 7 and 8 are illustrating some of them. Each curve on level surface represents the locus of points in which  $X$  has a constant value specified on the diagrams. Equal  $\Delta X$  intervals were chosen, so that the density of the level lines gives the measure of the rate of variation.

The rheological study implied the use of samples more concentrated in PAA. However, it was put in evidence that PAA concentration (between  $1 - 9 \cdot 10^{-2}$  mol monomer/l) has little influence on the structural diagrams, obtained by the superposition of level surfaces and given in Fig. 9.

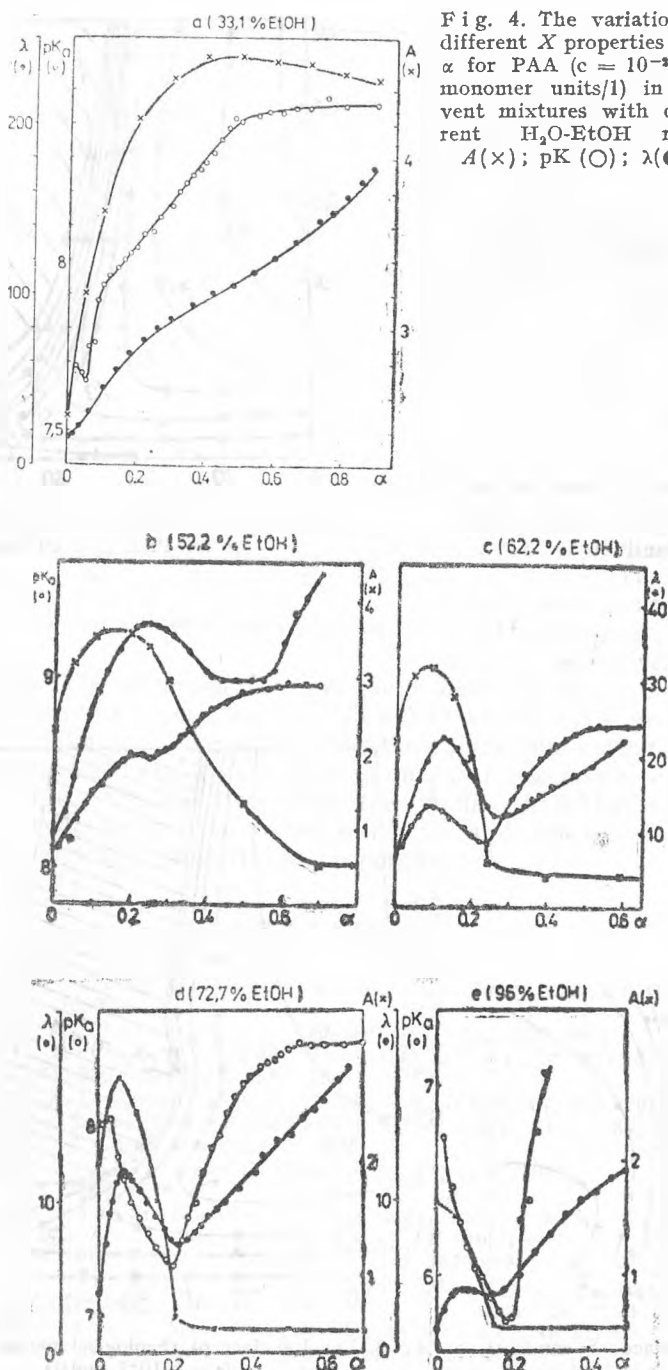


Fig. 4. The variation of different  $X$  properties with  $\alpha$  for PAA ( $c = 10^{-3}$  mol monomer units/l) in solvent mixtures with different  $H_2O$ -EtOH ratio.  
 $A(x)$ ;  $pK_a$ ;  $\lambda$ .

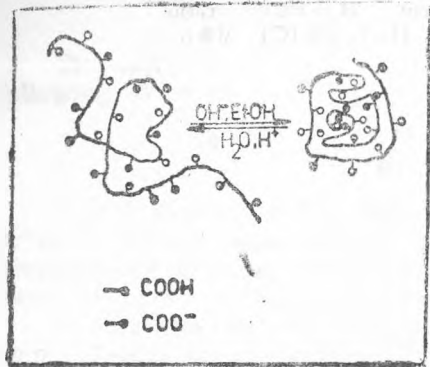


Fig. 5. Expanded coil-compact globule conformational transition for PAA.

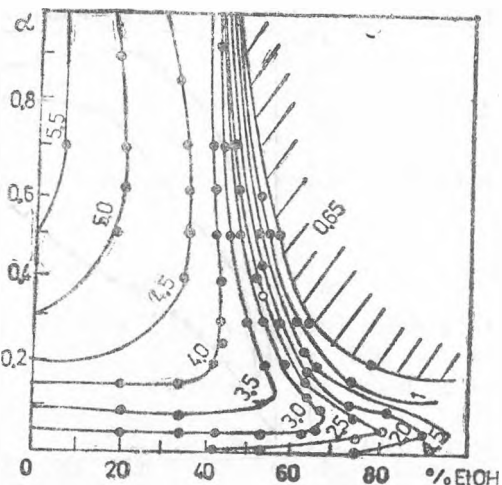


Fig. 6. Level surface of expansion coefficient  $A$  for PAA ( $c = 10^{-3}$  mol/l)

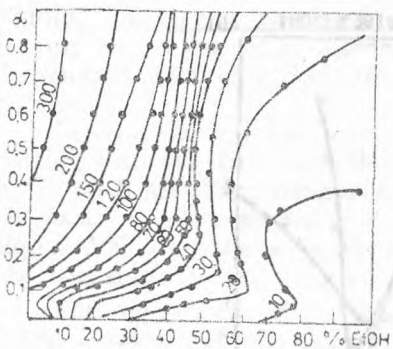


Fig. 7. Level surface of conductivity  $\lambda$  for PAA ( $c = 10^{-3}$  mol/l)

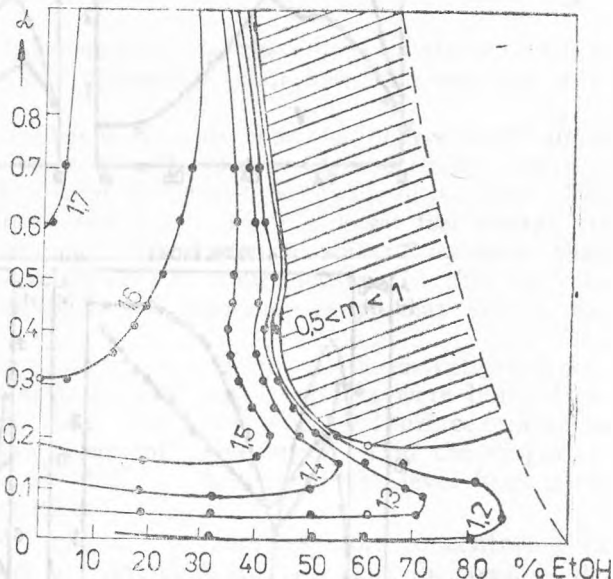


Fig. 8. Level surface of rheological parameter  $m$  for PAA ( $c = 9 \cdot 10^{-3}$  mol/l)

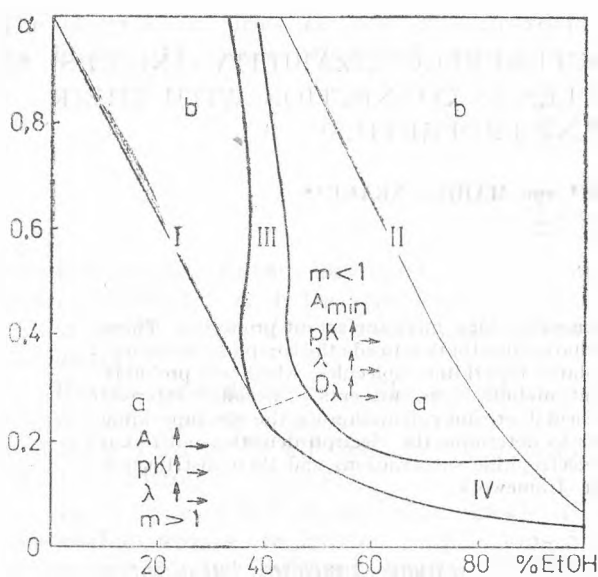


Fig. 9. Delimitation of structural zones for PAA.

**Conclusions.** The investigations of the transitions of the ionic solutions and micellar dispersions such as for P(EA-AA) as for PAA proved that polyacrylates may undergo in adequate solvent medium interesting conformational changes from extended coil to compact globules. These conformational changes are opposed and at the same time more spectacular than that put in evidence for polymethacrylic acid in aqueous solutions and play a decisive part in different technologically important properties.

#### REFERENCES

1. Kuhn W., Künzle O., Katchalsky A., *Helv. Chim. Acta*, **31**, 1994 (1948), *J. Polymer Sci.*, **5**, 283 (1950).
2. Katchalsky A., Lifson S., *J. Polymer Sci.*, **11**, 409 (1953).
3. Harris, F.E., Rice, S.A., *J. Phys. Chem.*, **58**, 725 (1954), **58**, 733 (1954), *J. Chem. Phys.*, **24**, 326 (1956), **24**, 336 (1956), **24**, 955 (1956).
4. Hermans, J.J., Overbeek, J.T.G., *Rec. Trav. Chim.*, **67**, 761 (1948).
5. Kimball, G.E., Cutler M., Samelson H., *J. Phys. Chem.*, **56**, 57 (1952).
6. Krieger, I.N., *J. Chem. Phys.*, **26**, 1 (1958).
7. Rinaudo M., Loiseleur B., *J. Chim. phys.*, **70**, 1305 (1973).
8. B.I.O.S. Trip. nr. 2788, 1946.
9. Kertész-Mureşan I., Kacsó E., *Stud. Univ. Babeş-Bolyai, Chem.*, **VIII**, 57 (1963).
10. Mureşan I., Zador L., *Rev. Roumaine Chim.*, **13**, 819 (1968).
11. Leyte, J.C., Mandel M., *J. Polymer Sci.*, **A 2**, 1879 (1964).
12. Barone G., Crescenzi V., Quadrifoglio F., *Ricerca Sci.*, **35(II A)** 393 (1965), **35**, 1069 (1965), **36**, 477 (1965).
13. Mureşan I., Zador L., *Stud. Univ. Babeş-Bolyai, Chem.*, **18 (1)** 89 (1973).
14. Zador L., Mureşan I., *Rev. Roumaine Chim.*, **19 (3)** 353 (1974).
15. Zador L., Mureşan I., *Stud. Univ. Babeş-Bolyai, Chem.*, **24 (1)** 47 (1979).

In the I ("coil") domain the shape of the chains changes from swollen to an expanded coil, as a function of their electrical charge. In its *b* zone, the peculiarities of the domain are screened by counterion binding.

The II ("globular") domain is characterized by opalescence and a less than unity value of the expansion coefficient. In its *a* zone rheopexy is present, proving that here the deformation energy may bring about the partial straightening of globular molecules, *i.e.* their conformational transition. In II *b* zone the association of globular chains into globular micelles occurs.

In the III and IV ("transition") domains the conformational transition at low EtOH% and low  $\alpha$ , respectively, takes place.

# CALCULATION OF FUKUI SUPERDELOCALIZABILITY INDICES $S_r^E$ FOR BIPYRIDINE MOLECULES IN CONNECTION WITH THEIR SURFACTANT PROPERTIES<sup>1</sup>

VICTOR NEAGU\* and MARIUS NEAGU\*\*

Received: September 8, 1986

Bipyridine complexes with some metallic ions have surfactant properties. These properties are determined by the charge distribution inside the complexe molecule. The charge distribution in the isolated bipyridine molecules, which are probably differently perturbed by different metallic ions, presents a peculiar interest. In this first report a Hückel molecular orbital calculation on the six bipyridine molecules was performed in order to determine the electron densities and Fukui superdelocalizability indices for electrophilic substitutions and their distribution in the corresponding molecular framework.

**Key-words:** *molecular orbital calculation, bipyridine complexes, Fukui superdelocalizability indices*

**Introduction.** Bipyridine complexes with some metallic ions have several interesting properties. For example, the photochemistry of the tris (2,2'-bipyridine) ruthenium (II) cation,  $\text{Ru}(\text{bpy})_3^{2+}$ , has been the subject of study, both for its intrinsic interest and because of possible promise for solar energy conversion processes [1]. Several reports have appeared concerned with the photochemistry of the water soluble  $\text{Ru}(\text{bpy})_3^{2+}$  or its surfactant derivatives in micellar systems [2, 3, 4, 5, 6]. The synthesis of several water insoluble derivatives of  $\text{Ru}(\text{bpy})_3^{2+}$  cation have been reported [7, 8]. These surfactant compounds can be dispersed readily in aqueous solutions of a variety of anionic, cationic and nonionic detergents.

These properties are determined by the charge distribution inside the complexe molecule. It is sure that the charge distribution in the isolated bipyridine molecules is differently perturbed by different metallic ions. In order to know this influence first of all is necessary to have a picture of the charge distribution in the bipyridine molecules. To obtain such information two reactivity indices were calculated, namely the electron densities and Fukui superdelocalizability indices for electrophilic substitutions and their distribution in the molecular framework.

**Molecular orbital calculations.** The calculations were carried out using an appropriate program of the Hückel approximation [9]. The values for the resonance and Coulomb integrals were taken from Streitwieser's book [10].

<sup>1</sup> Paper presented in the Symposium on Colloid and Surface Chemistry, Cluj-Napoca, September 8-10, 1986.  
Received: September 8, 1986

\* Faculty of Chemical Technology, University of Cluj-Napoca, 3400 Cluj-Napoca, Romania

\*\* Institute of Chemistry, Cluj-Napoca, 3400 Cluj-Napoca, Romania

The electron densities  $D_r^E$  and the superdelocalizability indices  $S_r^E$  introduced by Fukui [11] were calculated using the formulae:

$$D_r^E = f_j \sum_{j=1}^m c_{rj}^2 \quad (1)$$

$$S_r^E = f_j \sum_{j=1}^m \frac{c_{rj}^2}{\lambda_j} \quad (2)$$

where  $r$  represents atom number  $r$  inside the molecule,  $m$  is the highest occupied molecular orbital,  $c_{rj}$  is the coefficient of the  $r$ -th atomic orbital in the  $j$ -th molecular orbital,  $f_j = 2$  is the occupation number and  $\lambda_j$  is the Hückel energy parameter.

**Results and discussion.** The numbering of atoms inside the six bipyridine molecules is shown in Figures 1 to 6 and the reactivity indices are contained in Tables 1 to 6. In all cases the reactivity indices show the maximum value on the nitrogen atoms.

In the case of 2,2'-bipyridine molecule, Figure 1 and Table 1, the most reactive carbon atoms are located at positions 5 and 5'. Atoms 2,2' and 3,3' may be considered sterically hindered.

In the case of 3,3'-bipyridine molecule Figure 2 and Table 2, the most reactive carbon atoms are located at positions 5 and 5'. Those located at positions 2,2' and 3,3' are sterically hindered.

In the case of 4,4'-bipyridine molecule Figure 3 and Table 3, the most reactive carbon atoms are located at positions 3,3' and 5,5' while atoms 4 and 4' are sterically hindered.

As a consequence of the molecular symmetry of these three bipyridines the reactivity indices of the carbon atoms are symmetrically distributed in each molecular framework.

In the case of 2,3'-bipyridine molecule Figure 4 and Table 4, the most reactive carbon atoms are located at positions 3,5 and 5' while those located at positions 2 and 3' are sterically hindered.

In the case of 2,4'-bipyridine molecule Figure 6 and Table 5, the carbon atoms located at positions 3,5 and 3', 5' are the most reactive while atoms 2 and 4' are sterically hindered.

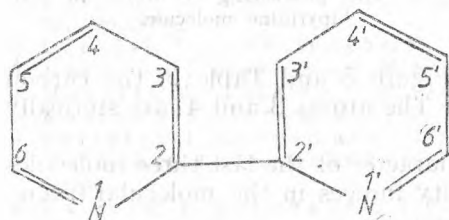


Fig. 1. The numbering of atoms in 2,2'-bipyridine molecule.

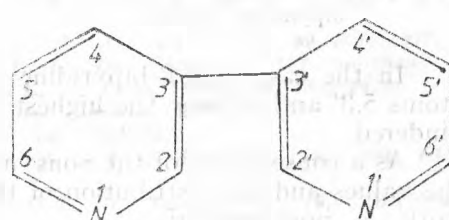


Fig. 2. The numbering of atoms in 3,3'-bipyridine molecule.

Table 1

$D_r^E$  and  $S_r^E$  reactivity indices for 2,2'-bipyridine molecule

Atom	$D_r^E$	$S_r^E$
1	1.2466	1.0828
2	0.9288	0.6854
3	0.9871	0.8766
4	0.9369	0.7234
5	0.9965	0.8571
6	0.9037	0.7558
1'	1.2466	1.0828
2'	0.9288	0.6854
3'	0.9871	0.8766
4'	0.9369	0.7234
5'	0.9965	0.8571
6'	0.9037	0.7558

Table 2

$D_r^E$  and  $S_r^E$  reactivity indices for 3,3'-bipyridine molecule

Atom	$D_r^E$	$S_r^E$
1	1.2439	1.0147
2	0.9034	0.8252
3	1.0032	0.7682
4	0.9353	0.7967
5	1.0048	0.8241
6	0.9090	0.8115
1'	1.2439	1.0147
2'	0.9034	0.8252
3'	1.0032	0.7682
4'	0.9353	0.7967
5'	1.0048	0.8241
6'	0.9090	0.8115

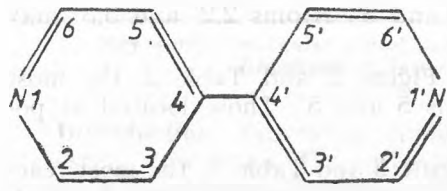


Fig. 3. The numbering of atoms in 4,4'-bipyridine molecule.

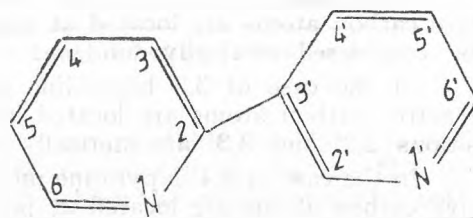


Fig. 4. The numbering of atoms in 2,3'-bipyridine molecule.

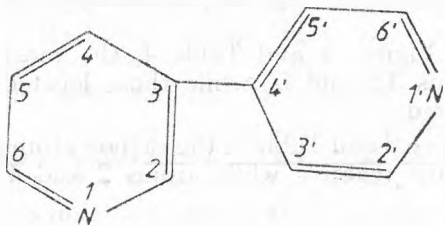


Fig. 5. The numbering of atoms in 3,4'-bipyridine molecule.

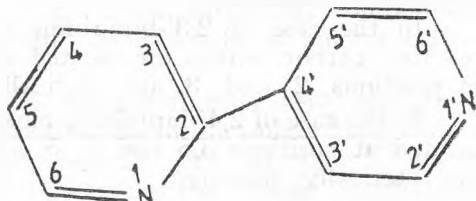


Fig. 6. The numbering of atoms in 2,4'-bipyridine molecule.

In the case of 3,4'-bipyridine molecule Figure 5 and Table 6, the carbon atoms 5,3' and 5' show the highest reactivity. The atoms 3 and 4' are sterically hindered.

As a consequence of the nonsymmetric character of the last three molecules the values and the distribution of the reactivity indices in the molecular framework is nonsymmetric.

In all cases the calculated reactivity indices for the carbon atoms in both rings show a similar variation to that existent in the isolated pyridine molecule.

Table 3

$D_r^E$  and  $S_r^E$  reactivity indices for 4,4' - bipyridine molecule

Atom	$D_r^E$	$S_r^E$
1	1.2415	1.0602
2	0.9105	0.7544
3	0.9963	0.8733
4	0.994	0.6617
5	0.9963	0.8733
6	0.9105	0.7544
1'	1.2415	1.0692
2'	0.9105	0.7544
3'	0.9963	0.8733
4'	0.9447	0.6617
5'	0.9963	0.8733
6'	0.9105	0.7544

Table 5

$D_r^E$  and  $S_r^E$  reactivity indices for 2,4' - bipyridine molecule

Atom	$D_r^E$	$S_r^E$
1	1.2476	1.0785
2	0.9253	0.6878
3	0.9891	0.8741
4	0.9366	0.7232
5	0.9974	0.8552
6	0.9039	0.7558
1'	1.2407	1.0634
2'	0.9109	0.7546
3'	0.9948	0.8760
4'	0.9476	0.6593
5'	0.9948	0.8760
6'	0.9109	0.7546

Table 4

$D_r^E$  and  $S_r^E$  reactivity indices for 2,3' - bipyridine molecule

Atom	$D_r^E$	$S_r^E$
1	1.2622	1.1102
2	0.9197	0.6847
3	1.0024	0.9071
4	0.9364	0.7224
5	1.0076	0.8835
6	0.9054	0.7613
1'	1.2442	1.0137
2'	0.6871	0.8027
3'	1.0090	0.7605
4'	0.9219	0.7712
5'	1.0053	0.8236
6'	0.8976	0.7834

Table 6

$D_r^E$  and  $S_r^E$  reactivity indices for 3,4' - bipyridine molecule

Atom	$D_r^E$	$S_r^L$
1	1.2441	1.0143
2	0.8898	0.8000
3	1.0067	0.7534
4	0.9235	0.7686
5	1.0052	0.8238
6	0.8985	0.7817
1'	1.2553	1.0953
2'	0.9103	0.7536
3'	1.0079	0.8998
4'	0.9398	0.6593
5'	1.0079	0.8989
6'	0.9103	0.7536

## REFERENCES

- Balzani, V., Bolletta, F., Scandola, F., Ballardini, R., *Pure Appl. Chem.*, **51**, 299(1979).
- Lachish, U., Ottolenghi, M., Rabani, J., *J. Am. Chem. Soc.*, **99**, 8062(1977).
- Meisel, D., Matheson, M.S., Rabani, J., *J. Am. Chem. Soc.*, **117**, 100(1978).
- Maestri, M., Infelta, P.P., Grätzel, M.J., *J. Chem. Phys.*, **69**, 1522(1978).
- Kalyanasundaram, K.J., *J. Chem. Soc., Chem. Commun.*, **628**(1978).
- Pelizzetti, E., Pramauro, E., *Inorg. Chem.*, **18**, 882(1979).
- Gaines, G.L. Jr., Behnken, P.E., Valenty, S.J., *J. Am. Chem. Soc.*, **100**, 6549 (1978).
- Valenty, S.J., Behnken, P.E., Gaines, G.L. Jr., *Inorg. Chem.*, **18**, 2160(1979).
- Hückel, E., *Z. Physik*, **76**, 628(1932).
- Streitwieser, A., "Molecular Orbital Theory for Organic Chemists", John Wiley and Sons, New York, 1961.
- Fukui, K., Yonezawa, T., Nagata, C.J., *Chem. Phys.*, **27**, 1247(1957).

# THE BEST PARAMETERS OF ADJUSTMENT OF COATING OBTAINED FROM AQUEOUS SUSPENSIONS USING ANODIC ELECTRODEPOSITION TECHNOLOGY<sup>1</sup>

RADU ȘERBAN\* and ECATERINA POROJAN\*

Received: September 8, 1986

In this work we have summarised epoxy-estheric electrodeposition system which works into eletropainting installation of 25 m<sup>3</sup> and the film-forming mechanism is imagined through anionic electrodeposition — anaphoresis. Through laboratory researches there were identified the main factors which influence the thickness of coating. These factors are created because of the constitutive elements of the film-forming product, as well as of the kinetic conditions during the electrodeposition and also of the electrical parameters of electropainting installation. After the analysis of concrete conditions created during the period of pilot researches and industrialization of the product there were established the best parameters for maintaining the thickness of the coating between 20–30 µm, this thickness assuring the equilibrium between anticorrosive characteristics and mechano-phisical characteristics.

Key-words: *electrodeposition, epoxy-esther, thickness of coating, anaphoretic mechanism, neutralization degree, pigment/binder ratio, organic cosolvent, throwing power, rate of recirculating, coating time, temperature of bath, electrical characteristics.*

**Introduction.** The coating products were used in industry starting with the 7<sup>th</sup> century, thanks to their economic and ecological advantages. The coating

products applied through the electrophoretic method are in continuous improvement, and electrodeposition installations increased very much especially in car industry and in the steel furniture industry for kitchen furniture [1, 2].

From the chemical point of view, the film forming products applied by electrodeposition are dispersed systems in which the disperse medium is deionised water and the dispersion stage is created from solid particles (pigments) filling materials included in a coating binder (synthetic resins, cosolvents and specific additives).

In this system discussed by us the coating's basis is an epoxy-estheric polymer synthesised at the Anticorrosive Paints and Varnishes Research Center — Bucureşti, starting from epoxy resin of type dig-

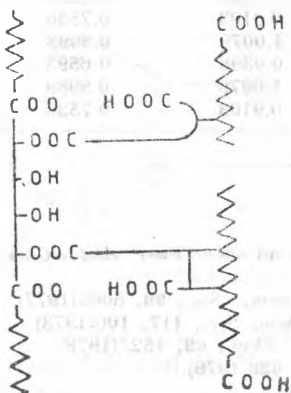


Fig. 1. General formula of epoxy — ester polymer.

<sup>1</sup> Paper presented in the Symposium on Colloid and Surface Chemistry, Cluj-Napoca, September 8–10, 1986.

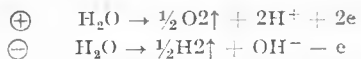
\* Anticorrosive Protection Paints and Varnishes Research Center — Bucureşti, Bdul Chimitoilor 309, sector 3, 74585 Bucureşti, Romania

lycidyl ether of bysphenol A which in the first stage partially reacts with fatty acids and a part of hydroxyl groups left freely is esterified with  $-COOH$  groups which are into adduct tricarboxylic hydrolysed [3,4].

The polymer, having the general formula as in Fig. 1, is neutralised by KOH becoming water soluble polymer; through dissociation anions of  $R-COO^-$  type are formed.

When through the dispersed system there passes a continuous electric current, coming from thyristor rectifier, and one of the electrodes (in this case the anode) is the same metal piece which must be protected, there are many effects, which lead to the electrodeposition of the paints.

**The mechanism of obtaining film-forming coats by anionic electrodeposition (anaphoresis).** Through electrolytic decomposition of water hydrogen is released at the cathode and oxygen at the anode.

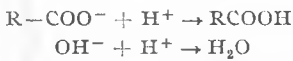


The anions carried by the electrical field to the anode are discharged

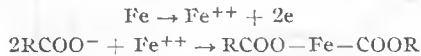


and this produces coagulation of neutral particles; this is the beginning of the coating creation.

The growth of film is produced near the anode where the resin becomes non-soluble.

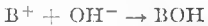


These chemical reactions are produced when the anode is totally non-soluble (for example platinum); but in the real case of iron anode a partial dissolution of metal [6] is produced and then the coagulation of the binder with metal ions takes place.



The formed film has an electrical resistance of  $10^5 - 10^6 \Omega/cm^2$ ; diminished current intensity; the electrical field having values of  $100 MK/cm$ , this fact explains the electro-osmosis of water (about 85%) from the film formed.

At the cathode, through the discharge of cations, free bases are formed and they are accumulated in the bath.



Elimination of bases and recovering of ionic equilibrium is produced through electrodialysis, the specific method for epoxyestheric primer which makes the accumulation of KOH in the cathodic space.

**Epoxy-estheric film-forming product.** The Painting primer EF 7301 elaborated by the Anti-corrosive Protection Paints and Varnishes Research Center - Bucureşti, which is used by Joint Venture OLTCIT - Craiova in the tanks of  $25 m^3$  is under the form of a fluid dispersed system, slightly thixotropic having a viscosity of maximum 100 P, of gray colour, containing about 40% solids content, is neutralised by KOH which gives it an alkaline pH and is diluted with water; this is sensitive to temperatures under  $10^\circ C$ , it is not inflammable and has a small toxicity in comparison with the classical products.

Through dilution of the primer with deionised water the electrodeposition bath is formed having a solids content of about 12.5%. Using the same electric voltage 120-200 V, we can obtain films correctly displayed which after drying at  $180^\circ C$  for 30 minutes are in accordance with actual international standards referring to the mechano-physical and to the corrosion property of the metal pieces pretreated with zinc phosphates.

**Thickness of coatings.** The thickness of coating is an important characteristic of the film. It is checked by non-destructive methods (with instruments of Permascop type). As a consequence of rigorous tests, it was established that in the case of epoxy-estheric system described above the thickness of 20–30 μm represents an optimum solution assuring an equilibrium between corrosion properties (with slight resistance to saline fog for small thickness) and mechanophysical characteristics (slight resistance for large thickness).

Starting from this premise which we consider very important, we made laboratory and pilot researches and then tested in electrodeposition installation of 25 m<sup>3</sup>, finally we improved the main factories involved in establishing the thickness of electrodeposited film-forming coats.

**Results of research tests.** We briefly present the influence of different factors which directly influence the thickness of coating in the case of epoxy esthetic system described by us in the first part of this paper.

**Factors which depend on the constituents of the formula.** Neutralization degree changes depending on neutraliser quantity from the formula; neutralisation degree influences inversely proportional the thickness of the films as it is illustrated in Fig. 2.

*Pigment/binder ratio* has an important role in providing the uniformity of films and of course changes the thickness of the coat.

In Fig. 3 we can see this variation simultaneously with the influence of the dilution deg-

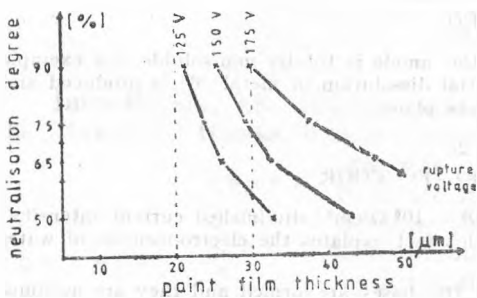


Fig. 2. Variation of films thickness with the neutralization degree and the deposition tension.

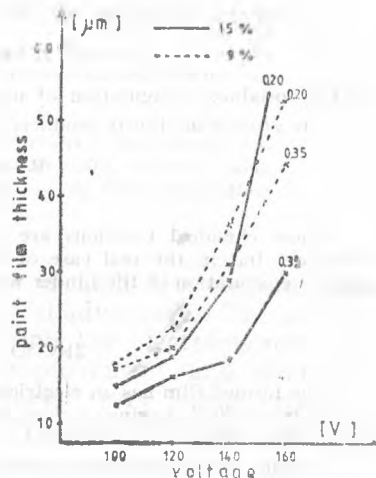


Fig. 3. Influence of P/B ratio and dilution degree.

ree of the bath; at constant voltages higher thicknesses provide primers with a less ratio P/L (approx. 0.20) and a greater dilution (9%).

Because of the quality it was established that pigment/binder ratio can vary round the value of 0.25, and from economic reasons dilution of the bath was established at 12.5% solids content.

The content of organic cosolvents improves the thickness of the film and it is more efficient if the product is fresher; the rate of growth is 2–3 μm in the case of *n*-butanol for 0.3% solvent.

*Pretreatment of surface*, more precisely the thickness of zinc phosphate coat influences inversely proportional the thickness of the film, this relation is illus-

trated in Fig. 4. The impurities located on the surface of the sheet iron change the thickness of the coating, which decreases when the electrical resistivity of the impurified areas increases.

**Factors which depend on kinetic conditions.** Rate of recirculating or stirring in electrodeposition bath composed of the product thinned at 12.5% solids content influences positively the growth of the film thickness, but this increasing is not significant (1–2  $\mu\text{m}$  for increasing the number of recirculating volumes from 20 to 25/h).

The bigger the distance to the cathode, the less is the value of the electrical field and at the same time the thickness of the paint coat decreases as in Fig. 5. This characteristic called *throwing power* was determined by us with the help of a closed body having a length of 24 cm, the deposition obtained representing 88% of the length of the sample.

The time of electrodeposition is an important factor of adjustment for film thickness as we can see in Fig. 6. In case of a normal deposit, at the speed of the conveyor 1.55–1.72 m/min the time of immersion of the pieces in the bath is limited between 3 min. 30 sec. and 4 min. We can see that the thickness of the films varies in the established limits of 20–30  $\mu\text{m}$  but in case of damage (when voltage of rectifier automatically decreases at 35–50 V the conveyor stops, therefore the metal pieces stay in the bath for a longer time). The time in which the film reaches these values can overpass 30 min.

The temperature of the bath influences directly proportional the speed of particles movement increasing the mobility of ions and it is an efficient mean of adjusting the thickness of the coating in electrodeposition installations which

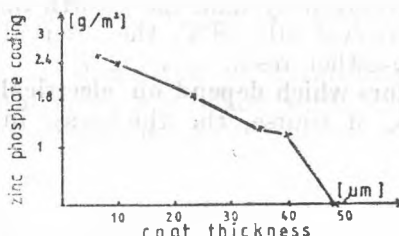


Fig. 4. Relation between phosphatic and paint film.

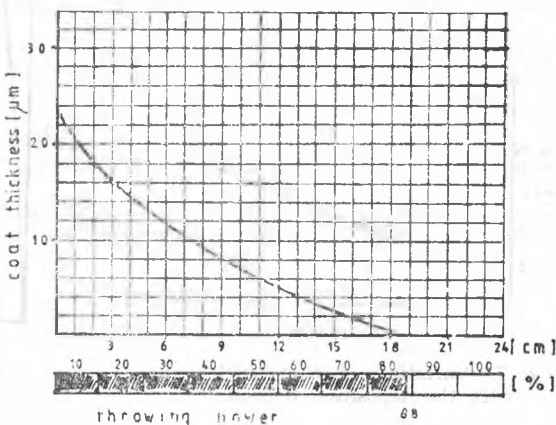


Fig. 5. Throwing power.

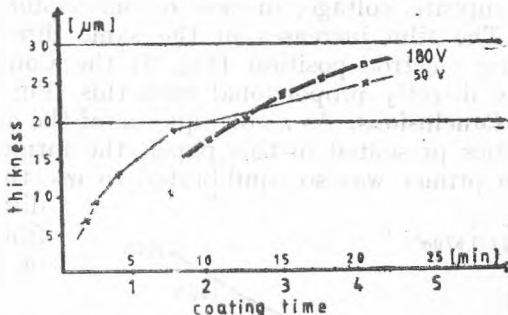


Fig. 6. Thickening of the film with electrodeposition time.

have thermostat system, the growth rate of the film thickness is  $1.5-2 \mu\text{m}/^\circ\text{C}$  in the interval  $20-28^\circ\text{C}$ , the interval imposed by the conditions of stability of epoxy-ester resin.

**Factors which depend on electrical characteristics.** When electrical voltage increases, of course, the thickness increases also as shown in Figs. 2, 3, 7.

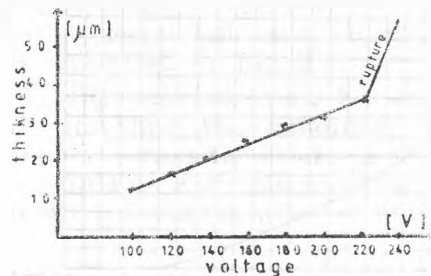


Fig. 7. Variation of film thickness with the deposition tension.

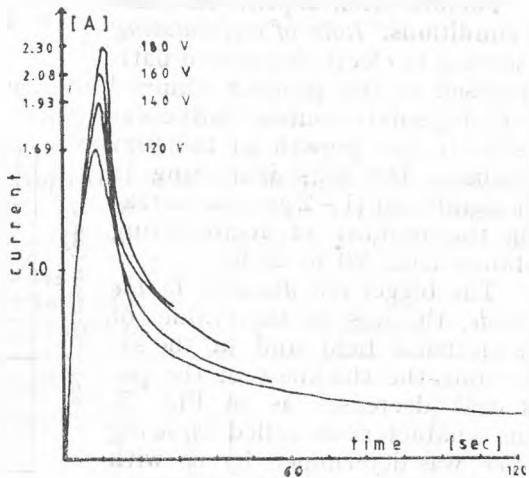


Fig. 8. Intensity curve during electrodeposition.

There is a limit voltage, after which the deposit is not realized uniformly, called the rupture voltage, in case of our system this is about 240 V.

The film increases in the same direction with the variation of *intensity* during electrodeposition (Fig. 8) the Coulombic consumption ( $\text{Coulombs}/\text{dm}^2$ ) being directly proportional with this (Fig. 9).

**Conclusions.** As a consequence of the analysis and correlation of the characteristics presented in this paper, the formula of the epoxyestheric electrodeposable primer was so equilibrated to use the real possibilities in industrial conditions to obtain the thickness of the film which cannot overpass the limits of the interval of  $20-30 \mu\text{m}$ .

The industrial process leads to the thickness increase of the film through: adding in the bath *n*-butanol up to 0.8%; increasing of temperature during deposition, but not above  $28^\circ\text{C}$ ; rising of application voltage within imposed limits;

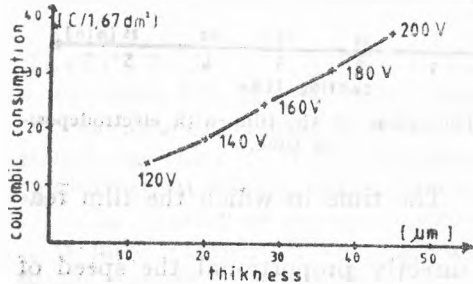


Fig. 9. Coulombic consumption and its influence upon the film thickness

The industrial process leads to the thickness decrease of the film through:

— decrease of bath temperature during application, but not under 20°C;  
decrease of deposition voltage;

— partial removing of the cosolvent by elimination of ultrafiltration.

The industrial optimization of film thickness was made with permanent assistance of specialists from the beneficiary entreprise Joint Venture OLTCIT — Craiova.

#### REFERENCES

1. Robu C., Serban R., "Protectia anticorosivă conferită caroseriilor auto de diferite tipuri de materiale aplicabile prin electroforeză" în *Coroziune-Buletin de informare tehnico-documentară a ICECHIM*, nr. 1, 1980, p. 67—72.
2. Robu C., Serban R., "Produse peliculogene solubile în ape indigene, utilizate în industria auto în România", *Simpozion Timișoara „Automobilul la intersecția cu anul 2000”*, 5—6 aprilie 1985, p. 389.
3. Domide T. et al., *Brevet RSR* 89, 229.
4. Serban R., Rosetti M., "Grund electroforetic epoxi-esteric. Prezentarea produsului și a peliculelor obținute", *Simpozion Timișoara „Automobilul la intersecția cu anul 2000”*, 5—6 aprilie, 1985, p. 373.
5. Yeates R. L., "Electropainting" Robert Draper LTD, Teeddington, october 1970, p. 21.
6. Machu W., "Handbook of Electropainting" Electrochemical Publications LTD, Bell & Bain LTD, Glasgow, 1978, p. 11.

# COLLAGEN POLYPEPTIDES AND REACTIVE BUTADIENE AND ACRYLIC CO-POLYMERS IN A DISPERSE SYSTEM — A COMPOSITE MATERIAL FOR FILLING AND STRENGTHENING LOOSE GRAIN LEATHERS<sup>1</sup>

IOAN BRĂDESCU\*, CRISTINA DANIELIUC\*, GABRIELA MACOVESCU\*, GABRIEL ZĂINESCU\*, JOHANNES BRANDSCH\*\*, CHIFOR AUGUSTIN\*\* and LUCIA DUMITRESCU\*\*

Received: September 8, 1986

It is a well known fact that some tanneries which process cattlehides sheep-goat-skins, and pigskins are faced sometimes with problems relating to the low quality of some groups of raw hides, as a result of the way of feeding and breeding the animals as well as the way of preserving storage and transport. With the view of diminishing and even eliminating some of these shortcomings of the Laboratory of Auxiliary Products in The Leather and Footwear Research Institute, new technological solutions or of any other kind are looked for, resorting to the synthetic polymer dispersions. A great part of these dispersions together with the collagen polypeptides chemically modified were successfully used as an active component for obtaining products of strengthening and filling leathers. The distribution of these products was made by the method of drum and float impregnation before tanning in chromium salts and in combination with the tanning materials during the retannage process. By the method of impregnation, a checked deposit of polymers in the interfibrillary spaces of the leather was carried out, so that the zones with few, spongy fibers may be filled selectively with polymer particles and especially the link between papillary and reticular layers (the lack of this bringing about the loose grain) must be strengthened. Collagen polypeptides, amphotolytes by their structure chemically modified have the role of „supplementary stabilizers” of the dispersions. They contribute to the obtaining of a fine grain and a soft touch generally counteracting the effect of “synthetic leather” given by the polymers.

Key-words: *leather field, butadiene and acrylic co-polymer dispersions, collagen polypeptides from pelt hide wastes, reactive products, filling and strengthening products loose grain, pickle, retannage.*

**Introduction.** Among the problems of a great importance in the modern leather industry, literature in this field deals with those problems connected with the elimination of shortcomings in the structure of the raw hide, a consequence of the way of feeding and breeding the animals, as well as the way of preserving, storage and transport.

So, in this way, abroad and in our country a lot of technological solutions and of any other kind are looked for meant to diminish or counteract a part of these shortcomings. Among these, in the last '30, for the different stages

<sup>1</sup> Paper presented at the *Symposium on Colloid and Surface Chemistry*, Cluj-Napoca, September 8–10, 1986.

\* *Leather and Footwear Research Institute, 70 Bucharest, Romania*

\*\* *I.C.P.A.O., 2221 Rîznov, Braşov County, Romania*

of processing leathers the dispersions or acrylic polymer solutions imposed, which penetrated during the process, both in the wet and finishing operations.

The direction of the leather industry towards synthetic polymers is explained by finding out the tanning properties of these, but especially of the reactive co-polymers containing reactive functional groups grafted on the macromolecule chain. These groups have the capacity of interacting both with leather collagen and with different vegetable and mineral tanning materials. Consequently in the literature, it was tried to account for the way of penetration and of binding the macromolecules to the synthetic polymers in leather, it has been found out among other problems that the fixation takes place by covalent, electrovalent and hydrogen bonds [1-6].

So this type of bonds for leather, assures a good retention of the polymers with collateral functional groups to the macromolecule chain. In this way, carboxyl, N-methyol, amine and even amide groups which besides their electrostatic action give reticulations in the structure of the leather have been pointed out.

The penetration of the polymers into leather, by the method of float impregnation is a complex phenomenon, if we take into account the necessity of dispersing them into the whole thickness of the leather.

The uniform dispersion of the polymer on the leather fibers and its deep penetration into the inter-structural spaces is carried out as a result of slowing down the process of hetero coagulation, by diminishing the sorption of emulsifier by the structural elements of leather.

On the other hand, in the impregnation process with polymer synthetic materials, another important element is the electrokinetic potential of leather and of the polymer particle [7].

Knowing this, we can explain the total and partial exhaustion of the acrylic dispersions in the float, the preferential distribution of the polymer particles depending on their size and the structure of the leather and finally the improvement of the physico-mechanical properties of the final product.

In order to subdue the physical-chemical processes which take place in different stages of processing leathers, it is necessary to know the electro-kinetic potential of the materials (leather and auxiliary materials), without being imperative this element only.

So, in this way, Prentiss W.C. from the University of Philadelphia [8] presents an interesting paper concerning „The Role of Acrylics in Pigskin Processing” which contains data about the composition of some acrylic syntans and the way of applying them in the process of processing the above mentioned leathers.

More types of acrylic polymers as aqueous dispersions with reactive functional groups with tanning ability are given here.

The characterization of one of them is made by methods of characteristic analysis of the tanning materials, for example: Dry Substance — 50%; Non tannins — 5%; Tannants — 35%; Purity — 88%; pH (10% sol.) — 3; Particle size — 0.07—0.15.

Polymer products for filling can penetrate into leathers, usually in drums, floats in the following stages of processing leathers: before tanning with chromium salts; in combination with a mineral tannage; at the end of mineral tan-

nage; in combination with tanning materials during retannage; after dyeing process; during or after fatliquoring.

The fixation of acrylic or butadiene co-polymers in the structure of leather is irreversible.

After using polymer filling materials in accordance with the data in literature we got: equal surfaces from point of view of absorption capacity as a result of selective penetration of the polymer; a fine structure of the grain diminution or elimination of the effect of loose grain; increase of tensile strength, tearing strength and scratching strength; improvement of the adhesive power of finishing process; greater strength towards micro-organisms chemical and atmospheric agents; high waterproof; high efficiency of "surface" and of sorting percentage.

Studying literature we found out that not all these advantages have been obtained from one type of leather which was impregnated with a certain polymer filling product. These improved characteristics depend on the origin and sort of the leathers and physico-chemical, structural characteristics of the polymers, as well as the technology applied in the impregnation process.

In order to be successful in this method of impregnation we must take into account more elements and mostly "the experience" in that field.

**Experimental Work.** In our country the polymeric products for leather field are manufactured usually at the chemical Factory — Rîšnov. They are dispersions of some co-polymers in an aqueous medium. Being known under commercial names, they can be divided into three big groups taking into account their reactivity.

a. *The group of reticulating polymer* which contains polymers with N-methylol ( $-\text{NH}-\text{CH}_2-\text{OH}$ ) reactive groups. They can form bridges of covalent groups between different macromolecules or of the same type by eliminating one water molecule at heat.

Besides these reactive groups; this type of polymers can also contain ester polar groups ( $-\text{COO}-\text{R}$ ) or nitrile ( $-\text{C}\equiv\text{N}$ ) groups and free carboxyl ( $-\text{COOH}$ ) groups which can combine with synthetic or vegetable tanning agents.

Among them, the dispersions EPS—2, E—41, ES, ERF, EFS—I, EFS—II, EPS<sub>1</sub>, ECP and EFPA—I are usually produced.

b. *The group of thickening and reticulating polymers* have the same physico-chemical characteristics but they can modify their viscosity with ammonia or other organic alkali as a result of an increased content of carboxyl groups.

In this group there are: D—2002, D—3003, EFPA<sub>2</sub> and M.

c. *The group of non reticulating polymers* consists of acrylic dispersions with the same chemical composition as we find in reticulating polymers but with difference in N-methylol groups responsible for reticulation.

In our country the following polymers are representative for this group: EPB, ESL, EL, F and E 17.

At the Leather and Footwear Research Institute in Bucharest the problem of obtaining synthetic proteinic products which can start from native polymers and which contribute to the improvement of quality of some leathers by brum impregnation, was developed. So, a great part fo acrylic dispersions was tested at the chemical Factory, Rîšnov above mentioned.

By laboratory tests concerning the selection of some acrylic and/or butadiene dispersions reactive polymers were chosen firstly.

These polymers with functional groups under certain conditions of pH, temperature and pressure can couple with other reactive groups in proteins. Another criterion which was the basis of the selection of polymer dispersions was an economic one, finally being a kind of compromise between this aspect and the functional one.

The impregnation of the leathers with acrylic and butadiene dispersions had the following results: the exhaustion of the floats was max. 50%, a characteristic percentage of an equilibrium absorption of the polymers; the polymer fixation was made preferably on the leather surface espe-

cially focussing on the papillary layer and providing an effect of synthetic touch. In this way, the lack of penetration of the polymers was noticed in all the thickness of the leather.

Starting from these disadvantages new solutions have been sought after for improving the penetration of the polymer particles in the whole leather thickness as well as for advanced exhaustion of the impregnation floats.

A lot of products based on collagen polypeptides in combination with aqueous polymer dispersions and bi-tricomponent, acrylic and/or butadiene co-polymers coupled with/or without redox system were tested. The synthetic component contains functional groups of one of these types: carboxyl, nitrile, N-methylol, ester C<sub>1</sub>—C<sub>4</sub>.

**Results and discussions.** In order to bring about the capacity of binding the proteins to the polymers in the proteinic synthetic impregnation product, we tested the loss of the films by solubilization in water 35°C for 3 hours. The results of the tests are given in Table 1. Taking into account the fact that

Table 1

No.	Symbol	Film Content				Redox System Yes = (+) No = (-)	The loss of the film by washing	The loss % related to PPC
		PPC (%)	P <sub>1</sub> A (%)	P <sub>2</sub> A (%)	P <sub>3</sub> B (%)			
1.	G <sub>1</sub>	16.70	83.30	—	—	(+)	2.22	13.89
2.	G <sub>2</sub>	16.70	83.30	—	—	(-)	3.81	22.81
3.	G <sub>3</sub>	16.70	—	83.3	—	(+)	2.74	16.41
4.	G <sub>4</sub>	16.70	—	83.3	—	(-)	5.10	30.54
5.	IE <sub>1</sub>	4.94	47.53	—	47.53	(+)	1.01	20.43
6.	IE <sub>2</sub>	8.53	45.73	—	45.73	(+)	2.41	28.00
7.	IE <sub>3</sub>	12.98	43.51	—	43.51	(+)	4.10	31.57

PPC — collagen polypeptides; P<sub>1</sub>A and P<sub>2</sub>A — acrylic copolymers; P<sub>3</sub>B — butadiene copolymers.

from the film mass only the collagen polypeptides can be extracted by dissolving in water, we found out that only 10–30% of the quantity introduced initially is lost by washing. It is interesting to notice that for the films in which the redox system is used, the losses by washing are the smallest (tests 1 compared with 2 and 3 compared with 4).

The loss by solubilization in water can be correlated with the nature of synthetic polymers as well as with the number of macromolecule species in the system (the tests 1, 2 compared with 3 and 4, as well as the tests 1 and 3 compared with the rest of tests 5–7).

For the tests G<sub>1</sub>—G<sub>4</sub> in the table we brought about the medium molecular masses, although there were no monomers in the system, we noticed that an increase of the medium molecular masses for the tests in which we used redox system took place (see diagram in the appendage).

Gel chromatography was employed, using Sephadex G 200 and as eluent — TRIS — HCl solution pH = 7, 5, 20°C.

After using column chromatography for bicomponent tests, many increases of medium molecular masses between 130.000–170.000 for those treated in redox system, resulted, a fact that suggests to us a coupling of macromolecules given by the redox system. The system being very complex the investigations are going on with the view of making clear the theoretical aspects concerning

the association and/or coupling of certain types of macromolecules in the redox system.

The dosage in leather of the synthetic proteinic product was made by the method "in the drum", in float in a series of stages of processing leathers.

By the method of impregnation, a checked deposit of polymers in the interfibrillary spaces of the leather was carried out, so that the zones with few, spongy fibers may be filled selectively with polymer particles and especially the link between papillary and reticular layers (the lack of this bringing about the loose grain) must be strengthened.

Collagen polypeptides ampholytes by their nature chemically modified contribute to the stabilization of the polymer dispersions against the structural elements of the leather so that the penetration and the distribution of the polymer particles must be made uniform, both in the thickness and on the topographical zones of it. For the leathers tested in the laboratory (cattlehides pigs-

Tabel 2

No.	Ratio dry leather/synthetic product d.s./g.g.	Coagulation substance content, % in float*	% Dry substance retained in leather	Float aspect	Notes
1.	100 : 2	0.04	98	clear	
2.	100 : 4	0.08	98	"	Total exhaustion
3.	100 : 6	0.18	97	"	
4.	100 : 8	0.36	95.5	"	
5.	100 : 10	0.70	93	opalescent	

\* The ratio float/leather was 100% and kept constantly

kins and sheepskins and dehaired rabbits) even with a different histological structure among the individuals of the same species, taking into account their age, the topographical zone and the way of preserving, the tested products are absorbed very well being bound in the leather irreversibly. The absorption and binding of the polymers were shown by pointing out the percentage of coagulation substance left in the float after impregnation.

The laboratory tests pointed out a good absorption capacity of the proteinic-synthetic products at the same time with an irreversible binding of it.

One of the products obtained in laboratory was tested on the dehaired rabbits with a technology established by The Leather and Footwear Research Institute obtaining finished rabbits with the physico-mechanical characteristics given in Table 3.

We can see clearly from this table the influence of penetrating proteinic-synthetic product in the structure of rabbit skins, in view of improving some physico-mechanical characteristics of these.

Furthermore, the observation of the tests against the control samples shows that the conjugated action polymer-collagen polypeptides leads to the obtaining of some leathers with "fine grain and soft touch generally counteracting the effect of" synthetic given by polymers.

Table 3

No.	The names of the characteristics	Control	Test
1.	Thickness	1.69	1.22
2.	Elongation	—	13.5
	— at a specified load 1 daN/mm <sup>2</sup>	48.0	44.0
	— cracking	48.0	44.0
	— breaking	—	—
3.	Tensile strength daN/mm <sup>2</sup>	0.41	1.62
	— at cracking	0.41	1.62
	— breaking	—	—
4.	Tearing resistance daN/mm <sup>2</sup>	19.7	21.5
5.	Stitch — resistance daN/cm	36.0	74.4

**Conclusions.** 1. As a result of the tests carried out in the Laboratory of Auxiliary Products for Leather Industry of our Institute in Bucharest a lot of proteinic-synthetic products "Polisin" with a capacity of penetrating into leather and strengthening the fibrous structure of the leathers, have been tested and produced. The products of "Polisin" range have been obtained by a scientific research in collaboration with ICPAO — Mediaș — Rîșnov — Section which offered us both reference material and acrylic dispersions for testing.

In obtaining and testing these products we took into account: the type of leathers (cattlehides, sheepskins, rabbit skins); the particle sizes of dispersions; medium molecular mass of the co-polimers and of the used polypeptides; the presence of reactive chemical groups of the polymer chain and especially carboxyl group.

2. The proteinic component of system contributes to a better stabilization of the dispersion towards the structural elements of the leather, making easier a better penetration and distribution of the polymers.

3. The penetration of the reactive polymers in leather is carried out by the method of "drum impregnation" in float.

4. The float exhaustion is 90—100% and it is carried out in about 45—60 minutes.

5. The values of the physical-mechanical characteristics of the impregnated leathers with the proteinic-synthetic product "Polisin" are high enough to the "control samples" for elongation break, tear and stitch resistance. The grain aspect, softness, and touch are well appreciated by the specialists.

6. Utilization of certain acrylic dispersions in obtaining proteinic-synthetic "Polisin" products led to; the possibility of diminishing chrome supply for some types of leather; high exhaustion of Cr<sub>2</sub>O<sub>3</sub> in the tanning float; the reduction of vegetable tanning materials used in retannage process.

#### R E F E R E N C E S

1. Ram cummar, S. C., Santhanam, S. P., "Acrylic Syntans for retanning leathers", Indofil Chem. Ltd. Madras 600 600.004/1978.
2. Smelkov, V. K., *Izvestia, Technology Light Industry*, No. 1, 1970.

3. B.V. 834-133, URSS.
4. Pfleiderer, R., Darmstadt, „Das Leder”, No. 10, 1981, p. 173-177.
5. Sovetkin, N.I.—KOP, No. 11, 1981, p. 46,
6. Izvestia, „Visih Tehnologii Legkoi Promislenosti”, no. 1, 1970. (The Theoretical Bases for treating leather in aqueous polymer dispersions).
7. Zöldy V., Doctoral Dissertation, „The Variation of the Electrokinetic Potential of the Leathers in the Wet Stages after Tanning in Chrome Salts” — Babeş-Bolyai University in Cluj-Napoca, Romania.
8. Prentiss W. C., „Röhm and Haas Company Philadelphia” — USA, 1978, „The Role of Acrylates in Pigskin Processing”.

## ACTIVITY AND STABILITY OF ENZYME MOLECULES FOLLOWING THEIR CONTACT WITH CLAY MINERAL SURFACES<sup>1</sup>

ȘTEFAN KISS\*, MIHAIL DRĂGAN-BULARDĂ\* and DANIELA PASCA\*\*

Received: September 8, 1986

The paper is a short review of the literature data concerning inhibitory and stabilizing effects of clay minerals on the invertase enzyme. Pure clay minerals (kaolinite, bentonite etc.) inhibit the activity of yeast invertase. The clay minerals added to soil stabilize and protect from degradation the invertase molecules produced by the soil microorganisms under the influence of inductor (sucrose).

Key-words: *clay minerals, invertase, enzyme adsorption, soil enzymes*

**Introduction.** Maintenance and perpetuation of life on our Planet are conditioned by the biological cycles of elements (C, N, P, S, etc.), in which photosynthesis and decomposition of organic (plant, animal, microbial and xenobiotic) residues are the basic processes. In the decomposition of organic residues, the enzymes accumulated in soil — besides the enzymes of the proliferating microorganisms — play a key role. Clay minerals contribute to this accumulation [1–3].

It has been proved in the case of many enzymes and different clay minerals that the contact between enzyme molecules and clay mineral surfaces leads, in general, to inhibition of enzyme activity, followed by stabilization and protection of the residual activity.

Our paper is a review which aims at exemplifying these investigations in the case of invertase. The review consists of two parts dealing with the inhibitory then with the stabilizing and protecting effects of clay minerals on invertase.

**I. Inhibitory Effect of Clay Minerals on Invertase.** The researches dealing with the inhibitory effect of clay minerals on the activity of enzymes may be grouped into 4 types, according to the source of clay minerals and that of enzymes:

*type 1*: pure clay minerals are used together with partially or completely purified enzyme preparations originating from microorganisms, plants or animals;

*type 2*: enzymatically active or inactivated soil samples are used together with enzyme preparations;

*type 3*: clay mineral — soil mixtures are used and the natural enzyme content of soil is the only enzyme source; and

*type 4*: clay mineral — soil mixtures are treated with enzyme preparations. In the case of invertase all types of researches are represented.

<sup>1</sup> Paper presented at the Symposium on Colloid and Surface Chemistry, Cluj-Napoca, September 8–10, 1986.

\* University of Cluj-Napoca, Department of Biology, 3400 Cluj-Napoca, Romania

\*\* Biological Research Centre, 3400 Cluj-Napoca, Romania

**1. Activity of Invertase in the Presence of Clay Minerals.** Willstätter and Schneider [4] found that adsorption of yeast invertase to kaolin resulted in a great loss of activity, but later the activity of adsorbate decreased only slowly. According to Fischer *et al.* [5], bentonite adsorbed the stabilizing polymannan component of yeast invertase and, therefore, inactivated the enzyme. Our data [6] indicated that there was a direct relationship between the amount of kaolinite and bentonite and their inhibitory effect on the invertase activity of yeast autolysate (Fig. 1). Zvyagintsev and Velikanov [7, 8] and Velikanov and Zvy-

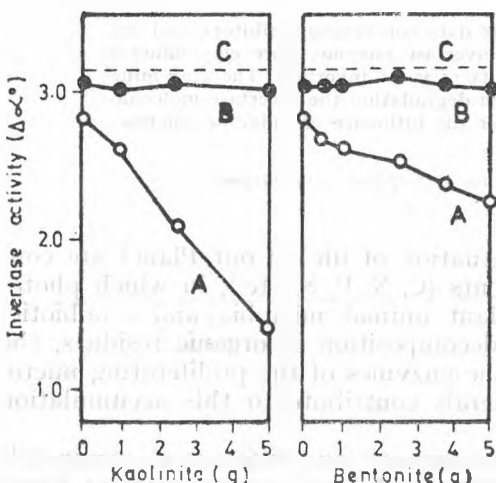


Fig. 1. Activity of yeast invertase in the presence of clay minerals (A), and of clay mineral — soil mixtures (B). The straight line C represents the sum of the activities of the soil invertase alone and of yeast invertase alone [6].

Table 1

Invertase activity of yeast autolysate added to samples of a leached chernozem [11]

Enzyme source	Invertase activity ( $\Delta\alpha^\circ$ )	
	Measured	Calculated
Autolysate	2.90	—
Soil	0.33	—
Soil + autolysate	3.03	3.23

gintsev [9] demonstrated that montmorillonitic clays (gumbrine, steatite, bentonite and nontronite) were stronger inhibitors of yeast invertase activity than kaolinite and monothermite.

Ross [10] also found significant decreases in yeast invertase activity in unbuffered and buffered clay suspensions. The inhibitory effect of clay minerals was in the order: montmorillonite > illite > kaolinite > allophane > muscovite. In the presence of 3 monomineralic clay fractions isolated from soils, the order of inhibition was: mica-beidellite > mica-vermiculite  $\approx$  muscovite. In buffered suspensions all clay minerals depressed invertase activity to a generally greater extent after 24-hour than after 1-hour contact; no activity was detectable after 24 hours in the presence of montmorillonite. The inhibitory effect of pedogenic clay fractions was, however, similar after 1 and 24 hours' contact time.

**2. Activity of Invertase Added to Soil Samples.** Our data [11] presented in Table 1 show that invertase activity of yeast autolysate added to samples of a leached chernozem suffered only a slight diminution. But according to Zvyagintsev and Velikanov [7, 8], the yeast invertase added to soil samples previously heated at 105°C for 3–4 hours lost a significant part of its activity. The effect of two chernozems was stronger than that of a soddy podzol. In the experiment of Ross [10], the two topsoils to which yeast invertase was added did not adsorb the enzyme or inhibit its activity.

Table 2

**Invertase activity in clay mineral — soil mixtures [11]**

Clay mineral and its amount (g) added to 20-g soil samples	Invertase activity ( $\Delta\alpha^\circ$ )
Kaolinite	0
	1
	5
	10
Bentonite	0
	1
	2.5
	5

Table 3

**Microbial synthesis and accumulation of invertase in incubated clay mineral — soil mixtures [12]**

Clay mineral and its amount (g) added to 50-g soil samples		Invertase activity ( $\Delta\alpha^\circ$ )		
		Experimental variants	Not moistened	Moistened with sucrose and moistened
Control	0	1.03	1.10	1.48
Kaolinite	1	1.00	1.12	1.58
	5	1.03	1.06	1.87
Bentonite	10	1.06	1.12	2.59
	1	1.06	1.11	1.59
	2.5	1.05	1.10	1.65
	5	1.07	1.15	2.04

*3. Activity of Soil Invertase in Clay Mineral — Soil Mixtures.* Invertase activity of a leached chernozem was not influenced by clay mineral additions [11] (Table 2). In other words, the invertase already accumulated in soil could not be inhibited by pure clay minerals. These minerals were able to inhibit only the free invertase present in yeast autolysate (cf. Fig. 1).

*4. Activity of Invertase Added to Clay Mineral — Soil Mixtures.* Fig. 1 shows that activity of yeast autolysate invertase added to clay mineral — soil mixtures remained unchanged in contrast to its strong inhibition which occurred when the enzyme was added to pure clay minerals. This means that the soil removed the inhibitory effect of pure clay minerals on the invertase activity [6].

**II. Stabilizing and Protecting Effect of Clay Minerals on Invertase.** Clay mineral — soil mixtures were amended with enzyme substrate (sucrose) and moistened, then incubated for 3 weeks to induce the microbial synthesis of invertase. Variants not amended and not moistened as well as variants without added clay minerals were also included. The results in Table 3 show that more invertase accumulated in the clay mineral — soil mixtures than in the soil samples. This proves that clay minerals stabilized and protected from degradation the invertase molecules produced by soil microorganisms under the inducing action of sucrose. Practically no change occurred in the invertase activity of variants without sucrose [12].

**Discussion.** The clay minerals, through their stabilizing and protecting effect on enzymes, contribute to the accumulation of enzymes in soil, to the "survival" of enzyme molecules

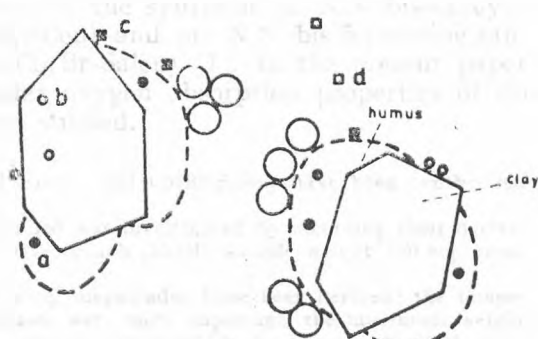


Fig. 2. Distribution of accumulated and free enzymes in the soil microenvironment [2]: a — Enzymes trapped within or complexed with humus; b — Enzymes adsorbed to clay, either on the surface or between the crystal lattices; c — Enzymes attached to surface of organic film; d — Free, ephemeral enzymes in the soil aqueous phase. The large circles represent microorganisms.

in the soil microenvironment. But the contribution of clay minerals to enzyme accumulation in soil, and probably in aquatic sediments as well, is achieved in association with humic substances. The accumulated enzymes are located at microsites in or on the organo-mineral (clay-humic) complexes. Fig. 2 presents a model [2] concerning distribution of accumulated and free enzymes in the soil microenvironment. The enzymes trapped inside the porous clay-humic complexes or attached to their surfaces are protected from proteolysis and other inactivations and yet accessible to substrates.

## REFERENCES

1. Kiss, S., Drăgan-Bulardă, M., Rădulescu, D., *Adv. Agron.*, **27**, 25 (1975).
2. Burns, R. G., Interaction of Microorganisms, Their Substrates and Their Products with Soil Surfaces, in "Adhesion of Microorganisms to Surfaces", D. C. Ellwood, J. Melling and P. Rutter, eds., Academic Press, London, (1979).
3. Stotzky, G., Burns, R. G., The Soil Environment: Clay — Humus — Microbe Interactions in "Experimental Microbial Ecology", R. G. Burns and J. H. Slater, eds., Blackwell, Oxford, (1982).
4. Willstätter, R., Schneider, K., *Z. Physiol. Chem.*, **133**, 193 (1924).
5. Fischer, E. H., Kohtès, L., Fellig, J., *Helv. Chim. Acta*, **34**, 1132 (1951).
6. Kiss, S., *Nature*, **182**, 203 (1958).
7. Zvyagintsev, D. G., Velikanov, L. I., *Pochvovedenie*, No. 6, 100 (1968).
8. Zvyagintsev, D. G., Velikanov, L. I., *Sb. Dokl. Simp. Ferment. Pochvy* (Minsk), p. 108 (1968).
9. Velikanov, L. I., Zvyagintsev, D. G., Adsorbsiya Fermentov i Ikh Aktivnost' na Granitse Razdela Tverdoi i Zhidkoi Fazy, in "Mikroorganizmy v Sel'skom Khozyaistve", Izd. Mosk. Univ., Moskva, (1970).
10. Ross, D. J., *Soil Biol. Biochem.*, **15**, 287 (1983).
11. Kiss, S., Talajenzimek, in "Talajtan", Csapó, M. J., ed., Ed. Agro-Silvică, Bucureşti, (1958).
12. Kiss, S., *Z. Pflanzenernähr., Düng. Bodenk.*, **81** (126), 117 (1958).

## THE THERMAL BEHAVIOUR AND THE MOLECULAR OXYGEN ABSORPTION PROPERTIES OF Co(SALEN) AND Co(BrSALEN) COMPLEXES

MARIANA RUSU\*, ALEXANDRU BOTAR\*\* and GHEORGHE MARCU\*

Eingegangen am 28 April 1987

Studies on thermal stability of Co (Salen) and Co (Br-Salen) complexes (Salen: N,N'-bis-salicylidene-ethylene-diamine and Br-Salen: N,N'-bis-5-bromine-salicylidene-ethylene diamine) and on molecular oxygen absorption properties of these complexes have been performed. It was established that Co (Salen) has a lower thermal stability and absorbs easier molecular oxygen than Co (Br-Salen).

**Introduction.** Numerous coordination compounds including the Co(II) complexes with different Schiff bases constitute a model for the study of reversible oxygenation mechanisms.

The reversible fixation of molecular oxygen, by the systems containing transition metals with variable oxidation states and different chelating agents, is an actual problem not only of bioinorganics but also of the technics to discover oxidation reactions in homogeneous phase, as well as in heterogeneous phases catalysed by different metals. Another application of the coordination compounds with molecular oxygen would be to obtain ultrapure oxygen by unconventional methods, the purification of different gases, respectively. In this context, the cobalt compounds with selective absorption-desorption properties for molecular oxygen have a special importance.

Our experiments were directed towards the synthesis of N,N'-bis-salicylidene-ethylene-diamine Co(II) noted Co(Salen) and of N,N'-bis-5-bromine-salicylidene-ethylene-diamine Co(II) noted Co(Br-Salen) [1]. In the present paper the thermal behaviour and the molecular oxygen absorption properties of Co (Salen) and Co (Br-Salen) complexes are studied.

**Materials and Methods.** Both complexes Co(Salen) and Co(Br-Salen) have been synthesized as described earlier [1].

Thermal decomposition of the complexes studied was investigated by recording their derivatograms, using an OD-102 type Paulik-Erdey derivatograph (MOM), sample weight 100 mg, constant heating rate 20°C/min.

From the recorded derivatograms the following magnitudes have been derived: the temperature ranges in which sample weight losses/increases were more important, the maximum weight loss rate temperatures (DTG peak temperatures), the domains in which the physico-chemical changes are exo- or endothermal (DTA peak temperatures).

An attempt is made to derive kinetic parameters for some thermal decomposition stages. For this purpose the validity of the rate equation [2,3]

$$\frac{d\alpha}{dt} = A \cdot e^{-E/RT} (1 - \alpha)^n \quad (1)$$

\* University of Cluj-Napoca, Faculty of Chemical technology, 3400 Cluj-Napoca, Romania

\*\* Institute of Chemistry, 3400 Cluj-Napoca Romania

has been presumed, where  $A$ ,  $E$  and  $n$  stand for the pre-exponential factor, activation energy and reaction order, respectively. The transformation degree ( $\alpha$ ) in a given decomposition stage (TG step) can be calculated by means of the relation:

$$\alpha_i = \frac{W_i - W_\infty}{W_0 - W_\infty} \quad (2)$$

where  $W_i$ ,  $W_0$  and  $W_\infty$  stand for the actual, initial and final weight of the sample, respectively. By taking logarithms of both sides of equation (1), one obtains:

$$\log \frac{d\alpha}{dt} = \log A - \frac{E}{2,3 RT} + n \log (1 - \alpha) \quad (3)$$

which is linear in both  $1/T$  and  $\log (1 - \alpha)$  allowing us to use the least square method [8] for deriving  $\log A$ ,  $E$  and  $n$  values, which will be referred to as kinetic parameters. For this purpose TG data, i.e. the  $W_i$  vs.  $t$  curve has been transformed into  $\alpha$  vs.  $T$  curve for the decomposition step considered, by using equation (2).  $\frac{d\alpha}{dt}$  vs.  $T$  curves have been constructed by using the DTG, i.e. the  $\frac{dW}{dt}$  vs.  $t$  and the  $T$  vs.  $t$  curves. In order to transform the DTG deviation from the base line into  $d\alpha/dt$  a direct proportionality was presumed between them and the maximum deviation corresponding to the DTG peak was equaled to the  $dW/dt$  value graphically determined from the TG curve [8].

The experimental  $\alpha_i$ ,  $d\alpha_i/dt$ ,  $T_i$  values have been processed accordingly to an adequate computer program [8].

The molecular oxygen absorption by Co(Salen) and Co(Br-Salen) complexes was practically followed by using an apparatus consisting of a three necked round bottom flask, an oxygen polarographic sensor, and an OH-102 Radelkis polarograph.

The bottom flask was filled with 300 ml water and then was bubbled with air. The oxygen absorption was followed by means of the recorded sensor current. The prepared complex-substance sample dissolved in 12.5 ml of dimethylformamide is introduced by injection at the moment when the sensor current remains constant (= O<sub>2</sub> saturation). Then the decrease of the sensor current is recorded being proportional to the decrease of the oxygen concentration as a result of oxygen absorption by the complex.

**Results and discussion.** The derivatogram recorded for Co (Salen) is presented in Fig. 1. As can be seen, a slight weight loss begins at about 90–100°C, presumably corresponding to the evaporation of moisture. The first true decomposition stage occurs between 290 and 390°C, characterized by a DTG and an exothermal DTA peak at 355 and 345°C, respectively. This is followed by a stage which is hardly observed on the TG curve, but is marked by a small DTG peak at 400°C and a small exothermal DTA peak at 395°C.

Further on, a more important weight loss occurs, the DTG curve exhibits a peak at 505°C and the DTA one an exothermal peak at 510°C. A very sharp exothermal peak is observed at 590°C together with a sharp DTG one at 595°C. The quite rapid weight loss continues and exhibits a maximum rate at about 665°C. The sample weight attains a minimum value at 795°C, corresponding to CoO. At this temperature the sample weight begins to increase due to the oxidation of the residue marked by a strong exothermal peak at 835°C, and attains a constant value, corresponding to Co<sub>3</sub>O<sub>4</sub> [4].

The weight losses in the successive exothermal stages correspond to no clear stoichiometric relations. Presumably, the ligand molecules are gradually oxidized by the atmospheric oxygen and gaseous products are evolved.

The TG and DTG curves in the temperature range comprised between 355 and 390°C were found to be suitable for kinetic calculations. This portion was processed, according to the above mentioned kinetic calculation method. The kinetic parameter values derived are  $E = 26.4$  Kcal/mole (110 KJ/mole) and  $n = 0.70$ , respectively, for the  $\alpha$  range  $0.66 < \alpha < 0.99$ .

The derivatogram of the Co(Br-Salen) complex is visualized in Fig. 2. As can be seen, the sample exhibits a weight loss up to about 120°C, marked by

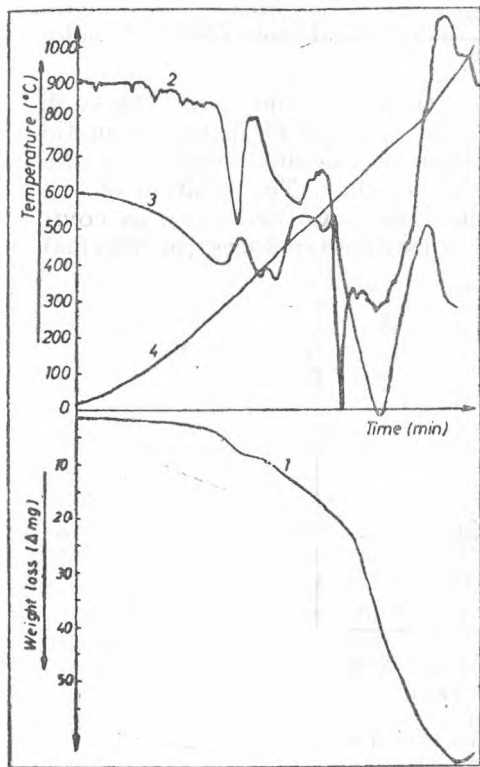


Fig. 1. Derivatogram of Co(Br-Salen); 1—TG curve; 2—DTG curve; 3—DTA curve; 4—temperature variation curve.

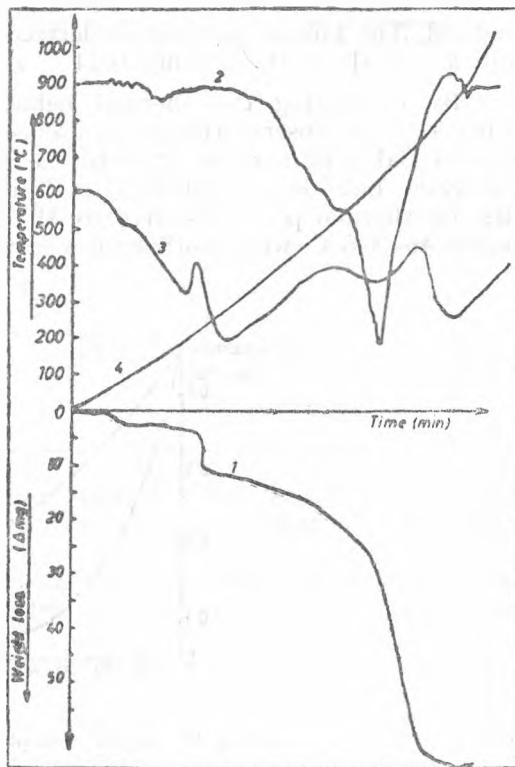


Fig. 2. Derivatogram of Co(Salen); 1—TG curve; 2—DTG curve; 3—DTA curve; 4—temperature variation curve.

a weak endothermal peak on the DTA curve, corresponding to the evaporation of moisture. Further begins a slow decomposition reaction, which gradually becomes very fast with a maximum rate at about 300°C, marked by a sharp exothermal peak at 310°C. The weight loss in this stage corresponds to no stoichiometric relation and presumably implies the oxydation of the ligand by the atmospheric oxygen, yielding gaseous products.

After a relatively short weight loss stop another exothermal process begins, with a DTA peak temperature equal to 670 °C. The decomposition rate becomes the largest only at 770 °C, presumably due to the superposition of another exothermal process, entailing the apparition of a sharp exothermal peak at 870 °C. From this temperature on the sample weight remains constant and it approximately corresponds to a residue of  $\text{CoO} + \text{CoBr}_2$ . Consequently, the ligand molecules seem to be combusted and volatilized, except the Br atoms. The formation of  $\text{CoBr}_2$  seems to hinder the oxydation of  $\text{CoO}$  into  $\text{Co}_3\text{O}_4$ .

For the first exothermal stage, the portions of the TG and DTG curves comprised between 285 and 315 °C were processed according to the kinetic method. The kinetic parameters derived are  $E = 57.8$  Kcal/mole (242 KJ/mole) and  $n = 0.51$  for the  $\alpha$  range  $0.24 < \alpha < 0.88$ .

By comparing the thermal behaviour of the two complexes with each other, one can observe that the presence of the Br substituent in the aromatic ring of Salen influences not only the composition of the final product of the pyrolysis, but also the thermal stability of the complex. The position of the first exothermal peak is shifted to 310 °C in the case of  $\text{Co}(\text{Br-Salen})$ , as compared to 345 °C with  $\text{Co}(\text{Salen})$ , i.e. the Br substituent reduces the thermal

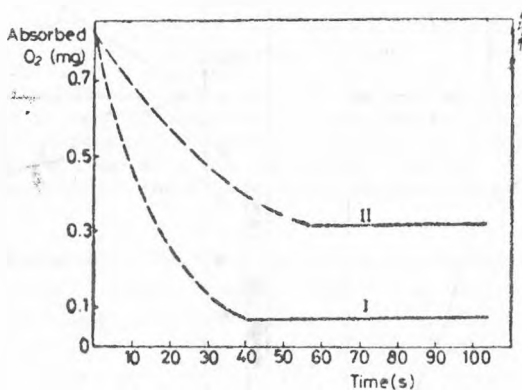


Fig. 3. Oxygen absorption as function of time:  
I— $\text{Co}(\text{Salen})$ ; II— $\text{Co}(\text{Br-Salen})$ .

stability of the complex. This effect might be due to the electron withdrawing properties of Br, entailing the diminution of the donor properties of both O and N atoms, i.e. the weakening of the Co-ligand bonds. The less thermal stability of  $\text{Co}(\text{Br-Salen})$  makes decomposition to occur in 3 successive and partially overlapped stages, as compared to  $\text{Co}(\text{Salen})$ , which exhibits 4 exothermal decomposition peaks. Further, the first decomposition stage is very rapid in the case of  $\text{Co}(\text{Br-Salen})$ , as compared to the slower process observed with  $\text{Co}(\text{Salen})$ .

The oxygen absorption properties of the complexes studied is shown by Fig. 3, giving the amount of  $\text{O}_2$  absorbed as function of time. As seen,  $\text{Co}(\text{Salen})$

absorbs the oxygen more rapidly as compared to Co(Br-Salen), the oxygen sensor indicating a saturation value after 42 s in the case of the former, as compared to 58 s with the latter. Concerning the amount of  $O_2$  absorbed, Table 1. is relevant, showing the absorption of one mole of  $O_2$  per two moles

Table 1

## Data for the oxygen absorption at saturation

Substances	Complex (mg)	$O_2$ absorbed (mg)	Mean of $O_2$ absorbed (mg)	Moles of $O_2$ absorbed by two moles of complexes
Co(Salen)	16	0.751	0.752	0.9953
	16	0.758		
	16	0.747		
	16	0.754		
	16	0.748		
Co(Br-Salen)	16	0.5070	0.510	0.9621
	16	0.5080		
	16	0.5118		
	16	0.511		
	16	0.5012		

of complex in the case of both complexes studied. These results are in good agreement with literature data [5-7], and indicate the formation of binuclear products, with bridged molecular oxygen.

The influence of the Br-substituent in the aromatic ring consists of reduced absorption rate, suggesting the idea that the inductive effect of Br entails the increase of the activation energy of the process.

## REFERENCES

1. Gh. Marcu, A. Botar and A. Naumescu, *Rev. Roumaine Chim.*,
2. J. Sesták and G. Berggren, *Thermochim. Acta.*, **3**, 1 (1971).
3. E. Segal and D. Fătu, „Introducere în cinetica neizotermă”, Ed. Acad. R.S.R., Bucureşti, 1983, p. 69.
4. G. Liptay, *Rev. Chim.*, **26**, 149 (1979).
5. T. Tsumaki, *Bull. Chem. Soc. Japon.*, **13**, 252 (1938).
6. R. H. Bailes and M. Calvin, *J. Amer. Chem. Soc.*, **69**, 1886 (1947).
7. F. Calderazzo, F. Floriani and J. J. Salzmann, *Inorg. Nucl. Chem. Letters*, **2**, 379 (1966).
8. V. Liteanu, unpublished results.

## RATIONALISIERUNG UND VEREINFACHUNG EINIGER ANALYTISCH-CHEMISCHEN BERECHNUNGEN

DUMITRU CEAUŞESCU\* und MARINA ELIU-CEAUŞESCU\*

Eingegangen am 28 April 1987

**Rationalisation and Simplification of Some Analytical-chemical Calculations.** The present report refers to the computation of the equilibrium concentrations of species in aqueous media of  $AB_n$ - type substances (weak acids —  $H_nA^-$ , or complexes —  $ML_m^-$ ). When the consecutive equilibrium constants differ with more than 3 orders or complexes —  $ML_m^-$ ). When the consecutive equilibrium constants differ with more than 3 orders of power, computation is made using molecular fractions obtained through tabular computation (using previously computed table for substances of type  $AB$ ). When the consecutive equilibrium constants have nearer values, computation is performed graphically (using *ad-hoc* constructed logarithmical diagrams). The concentration of  $B$  is obtained by successive approximation, combining a simple numerical computation with tabular or graphical one.

Vorliegende Arbeit bezieht sich auf die Konzentrationsberechnung der anwesenden Spezien im Falle der wässrigen Lösungen der Substanzen vom Typus  $AB_n$  (schwache Säuren  $H_nA$ , Komplexe  $ML_m$ ). Die Berechnungen werden auf Grund der Molbrüche gemacht, welche entweder tabellarisch (aus vorher berechneten Tabellen), oder graphisch (aus *ad-hoc* aufgebauten Diagrammen) erhalten werden. Für die Spezie  $B$  werden die Berechnungen auf Grund der Molbrüche gemacht, durch iteratives Näherungsverfahren, indem man einfache numerische Berechnungen mit tabellaren oder graphischen Berechnungen kombiniert.

Zur Vereinfachung beziehen wir uns auf die Substanz  $AB_3$ , von der analytischen Konzentration  $C$ , charakterisiert durch die sukzessiven Dissoziationskonstanten  $K_1 = \frac{[AB_2][B]}{[AB_3]}$ ,  $K_2 = \frac{[AB][B]}{[AB_2]}$ ,  $K_3 = \frac{[A][B]}{[AB]}$ . Die Konzentrationen der verschiedenen Spezien erhält man aus den Ausdrücken :

$$[A] = \frac{C}{\alpha_{(B)}}; [AB] = \frac{C[B]}{\alpha_{(B)} K_3}; [AB_2] = \frac{C[B]^2}{\alpha_{(B)} K_3 K_2}; [AB_3] = \frac{C[B]^3}{\alpha_{(B)} K_1 K_2 K_3}$$

wobei :

$$\alpha_{(B)} = 1 + \frac{[B]}{K_3} + \frac{[B]^2}{K_3 K_2} + \frac{[B]^3}{K_3 K_2 K_1}$$

$$[B] = 3C - [AB] - 2[AB_2] - 3[AB_3], \text{ oder } [B] = 3[A] + 2[AB] + [AB_2]$$

welche leicht abzuleiten sind.

\* Universität Timișoara, Fakultät für Naturwissenschaft, 1900 Timișoara, Rumänien

Wenn man im Ausdruck für  $[B]$  die Konzentrationen der verschiedenen Spezien durch ihre oben formulierten Werte ersetzt, auf  $C$ ,  $[B]$  und die Dissoziationskonstanten bezogen, erhält man komplizierte Beziehungen, die wir nicht wiedergeben. Im Vergleich dazu, sind die analogen Beziehungen, die auf die Molbrüche  $x_A$ ,  $x_{AB}$ , ... bezogen formuliert werden, sehr einfach:

$$[B] = 3C - C(x_{AB} + 2x_{AB_2} + 3x_{AB_3}), \text{ oder } [B] = C(3x_A + 2X_{AB} + x_{AB_2})$$

Wenn die Möglichkeit einer einfachen Berechnung der Molbrüche in Funktion von  $[B]$  bestehen würde, könnten diese Beziehungen für eine bequeme Berechnung von  $[B]$  durch iteratives Näherungsverfahren eingesetzt werden.

Im Falle der Substanzen vom Typus AB erlaubt die vorher berechnete und tabellierte Beziehung  $\rho B - \rho K = \lg \frac{[A]}{[AB]} = \lg \frac{x_A}{x_{AB}}$  eine rasche Berechnung auf tabellarem Weg der Konzentrationen der Spezien einer beliebigen Substanz AB (charakterisiert durch  $K$  und  $C$ ), für einen gegebenen  $\rho B$ -Wert ( $x_A$  und  $x_{AB}$ , welche der Differenz  $\rho B - \rho K$  entsprechen, werden mit  $C$  multipliziert). Die Aufstellung der Distributionsdiagramme wird somit überflüssig. Für eine zufriedenstellende Präzision ist es notwendig, dass die Tabelle  $x$ -Werte enthält, die sich voneinander um 0,005 unterscheiden (welches einer Präzision von  $\pm 0,001$  durch Interpolation entspricht). Wir fügen — zur Illustrierung — eine solche Tabelle bei (Tab. 1), in welcher die  $x$ -Werte sich voneinander mit 0,02 unterscheiden. Das Existenzbereich der Spezien A und B ist (praktisch):  $\rho B = \rho K \mp 3$ . Aus dieser Beziehung folgt, dass die Tabelle für die Berechnung der Konzentrationen der anwesenden Spezien der Substanzen AB verwendbar ist, wenn die sukzessiven  $K$ -Werte sich untereinander mehr als  $10^3$ -mal unterscheiden. Somit können im Fall der Substanz  $AB_3$ , wenn  $\rho B \leq \rho K_1$  oder  $\rho B \geq \rho K_3$ , nur zwei

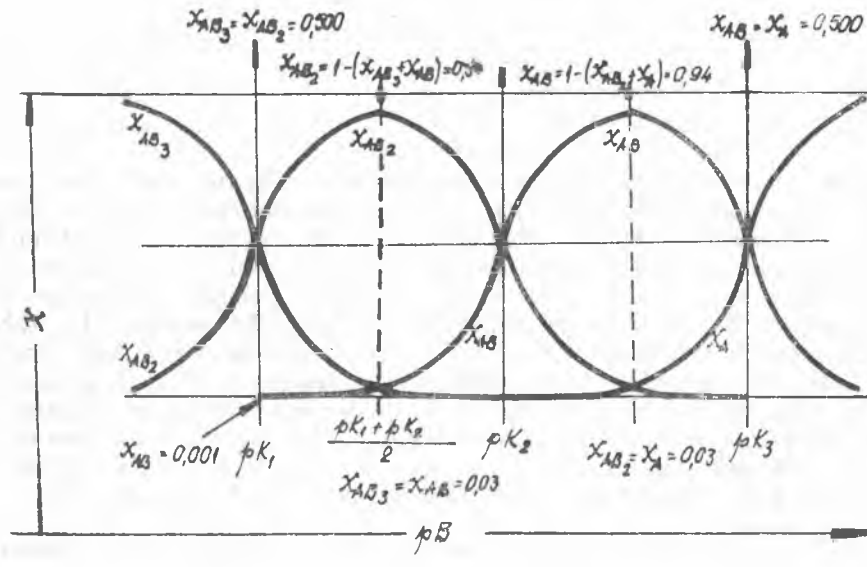


Abb. 1

Tabelle 1

$pB - pK$	$x_{AB}$	$x_A$	
-5	0,99999	0,00001	+5
-4	0,9999	0,0001	+4
-3	0,999	0,001	+3
-2,30	0,995	0,005	+2,30
-1,996	0,99	0,01	+1,996
-1,62	0,98	0,02	+1,62
-1,38	0,96	0,04	+1,38
-1,20	0,94	0,06	+1,20
-1,06	0,92	0,08	+1,06
-0,954	0,90	0,10	+0,954
-0,865	0,88	0,12	+0,865
-0,788	0,86	0,14	+0,788
-0,720	0,84	0,16	+0,720
-0,658	0,82	0,18	+0,658
-0,602	0,80	0,20	+0,602
-0,550	0,78	0,22	+0,550
-0,500	0,76	0,24	+0,500
-0,454	0,74	0,26	+0,454
-0,410	0,72	0,28	+0,410
-0,368	0,70	0,30	+0,368
-0,327	0,68	0,32	+0,327
-0,288	0,66	0,34	+0,288
-0,250	0,64	0,36	+0,250
-0,213	0,62	0,38	+0,213
-0,176	0,60	0,40	+0,176
-0,140	0,58	0,42	+0,140
-0,105	0,56	0,44	+0,105
-0,070	0,54	0,46	+0,070
-0,035	0,52	0,48	+0,035
0	0,50	0,50	0

Spezien anwesend sein, beziehungsweise  $AB_3$  und  $AB_2$  im ersten Fall, oder  $AB$  und  $A$  im zweiten Fall. Wenn  $pB$  zwischen den Werten  $pK_1$  und  $pK_2$ , oder zwischen den Werten  $pK_2$  und  $pK_3$  liegt, sind drei Spezien anwesend, und zwar  $AB_3$ ,  $AB_2$  und  $AB$  im ersten Fall, oder  $AB_2$ ,  $AB$  und  $A$  im zweiten Fall. In diesen Fällen werden die Differenzen zwischen  $pB$  und beiden  $pK$ -Werten, welche beiderseits von  $pB$  gelegen sind, in Betracht gezogen. In Abbildung 1 ist das Distributionsdiagramm einer (imaginären) Substanz  $AB_3$  gegeben, in deren Fall sich die sukzessiven  $K$ -Werte voneinander  $10^3$ -mal (genau) unterscheiden. Das Diagramm illustriert das oben Gesagte. Pregnante Werte:  $pB = pK_1$ , wenn  $x_{AB_3} = x_{AB_2} = 0,50$ ;  $pB = pK_1 + 1,5 = pK_2 - 1,5$ , wenn  $x_{AB_3} = x_{AB_2} = 0,03$  und folglich  $x_{AB_2} = 1 - (x_{AB_3} + x_{AB_2}) = 1 - 0,06 = 0,94^*$  u.s.w. (weiterhin ist die Abbildung zu verfolgen). Für die Berechnung von  $[B]$ , im

\* Für andere Zvischenwerte ist die Überlegung die gleiche. Zum Beispiel für  $pB = pK_1 + 1 = pK_2 - 2$  finden wir tabellarisch  $x_{AB_3} = 0,09$  und  $x_{AB_2} = 0,01$ . Daraus folgt, dass  $x_{AB_2} = 1 - (0,09 + 0,01) = 0,90$ .

Fall der reinen Substanz  $\text{AB}_3$ , durch iterative Näherungsverfahren, geht man von  $[\text{B}]_0$  aus, welche aus  $K_1$  erhalten wurde, wo man  $[\text{AB}] \approx [\text{B}]$  und  $[\text{AB}] \approx \approx C$  nimmt, wonach man die Tabelle benutzen kann ( $p\text{B} < pK_1$  — folglich sind nur die Spezien  $\text{AB}_3$  und  $\text{AB}_2$  anwesend).

*Beispiel.* Es gibt eine 0,1 M Lösung der Substanz  $\text{AB}_3$ , welche  $K_1 = 10^{-3}$ ,  $K_2 = 10^{-6}$ ,  $K_3 = 10^{-9}$  hat. Man verlangt die Berechnung von  $[\text{B}]$ .

Man erhält:  $[\text{B}]_0 = \sqrt{K_1 C} = \sqrt{10^{-3} \cdot 10^{-1}} = 10^{-2} \text{ M}$ . Für  $p\text{B} - pK_1 = 2 - 3 = -1$  finden wir tabellarisch  $x_{\text{AB}_3} = 0,91$ ,  $x_{\text{AB}_2} = 0,09$ . Wir haben weiter  $[\text{B}]_1 = C(3x_A + 2x_{\text{AB}} + x_{\text{AB}_3}) = 0,1 \cdot 0,09 = 9 \cdot 10^{-3} = 10^{-2,05}$ . Für  $p\text{B} - pK_1 = 2,05 - 3 = -0,95$  finden wir  $x_{\text{AB}_2} = 0,10$ . Es folgt, dass  $[\text{B}]_2 = 10^{-2} \text{ M}$ .  $[\text{B}]_{\text{Mittelwert}} = 10^{-2,03} = 9,5 \cdot 10^{-3} \text{ M}$ .

Im Fall, dass die sukzessiven  $K$ -Werte weniger als  $10^3$ -mal untereinander verschieden sind, kann die Tabelle 1 nicht mehr benutzt werden, und man muss als Hilfsmittel ein ad-hoc Diagramm anfertigen, welches auf den Beziehungen:

$$[\text{AB}_3] = \frac{[\text{A}][\text{B}]^3}{K_3 K_2 K_1}; \quad [\text{AB}_2] = \frac{[\text{A}][\text{B}]^2}{K_3 K_2}; \quad [\text{AB}] = \frac{[\text{A}][\text{B}]}{K_3}$$

fusst. In diesen Beziehungen bemerken wir, dass in der Beschaffenheit der Konzentrationen aller Spezien mit A, als gemeinsamer Faktor  $[\text{A}]$  erscheint. Es folgt also, dass in den relativen Konzentrationsbeziehungen jeder Spezie in bezug auf die Summe der Konzentrationen, dieser Faktor  $[\text{A}]$  sich reduziert. Diese Tatsache bedeutet, dass  $[\text{A}]$  entweder den reellen Wert, oder jedwelchen anderen arbiträren Wert haben kann, und dass diese relativen Konzentrationen nichts anders als die Molbrüche darstellen. Durch Logarithmieren der obigen Beziehungen erhält man:

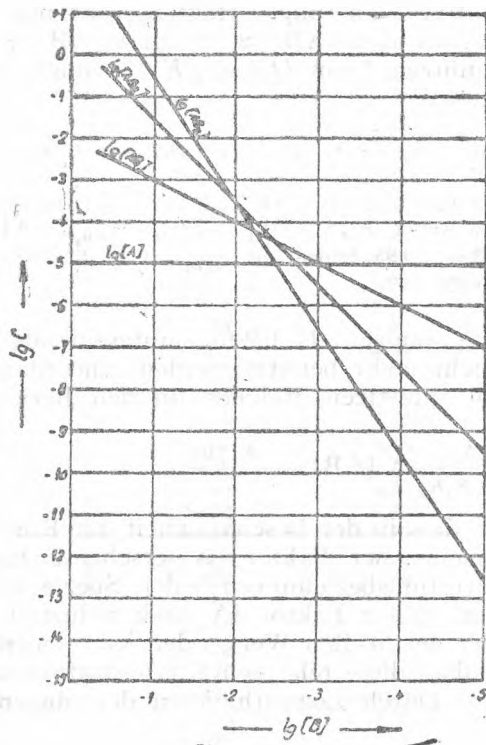
$$\begin{aligned}\lg [\text{AB}_3] &= \lg [\text{A}] - \lg K_3 K_2 K_1 + 3 \lg [\text{B}] \\ \lg [\text{AB}_2] &= \lg [\text{A}] - \lg K_3 K_2 + 2 \lg [\text{B}] \\ \lg [\text{AB}] &= \lg [\text{A}] - \lg K_3 + \lg [\text{B}] \\ \lg [\text{A}] &= \text{Konstante (arbiträr)}\end{aligned}$$

Das Diagramm der Gesamtheit solcher logarithmischer Geraden benutzt man bei der Erhaltung der Molbrüche für gegebene  $[\text{B}]$ -Werte, in Anbetracht der Errichtung der Distributionsdiagramme der Komplexverbindungen (siehe z.B. (1)). Wir werden sie nicht nur für die Erhaltung der Molbrüche für gegebene  $[\text{B}]$ -Werte benutzen, sondern auch für die Berechnung der Unbekannten  $[\text{B}]$  durch iterative Näherungsverfahren.

*Beispiel.* Gegeben ist eine 0,1 M Lösung der Substanz  $\text{AB}_3$  mit  $K_1 = 10^{-3}$ ,  $K_2 = 10^{-2,5}$ ,  $K_3 = 10^{-3}$ . Man soll  $[\text{AB}_3]$ ,  $[\text{AB}_2]$ ,  $[\text{AB}]$  und  $[\text{A}]$  berechnen für  $[\text{B}] = 10^{-2,75} \text{ M}$ , und  $[\text{B}]$  im Fall der reinen Substanz  $\text{AB}_3$ .

Um die logarithmischen Geraden zu errichten, brauchen wir zwei Punkte. Wir nehmen  $[\text{B}] = 10^{-2} \text{ M}$ , und  $[\text{B}] = 10^{-5} \text{ M}$ . Wir nehmen noch — arbiträr —  $[\text{A}] = 10^{-5} \text{ M}$ . Wir erhalten:

	$[\text{B}] = 10^{-2} \text{ M}$	$[\text{B}] = 10^{-5} \text{ M}$
$\lg [\text{AB}_3]$	$-5 + 7,5 - 3 \cdot 2 = -3,5$	$-5 + 7,5 - 3 \cdot 5 = -12,5$
$\lg [\text{AB}_2]$	$-5 + 5,5 - 3 \cdot 2 = -5,5$	$-5 + 5,5 - 2 \cdot 5 = -9,5$
$\lg [\text{AB}]$	$-5 + 3 - 2 = -4$	$-5 + 3 - 4 = -7$
$\lg [\text{A}]$	$-5$	$-5$



A b b . 2

In Abbildung 2 ist auf Millimeterpapier das Diagramm der Gesamtheit der vier Geraden dargestellt. Die Koordinatenachsen werden so gradiert, dass sie die Präzisionsbedingung erfüllen.

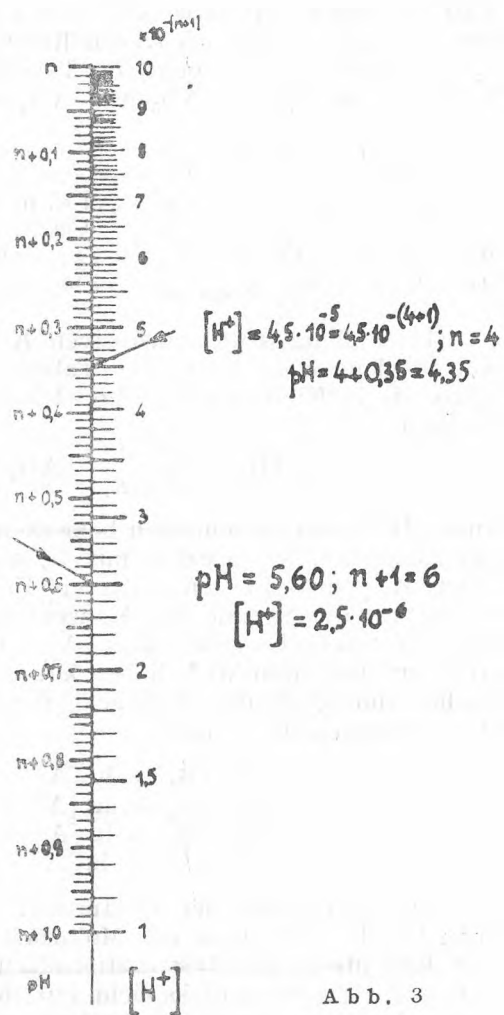
- 1) Auf der Vertikalen  $[B] = 10^{-8,75} M$  finden wir, von oben nach unten:

$$[AB] = 10^{-4,77} = 1,67 \cdot 10^{-5}$$

$$[AB_1] = 10^{-5} = 1 \cdot 10^{-5}$$

$$[A] \parallel = 10^{-5} = 1 \cdot 10^{-5}$$

$$[AB_3] = 10^{-5,8} = \frac{0,16 \cdot 10^{-5}}{3,83 \cdot 10^{-5}}$$



A b b . 3

$$x_{AB} = \frac{1,67}{3,83} = 0,436$$

$$x_{AB_1} = \frac{1}{3,83} = 0,261$$

$$x_A \parallel = \frac{1}{3,83} = 0,261$$

$$x_{AB_3} = \frac{0,16}{3,83} = 0,042$$

1,000

Die Umwandlungen von  $10^{\lg \gamma} = 10^{-\frac{1}{2}y}$  in  $y$  werden nomographisch gemacht. In Abbildung 3 ist das entsprechende Nomogramm (2)\* gegeben. Es folgt:

$$[\text{AB}_3] = C_{\text{AB}_1} \cdot x_{\text{AB}_3} = 0,1 \cdot 0,042 = 0,0042 M$$

$$[\text{AB}_2] = 0,1 \cdot 0,261 = 0,0261 M$$

$$[\text{AB}] = 0,1 \cdot 0,436 = 0,0436 M$$

$$[\text{A}] = 0,1 \cdot 0,261 = 0,0261 M$$

2) [B] in reiner  $\text{AB}_3$ -Lösung. Wir nehmen ursprünglich  $[\text{AB}_2] \approx [\text{B}]$  und  $[\text{AB}_3] \approx C$ . Wir haben:

$$[\text{B}]_0 = \sqrt{K_1 C} = \sqrt{10^{-2} \cdot 10^{-1}} = 10^{-1,5}$$

Tabelle 2

[B] sukzessiv		$C_{\text{AB}_3}(3x_A + 2x_{\text{AB}} + x_{\text{AB}_3}) = [\text{B}]$
$10^{-1,5}$	$[\text{AB}_3] = 10^{-2,05} = 8,9 \cdot 10^{-3}; x_{\text{AB}_3} = \frac{8,9}{11,99} = 0,742$ $[\text{AB}_2] = 10^{-2,55} = 2,8 \cdot 10^{-3}; x_{\text{AB}_2} = \frac{2,8}{11,99} = 0,234$ $[\text{AB}] = 10^{-3,55} = 0,28 \cdot 10^{-3}; x_{\text{AB}} = \frac{0,28}{11,99} = 0,023$ $[\text{A}] = 10^{-5} = 0,01 \cdot 10^{-3}; x_A = \frac{0,01}{11,99} = 0,0008$ $\underline{11,99 \cdot 10^{-3}}$	$0,1(3 \cdot 0,0008 + 2 \cdot 0,023 + 0,234) = 0,0284 = 10^{-1,55} M$
$10^{-1,55}$	$[\text{AB}_3] = 10^{-2,15} = 7,1 \cdot 10^{-3} x_{\text{AB}_3} = \frac{7,1}{9,89} = 0,718$ $[\text{AB}_2] = 10^{-2,6} = 2,5 \cdot 10^{-3}; x_{\text{AB}_2} = \frac{2,5}{9,89} = 0,253$ $[\text{AB}] = 10^{-3,55} = 0,28 \cdot 10^{-3}; x_{\text{AB}} = \frac{0,28}{9,89} = 0,028$ $[\text{A}] = 10^{-5} = 0,01 \cdot 10^{-3}; x_A = \frac{0,01}{9,89} = 0,001$ $\underline{9,89 \cdot 10^{-3}}$	$0,1(3 \cdot 0,001 + 2 \cdot 0,028 + 0,253) = 0,0312 = 10^{-1,52} M$
$10^{-1,52}$	$[\text{B}]_{\text{Mittelwert}} = 10^{-1,53}$	

## B I B L I O G R A P H I E

1. L. Kékedy, „Chimie analitică calitativă“, Ed. Scrisul Românesc Craiova 1982, S. 178.
2. E. Flück, M. Becke - Goehring, „Einführung in die Theorie der quantitativen Analyse“, Dresden 1972, S. 40.

\* Das Nomogramm wurde für die  $pH \Leftrightarrow [\text{H}^+]$  Umwandlungen errichtet, aber es hat eine allgemeine Anwendbarkeit. Die Notwendigkeit einer solcher Umwandlung ist sehr häufig in der analytischen Chemie und daher ist seine praktische Wichtigkeit gross

## THE STUDY OF THE FORMATION OF HETEROPOLYANIONS OF TYPE ML, WHERE M=Co<sup>2+</sup> AND V<sup>3+</sup>, RESPECTIVELY, L=P<sub>W</sub><sub>9</sub>Mo<sub>2</sub>O<sub>39</sub><sup>7-</sup> AND P<sub>2</sub>W<sub>16</sub>Mo<sub>61</sub><sup>10-</sup>, RESPECTIVELY, USING PAPER ELECTROPHORESIS

A. BOTAR\*, D. ITUL\* and GH. MARCU\*\*

Received: May 20 1987

Reaction of the formation of ML-type heteropolyanions, where M=Co<sup>2+</sup> and V<sup>3+</sup>, respectively, L=P<sub>W</sub><sub>9</sub>Mo<sub>2</sub>O<sub>39</sub><sup>7-</sup> and P<sub>2</sub>W<sub>16</sub>Mo<sub>61</sub><sup>10-</sup>, respectively, was studied by high tension paper electrophoresis. The forming and stability ranges of the heteropolyanions and the values of the stability constants, respectively, have been determined.

**Introduction.** The high tension paper electrophoresis is an investigation method for the formation of the complex compounds. The mechanism of the formation of complex compounds, their constants of stability, respectively, were studied using this method [1-4]. The experimental values are in good agreement with the values obtained by other methods.

The paper electrophoresis method has been successfully used in determining the stability constants of heteropolycompounds; this method has incontestable advantages as compared to other methods [5-7]. The formation of ML-type heteropolyanion, where M=Co<sup>2+</sup> and V<sup>3+</sup>, respectively, while L=P<sub>W</sub><sub>9</sub>Mo<sub>2</sub>O<sub>39</sub><sup>7-</sup> and P<sub>2</sub>W<sub>16</sub>Mo<sub>61</sub><sup>10-</sup>, respectively, takes place after the reaction between the metal ion and the unsaturated heteropolyanion, as follows:



In this case, the equilibrium constant ( $K'$ ) is:

$$K' = \frac{[ML]}{[M] \cdot [L]}$$

The sum of the ion mobilities  $u$ , in the case of electromigration on the chromatographic paper, is given by the relation:

$$u = \frac{u_M \cdot [M] + u_{ML} \cdot [ML]}{[M] + [L]}$$

where  $u_M$  is the metal ion migration, M,  $u_{ML}$  stands for migration of the new heteropolyanion.

Applying the Consden [8] relation to the studied system, it follows:

$$\lg \frac{u - u_M}{u_{ML} - u} = \lg K' + \lg C$$

where  $C$  is the concentration of the unsaturated heteropolyanion, mole/litre.

\* Institute of Chemistry, 3400 Cluj-Napoca, Romania

\*\* University of Cluj-Napoca, Faculty of Chemical Technology, 3400 Cluj-Napoca, Romania

The values for the electrophoretic mobilities  $u_M$  and  $u_{ML}$ , were determined by paper electrophoresis; the equilibrium constant  $K'$  was calculated from the concentration of the unsaturated heteropolyanion.

The constant of stability  $\beta$  of the  $M_1$  heteropolyanions, is calculated according to the relation:

$$\lg \beta = \lg K' + \lg C$$

**Experimental part.** An installation for high tension paper electrophoresis Pherograph-Original-Frankfurt, type 64, was used. Experiments were performed in a solution of unsaturated heteropolyanion, of concentration  $c = 10^{-2} M$  in the range of  $pH = 2.0 - 6.5$ . A Whatman No 1 paper was used; the  $pH$  of the solutions was adjusted using  $HCl 0.1N$ ; the ionic strength was constantly maintained by adding  $NaClO_4$ .

The solution containing the metal ion was put on the chromatographic paper ( $40/4$  cm) using a micropipette; the potential difference was of  $1500$  V for  $30$  minutes at a  $6^\circ C$  temperature.

Displacement of the ionic species, which are formed after electromigration, was pursued by watching the colour of the heteropolyanions.

The sum of the electrophoretic mobilities is calculated according to the relation [9]:

$$u_d = \frac{d \cdot k \cdot 1}{t \cdot V} \text{ cm}^2 \text{ V}^{-1} \text{ sec}^{-1}$$

where  $u_d$  = the sum of the experimental electrophoretic mobilities;  $d$  = the migration of the ionic species (cm);  $t$  = time of electromigration (second);  $V$  = the applied potential difference (volt);  $k$  = factor which is dependent on the type of the chromatographic paper.

For the actual determination of the electrophoretic mobilities,  $u$ , the absorption of the ions on the chromatographic paper must be also taken into account, according to the relation:

$$u = u_d \cdot \frac{1}{R_f}$$

The  $R_f$  values were experimentally determined by chromatographic method, so for:



and for;



The ion migrations and the sum of electrophoretic mobilities, as function of  $pH$  values, are given in Tables 1 and 2.

Table 1

The migration and the sum of electrophoretic mobilities for the system  $Co^{2+}(V^{3+}) - PW_9Mo_2O_{30}^{3-}$

No.	pH	d(cm)		$u \cdot 10^{-4}$	
		$Co^{2+}$	$V^{3+}$	$Co^{2+}$	$V^{3+}$
1	2.0	-2.4	-1.9	-1.03	-0.84
2	2.5	-1.4	-0.8	-0.60	-0.36
3	3.0	+2.4	+2.5	+1.04	+1.11
4	3.5	+4.1	+3.8	+1.77	+1.69
5	4.0	+4.4	+3.8	+1.89	+1.69
6	4.5	+4.7	+4.2	+2.03	+1.87
7	5.0	+4.8	+4.3	+2.07	+1.91
8	5.5	+4.7	+4.2	+2.03	+1.87
9	6.0	+4.9	+4.3	+2.12	+1.91
10	6.5	+4.7	+4.2	+2.03	+1.87

Table 2

The migration and the sum of electrophoretic mobilities for the system  $Co^{2+}(V^{3+}) - P_2W_{16}MoO_{61}^{10-}$

No.	pH	d(cm)		$u \cdot 10^{-4}$	
		$Co^{2+}$	$V^{3+}$	$Co^{2+}$	$V^{3+}$
1	2.0	-2.3	-1.8	-1.02	-0.82
2	2.5	-1.5	-1.1	-0.67	-0.51
3	3.0	+0.6	+0.9	+0.25	+0.42
4	3.5	+3.3	+2.7	+1.44	+1.21
5	4.0	+4.0	+3.4	+1.75	+1.52
6	4.5	+4.2	+3.7	+1.86	+1.68
7	5.0	+4.3	+3.7	+1.90	+1.68
8	5.5	+4.4	+3.8	+1.92	+1.72
9	6.0	+4.5	+3.8	+1.97	+1.72
10	6.5	+4.4	+3.9	+1.94	+1.75

The variation of electrophoretic mobility as function of the concentration of the unsaturated heteropolyanion was experimentally determined. Experimental results are given in Tables 3-4.

Table 3

**The values of electrophoretic mobilities as a function of the concentration of  $K_2PW_9Mo_2O_{39}$**

The concentra- tion mole/litre	$Co^{2+}$ ion		$V^{3+}$ ion	
	$u \cdot 10^{-4}$	$\frac{u - u_{Co}}{u_{CoL} 1 - u}$	$u \cdot 10^{-4}$	$\frac{u - u_V}{u_{VL} 1 - u}$
$10^{-2}$	+2.09	188	+1.88	114
$5 \cdot 10^{-2}$	+2.04	52.4	+1.83	51.30
$10^{-1}$	+1.57	6.06	+1.64	6.24
$5 \cdot 10^{-1}$	+1.21	3.21	+1.40	2.82

Table 4

**The values of electrophoretic mobilities as a function of the concentration of  $K_{10}P_2W_{16}MoO_{61}$**

The concentra- tion mole/litre	$Co^{2+}$ ion		$V^{3+}$ ion	
	$u \cdot 10^{-4}$	$\frac{u - u_{Co}}{u_{CoL} 2 - u}$	$u \cdot 10^{-4}$	$\frac{u - u_V}{u_{VL} 2 - u}$
$10^{-2}$	+1.90	173	+1.72	156.5
$5 \cdot 10^{-2}$	+1.87	70.14	+1.69	63.20
$10^{-1}$	+1.50	7.23	+1.39	8.12
$5 \cdot 10^{-1}$	+1.01	2.83	+0.87	2.62

**Discussion.** By plotting the sum of electrophoretic mobilities as a function of pH values, curves having „S” shape were obtained (Fig. 1-2). These curves are specific to the formation of complex compounds. This fact represents an evidence for the formation of unit complexes and not for the formation of mixtures of heteropolyanions.

By extrapolation, at the „S” shape curves ordinate of the extreme (Fig. 1-2), the values of electrophoretic mobilities are determined for the ionic species.

By plotting the dependence  $\lg \frac{u - u_M}{u_{ML} - u}$  as a function of “ $\lg c$ ”, the value “ $\lg c$ ” is determined for the case when  $\frac{u - u_M}{u_{ML} - u} = 0$ .

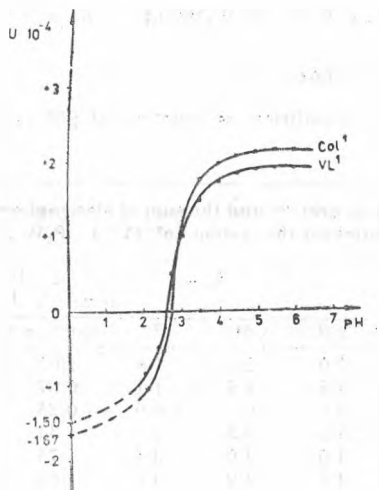


Fig. 1. The sum of electrophoretic mobilities as a function of pH values for the system  $Co^{2+}(V^{3+})PW_9Mo_2O_{39}$

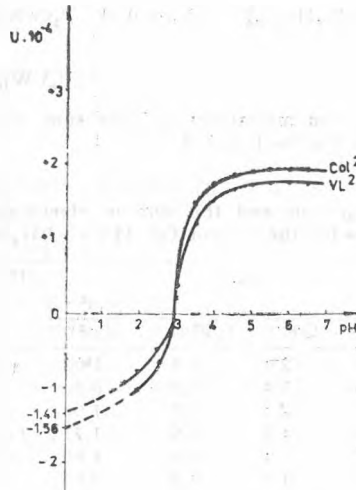


Fig. 2. The sum of electrophoretic mobilities as a function of pH values for the system  $Co^{2+}(V^{3+})P_2W_{16}MoO_{61}$

Table 5

The values of the constants of stability and instability,  
respectively

The heteropolyanion	The constant of stability	The constant of instability $K$
$\text{PCoW}_9\text{Mo}_6\text{O}_{39}^{5-}$	$0.16 \cdot 10^6$	$6.02 \cdot 10^{-5}$
$\text{PVW}_9\text{Mo}_6\text{O}_{39}^{4-}$	$0.14 \cdot 10^6$	$7.24 \cdot 10^{-1}$
$\text{P}_2\text{CoW}_{16}\text{MoO}_{61}^{8-}$	$0.32 \cdot 10^6$	$3.09 \cdot 10^{-6}$
$\text{P}_2\text{VW}_{16}\text{MoO}_{61}^{7-}$	$0.29 \cdot 10^6$	$3.38 \cdot 10^{-5}$

The values of the constants of stability and instability, respectively, for the ML heteropolyanions, are given in Table 5.

**Conclusions.** On the basis of the experimental results obtained by paper electrophoresis studies concerning the reactions between  $\text{Co}^{2+}(\text{V}^{3+})$  and the unsaturated heteropolyanions  $\text{PW}_9\text{Mo}_6\text{O}_{39}^{7-}$  and  $\text{P}_2\text{W}_{16}\text{MoO}_{61}^{10-}$ , it follows that:

- the ML heteropolyanions are unit complex compounds and not mixtures of heteropolywolframates;

- the heteropolyanions of  $\text{M}(\text{PW}_9\text{Mo}_6\text{O}_{39})$  and  $\text{M}(\text{P}_2\text{W}_{16}\text{MoO}_{61})$  types are formed in the range of  $\text{pH} = 2.6 - 4.5$  and  $\text{pH} = 3.0 - 5.0$ , respectively;

- the values of stability constants indicate that the studied heteropolyanions have nearly identical stability, these values being comparable with the stability of the other heteropolyanions from the literature.

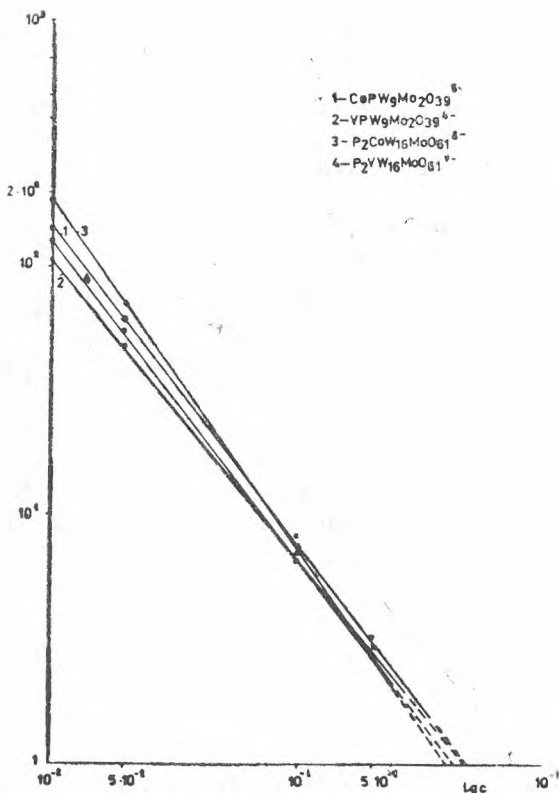


Fig. 3. The dependence  $\lg \frac{u - u_M}{u_{ML} - u}$  as a function of  $\lg c''$ .

## REF E R E N C E S

1. Gh. Marcu and A. Botar, *Stud. Univ. Babeş-Bolyai, Chem.*, **12**, 11 (1967).
2. Gh. Marcu and A. Botar, *Stud. Univ. Babeş-Bolyai, Chem.*, **13**, 111 (1968).
3. Gh. Marcu and A. Botar, *Rev. Roumaine Chim.*, **17**, 93 (1972).
4. Gh. Marcu and A. Botar, *Stud. Univ. Babeş-Bolyai, Chem.*, **2**, 109 (1971).
5. R. Ripan and A. Botar, *Rev. Roumaine Chim.*, **13**, 805 (1968).
6. R. Ripan, A. Botar and V. Cordiș, *Rev. Roumaine Chim.*, **16**, 1717 (1971).
7. Gh. Marcu, I. Todoruț and A. Botar, *Rev. Roumaine Chim.*, **16**, 829 (1971).
8. R. Consden, A. H. Gordon and A. P. Martin, *J. Biochem.*, **40**, 33 (1946).
9. H. G. Kunkel and A. Tiselius, *J. Gen. Physiol.*, **35**, 89 (1951).

<sup>1</sup>H-NMR SPECTRA AND STEREOCHEMISTRY OF SOME 2-ARYL-5,5-SUBSTITUTED 1,3-DIOXANES

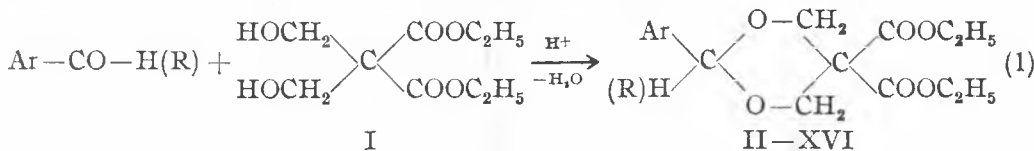
SOBIN MAGER\* and JON GROSE\*\*

Received: June 19, 1987

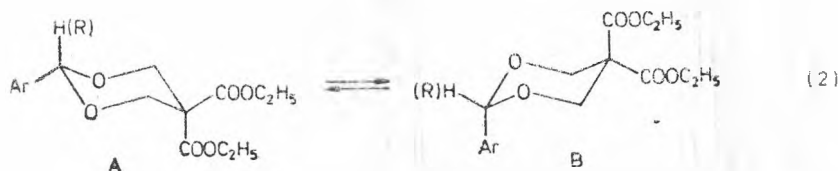
Some new 2-aryl-5,5-disubstituted 1,3-dioxanes were synthesized by the condensation reaction between bis(hydroxymethyl)malonic diethylester and aromatic aldehydes or ketones. The stereochemical investigations by means of the  $^1\text{H}$ -NMR-spectroscopy show "mobile" structures for the 1,3-dioxanes obtained from symmetric ketones, and "fixed" structures for those obtained from aldehydes or unsymmetrical ketones. The 1,3-dioxanes obtained by ketalisation of some aryl-methyl ketones show a preference of the phenyl group in the axial-orthogonal orientation. The spatial orientation of the magnetic lines of force induced by the anisotropy of the phenyl ring is proved by its shielding influence on the  $-\text{CH}_2-$  and  $-\text{CH}_3$  protons of the equatorial ethyloxycarbonyl group.

Earlier stereochemical studies in the field of substituted 1,3-dioxanes [1-6] were continued with the synthesis and stereochemical investigation by means of the  $^1\text{H-NMR}$  spectroscopy, of some 2-aryl-5,5-bis(ethyloxycarbonyl)-1,3-dioxanes.

Aromatic aldehydes and ketones were condensed with bis(hydroxymethyl)malonic diethylester (I) resulting (1) the corresponding 1,3-dioxanes (II-XVI):



The condensation with a symmetric ketone (benzophenone) leads to a "mobile" structure (II) while aldehydes or unsymmetrical ketones yield "fixed" (anacomeric) structures (III–XVI), as shown by the conformational equilibrium (2):



Concerning the mobile structure of compound II ( $R=Ar=C_6H_5$ ) without  $\Delta G = 0$  for the equilibrium A  $\rightleftharpoons$  B, the very simple  $^1H$ -NMR spectrum (Fig. 1)

\* University of Cluj-Napoca, Faculty of Chemical Technology, 3400 Cluj-Napoca, Romania  
 \*\* High School for Mathematics and Physics, Nr. 2, 3400 Cluj-Napoca, Romania

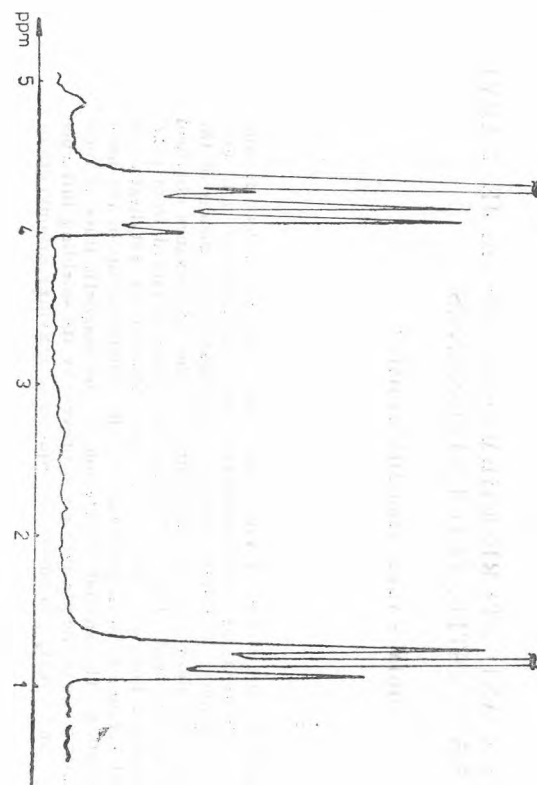


Fig. 1.

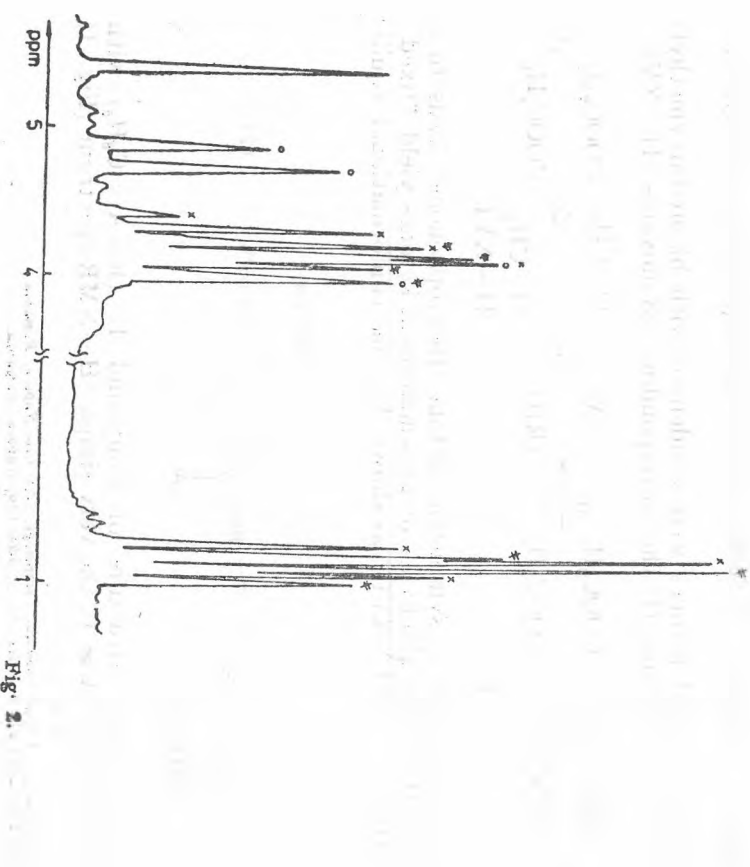


Fig. 2.

Table 1

## 1H-NMR parameters for compounds II-XVI

Nr.	Aryl	R	δ values; ppm										
			C <sup>a</sup>			C <sup>b</sup> , C <sup>c</sup>			C <sup>d</sup>				
			CH <sub>3</sub>	Ha	He	Ha	Δe, a	CH <sub>2</sub> a	CH <sub>2</sub> e	Δa,e	CH <sub>3</sub> a	CH <sub>2</sub> e	Δa,e
II	phenyl	C <sub>6</sub> H <sub>5</sub>	—	—	4.32	4.32	0	4.15	4.15	0	1.15	1.15	0
III	phenyl	H	—	5.14	4.55	3.84	0.71	4.07	3.95	0.12	1.10	1.03	0.07
IV	o-nitrophenyl	H	—	6.11	4.83	4.20	0.63	4.29	4.20	0.09	1.27	1.23	0.04
V	m-nitrophenyl	H	—	5.55	4.87	4.15	0.72	4.31	4.18	0.13	1.25	1.20	0.05
VI	p-nitrophenyl	H	—	5.46	4.79	4.08	0.71	4.23	4.11	0.12	1.21	1.16	0.05
VII	o-chlorophenyl	H	—	5.40	4.81	4.13	0.68	4.25	4.12	0.13	1.25	1.18	0.07
VIII	m-chlorophenyl	H	—	5.45	4.85	4.12	0.73	4.27	4.15	0.12	1.20	1.15	0.05
IX	p-chlorophenyl	H	—	5.40	4.82	4.10	0.72	4.28	4.15	0.13	1.25	1.20	0.05
X	p-methoxyphenyl	H	—	5.40	4.81	4.10	0.71	4.30	4.16	0.14	1.28	1.23	0.05
XI	phenyl	CH <sub>3</sub>	1.33	—	4.31	3.80	0.51	4.18	3.80	0.28	1.17	1.00	0.17
XII	o-nitrophenyl	CH <sub>3</sub>	1.45	—	4.25	3.56	0.69	4.10	3.86	0.24	1.08	0.95	0.13
XIII	m-nitrophenyl	CH <sub>3</sub>	1.42	—	4.37	3.70	0.67	4.19	3.91	0.28	1.22	1.06	0.16
XIV	p-nitrophenyl	CH <sub>3</sub>	1.37	—	4.32	3.70	0.62	4.16	3.90	0.26	1.22	1.05	0.17
XV	α-naphthyl	CH <sub>3</sub>	1.50	—	4.50	3.95	0.55	4.31	3.97	0.34	1.30	1.07	0.23
XVI	β-naphthyl	CH <sub>3</sub>	1.48	—	4.50	3.95	0.55	4.40	3.97	0.43	1.27	1.05	0.22

of 2,5-diphenyl-5,5-bis(ethyloxycarbonyl)-1,3-dioxane (II) shows only one peak (medium value,  $\delta = 4.32$  ppm, for equatorial and axial protons) for the four protons of the C<sup>4</sup> and C<sup>6</sup> atoms (Table 1). At the same time, only one triplet (medium value  $\delta = 1.15$  ppm) and one quartet (medium value  $\delta = 4.15$  ppm) for the two —CH<sub>2</sub>—CH<sub>3</sub> groups are shown.

In the case of the anancomeric 1,3-dioxanes bearing substituents with large values of the conformational free enthalpy, the equilibrium (2) is practically completely shifted towards the conformation having the substituent with larger conformational free enthalpy in the equatorial orientation. The <sup>1</sup>H-NMR spectra of this kind of compounds (III—X) lead to the differentiation of the equatorial and axial protons at the C<sup>4</sup> and C<sup>6</sup> carbon atoms as shown in Table 1 and in Fig. 2, which represent, as a model, the spectrum of the fixed 5,5-bis(ethylloxycarbonyl)-2-p-methoxyphenyl-1,3-dioxane (X).

The different environment of the equatorial and axial ethyloxycarbonyl groups is proved by the presence in the NMR spectrum of two quartets corresponding to the equatorial ( $\delta = 4.16$  ppm) and axial ( $\delta = 4.30$  ppm) —CH<sub>2</sub>— fragments, and of two triplets corresponding to the equatorial ( $\delta = 1.23$  ppm) and axial ( $\delta = 1.28$  ppm) —CH<sub>3</sub> groups. The influence of the unshared pairs of electrons of the two oxygen atoms belonging to the 1,3-dioxanic structure is reflected in the deshielding of the axial ethyloxycarbonyl group. The influence represents  $\Delta\delta = 0.12$  ppm for the —CH<sub>2</sub>— group and about 0.05 ppm for the —CH<sub>3</sub> group (Table 1). Concerning the equatorial and axial protons of the C<sup>4</sup> and C<sup>6</sup> atoms of the dioxanic ring, the spectrum shows two AB doublets located at  $\delta = 4.81$  ppm and 4.10 ppm, respectively; the second one overlaps the two quartets of the ethyloxycarbonyl groups, but (Fig. 2) is still easy to locate between the peaks of the multiplet. This difference represents 0.71—0.73 ppm for compounds III—X derived from aldehydes and 0.51—0.69 ppm for compounds XI—XVI derived from methylketones (excepting compound IV where Ar=o-nitrophenyl, with a smaller value, 0.63 ppm for  $\Delta\delta_{ea}$ ).

Table 1 also shows the influence of the substituents located on the phenyl ring (Cl, NO<sub>2</sub>, OCH<sub>3</sub>) upon the axial proton belonging to C<sup>2</sup> atom of the dioxanic ring, in compounds III—X.

An important feature of compounds XI—XVI obtained by ketalisation of some aryl-methyl ketones with diol I is the shifting of the conformational equilibrium (2) towards conformation B (R=CH<sub>3</sub>) bearing the methyl group in the equatorial orientation and the aryl group in the axial one. This preference is confirmed by means of thermodynamic determinations which show a significant larger  $\Delta G$  value for the conformational equilibrium of some substituted 1,3-dioxanes [7] as than expected from the calculations based on the  $\Delta G$  differences of the —CH<sub>3</sub> and —C<sub>6</sub>H<sub>5</sub> groups [8, 9].

The phenyl group, because of its steric interaction with the protons belonging to C<sup>4</sup> and C<sup>6</sup> atoms, is supposed to adopt an orthogonal orientation [10, 11]. As a consequence, the shielding influence of the aryl group is undergone by the protons of the equatorial ethyloxycarbonyl group as shown in Table 1 and Fig. 3 which presents the spatial orientation of the magnetic lines of force induced by the presence of the anisotropic phenyl ring in orthogonal orientation.

As shown by Haigh and Mallion [12], one can estimate by means of the isoshielding curves (Fig. 3), the shielding influence of the phenyl ring on the  $-\text{CH}_2-$  and  $-\text{CH}_3$  protons of the equatorial ethyloxycarbonyl group. Because of the shielding effect the differences,  $\Delta\delta$ , of the chemical shifts between the equatorial and axial groups become larger: about 0.26 ppm (instead of 0.12) for the  $-\text{CH}_2-$  protons and about 0.16 ppm (instead of 0.05) for the  $-\text{CH}_3$  protons. The shielding power of the benzenic ring can be estimated to about 0.14 ppm for the methylenic protons and about 0.1 ppm for the methyllic protons, in agreement with the supposed spatial orientation of the ethyl chain.

In the case of compounds XV and XVI with an  $\alpha$ - or  $\beta$ -naphthyl ring, the shielding effect becomes stronger, so that the differences for the  $-\text{CH}_2-$  protons are now about 0.4 ppm and for the  $-\text{CH}_3$  protons about 0.22 ppm.

The shielding effect of the aromatic ring is also undergone by the protons belonging to the  $\text{C}^4$  and  $\text{C}^6$  atoms of the 1,3-dioxanic ring, being stronger for the axial protons. As a consequence, the difference between the chemical shifts to the equatorial and axial protons becomes smaller, as it is easy to observe from the  $\delta$  values shown in Table 1.

**Experimental part.** Compounds II—XVI were obtained by the following general procedure: equimolecular amounts of diol I and corresponding aldehydes or ketones were refluxed in benzene, under stirring, in the presence of catalytical amounts of p-toluenesulphonic acid. The reaction flask is provided with a trap for the separation of the water resulted from the reaction. After the whole reaction water had been separated, the reaction product was neutralized with sodium acetate then washed with water. After distillation of the benzene, the pure product was obtained by vacuum distillation or by crystallization from a suitable solvent (ethanol).

The following new compounds were obtained:

- II 2,2-di(phenyl)-5,5-bis(ethyloxycarbonyl)-1,3-dioxane
- III 2-phenyl-5,5-bis(ethyloxycarbonyl)-1,3-dioxane
- IV 2-o-nitrophenyl-5,5-bis(ethyloxycarbonyl)-1,3-dioxane
- V 2-m-nitrophenyl-5,5-bis(ethyloxycarbonyl)-1,3-dioxane
- VI 2-p-nitrophenyl-5,5-bis(ethyloxycarbonyl)-1,3-dioxane
- VII 2-o-chlorophenyl-5,5-bis(ethyloxycarbonyl)-1,3-dioxane
- VIII 2-m-chlorophenyl-5,5-bis(ethyloxycarbonyl)-1,3-dioxane
- IX 2-p-chlorophenyl-5,5-bis(ethyloxycarbonyl)-1,3-dioxane
- X 2-p-methoxyphenyl-5,5-bis(ethyloxycarbonyl)-1,3-dioxane
- XI 2-methyl,2-phenyl-5,5-bis(ethyloxycarbonyl)-1,3-dioxane
- XII 2-methyl,2-o-nitrophenyl-5,5-bis(ethyloxycarbonyl)-1,3-dioxane
- XIII 2-methyl,2-m-nitrophenyl-5,5-bis(ethyloxycarbonyl)-1,3-dioxane
- XIV 2-methyl,2-p-nitrophenyl-5,5-bis(ethyloxycarbonyl)-1,3-dioxane
- XV 2-methyl,2- $\alpha$ -naphthyl-5,5-bis(ethyloxycarbonyl)-1,3-dioxane
- XVI 2-methyl,2- $\beta$ -naphthyl-5,5-bis(ethyloxycarbonyl)-1,3-dioxane

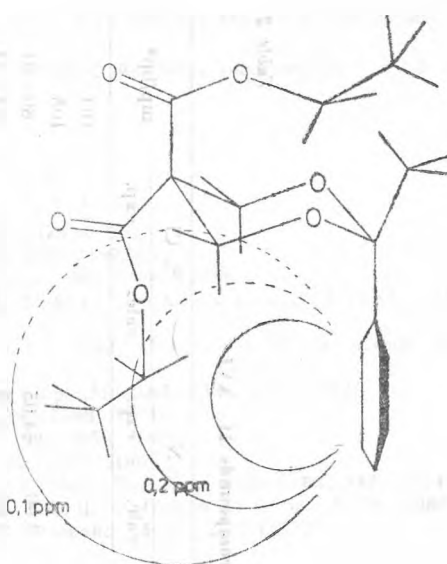


Fig. 3.

Table 2

Physical constants and elemental analysis of compounds II-XVI

Nr.	Formula	M.W.	% C		% H		% N		% Cl		mp/bp*
			calc.	exp.	calc.	exp.	calc.	exp.	calc.	exp.	
II	$C_{22}H_{24}O_6$	384.43	68.73	68.17	6.29	6.32	—	—	—	—	104
III	$C_{16}H_{20}O_6$	308.33	62.32	61.95	6.53	6.33	—	—	—	—	105
IV	$C_{16}H_{19}NO_8$	353.33	54.38	54.08	5.42	5.72	3.96	4.05	—	—	60-61
V	$C_{16}H_{19}NO_8$	353.33	54.38	54.11	5.42	5.75	3.96	4.10	—	—	63-64
VI	$C_{16}H_{19}NO_8$	353.33	54.38	54.86	5.42	5.51	3.96	4.16	—	—	62-63
VII	$C_{16}H_{19}ClO_6$	342.78	56.06	55.65	5.58	5.72	—	—	10.34	10.47	180-182*
VIII	$C_{16}H_{19}ClO_6$	342.78	56.06	55.45	5.58	5.87	—	—	10.34	10.49	188-190*
IX	$C_{16}H_{19}ClC_6$	342.78	56.06	55.63	5.58	5.79	—	—	10.34	10.41	40-42
X	$C_{17}H_{22}O_7$	338.36	60.34	60.22	6.55	6.86	—	—	—	—	39-40
XI	$C_{17}H_{22}O_6$	322.36	63.34	62.96	6.88	7.08	—	—	—	—	77
XII	$C_{17}H_{24}NO_8$	367.36	55.58	55.44	5.76	5.39	3.81	4.02	—	—	110
XIII	$C_{17}H_{21}NO_8$	367.36	55.58	55.09	5.76	5.43	3.81	4.11	—	—	119
XIV	$C_{17}H_{21}NO_8$	367.36	55.58	55.24	5.76	5.57	3.81	4.25	—	—	90-91
XV	$C_{21}H_{24}O_6$	372.42	67.72	67.22	6.49	6.80	—	—	—	—	128-130
XVI	$C_{21}H_{24}O_6$	372.42	67.72	67.52	6.49	6.80	—	—	—	—	132-134

\* Compounds VII and VIII are liquids, boiling points at 2 mm/Hg.

Table 2 shows the physical constants of compounds II—XVI and the results of the elemental analysis.

The  $^1\text{H}$ -NMR spectra were run with a TESLA-BS487C 80-MHz spectrometer, in  $\text{CDCl}_3$ , with TMS as standard.

#### R E F E R E N C E S

1. S. Mager, E. Eliel, *Rev. Roumaine Chim.*, **18**, 1379 (1973).
2. S. Mager, E. Eliel, *Rev. Roumaine Chim.*, **18**, 2097 (1973).
3. G. Binsch, E. Eliel, S. Mager, *J. Org. Chem.*, **38**, 4079 (1973).
4. M. Kaloustian, N. Dennis, S. Mager, S. Evans, F. Alcudia, E. Eliel, *J. Amer. Chem. Soc.*, **98**, 956 (1976).
5. S. Mager, I. Popărean, M. Horn, I. Grosu, *Stud. Univ. Babes-Bolyai, Chem.*, **24** (1), 32 (1979).
6. S. Mager, R. Tărănu, M. Horn, M. Mureșan, *Monatsh.* **113**, 565 (1982).
7. V. F. Bailey, E. Eliel, *J. Amer. Chem. Soc.*, **96**, 1698 (1974).
8. F. W. Nader, E. Eliel, *J. Amer. Chem. Soc.*, **92**, 3050 (1970).
9. K. Pihlaya, S. Luoma, *Acta Chem. Scand.*, **22**, 2401 (1968).
10. E. Bernaert, M. Anteunis, D. Tavernier, *Bull. Soc. chim. belges*, **83**, 357 (1974).
11. E. S. Drewes, M. W. Drewes, I. J. McNaught, *S. African J. Chem.*, **3**, 38 (1985).
12. C. W. Haigh, R. B. Mallion, *J. Org. Magn. Resonance*, **4** (2), 203, (1972).

## ÉTUDE EN SPECTROMÉTRIE DE MASSE DES ARYLSULPHONAMIDES THIOPHOSPHORORGANIQUES

### I. Arylsulphonamides de l'acide diéthylthiophosphinique

RODICA POPESCU\*, IOAN OPREAN\*, NICOLAE PALIBRODA\*\* et  
ZAHARIA MOLDOVAN\*\*

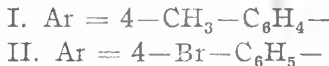
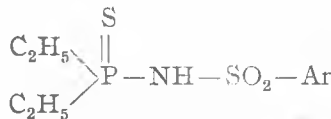
Reçu : Juillet 11, 1987

**Mass Spectra of the Arylsulphonamides of the Diethylthiophosphinic Acid.** The mass spectra of the arylsulphonamides of the diethylthiophosphinic acid I and II were recorded and interpreted. The spectra are typical for compounds of low stability under electron impact, showing molecular ion intensities of 2 and 4%, respectively. The fragmentation pathways were established by means of metastable ion transitions and confirmed by high resolution determinations and also by means of mass spectra of the deuterium labelled compound ID. For two substituents (Br and CH<sub>3</sub>) in the paraposition of the benzene ring only slight differences were found in the fragmentation patterns. Only the intensities of two fragment ions having the same origin show a correlation to the nature of the substituent placed on the benzene ring.

**Introduction.** Dans le cadre des travaux de notre laboratoire on a synthétisé et étudié plusieurs classes des dérivés thiophosphorylés renfermant un ou deux groupements arylsulphonamides [1—11]. Sur ces composés a été établie l'influence de la nature des substituants liés à l'atome de phosphore sur les constants de dissociation acide, sur l'énergie des liaisons hydrogène intermoléculaire et sur l'acidité „dynamique” des deux formes tautomères.

Les composés thiophosphororganiques ont été moins étudiés par la spectrométrie de masse [12—23]. Les arylsulphonamides des acides thiophosphororganiques n'ont pas été examinés par la spectrométrie de masse. C'est pourquoi dans une série de mémoires nous nous proposons d'étudier le comportement sous l'impact électronique de quelques classes de ces composés, pour confirmer d'une part, la structure chimique proposée, et d'autre part, pour déterminer les masses moléculaires de ceux-ci.

Le présent mémoire est consacré à l'étude de deux représentants de la classe des arylsulphonamides de l'acide diéthylthiophosphinique :



\* Institut de Chimie de Cluj-Napoca, 3400 Cluj-Napoca, Roumanie

\*\* Institut de Technologie Isotopique et Moléculaire, 3400 Cluj-Napoca, Roumanie

**Partie expérimentale.** Les spectres de masse ont été enregistrés sur un spectromètre Varian MAT 311, avec double focalisation en utilisant un système d'introduction direct. L'énergie d'ionisation était de 70 eV et la température d'enregistrement de 100°C.

Les transitions métastables ont été détectées par la technique de défocalisation et par l'analyse directe des ions fragments.

Les mesures de masse en haut résolution ont été effectuées à une résolution de 10.000 (10% vole).

Les substances étudiées ont été synthétisées d'après la procédure décrite dans le travail [1].

Le composé déuterié ID a été préparé à partir du composé I par échange isotopique en présence de D<sub>2</sub>O.

**Résultats et dissections.** Les spectres de masse correspondant aux composés I et II sont présentés dans les tableaux 1 et 2.

Le spectre de masse du composé I

Tableau 1

$\frac{m}{e}$	1%	$\frac{m}{e}$	1%	$\frac{m}{e}$	1%								
39	7	76	9	106	9	136	2	167	4	228	13		
46	19	77	8	107	13	138	38	170	21	229	4		
47	2	80	26	108	28	139	48	171	51	291	8		
48	16	91	69	109	11	140	5	172	7				
49	2	92	19	119	25	154	28	198	6				
61	6	93	5	120	2	155	14	199	62				
63	16	104	52	121	6	156	2	200	6				
65	33	105	7	123	7	166	13	227	100				

Le spectre de masse du composé II

Tableau 2

$\frac{m}{e}$	1%	$\frac{m}{e}$	1%	$\frac{m}{e}$	1%	$\frac{m}{e}$	1%	$\frac{m}{e}$	1%	$\frac{m}{e}$	1%	$\frac{m}{e}$	1%
46	41	78	3	109	17	158	3	205	12	262	2		
47	1	79	7	110	5	170	3	206	1	263	27		
48	23	80	51	121	9	171	3	218	11	264	4		
50	11	81	2	122	2	172	9	219	4	265	28		
51	3	82	3	123	2	173	3	220	11	266	3		
57	1	87	3	124	2	174	2	221	4	267	1		
59	5	89	2	136	1	183	1	230	3	291	32		
61	11	91	3	137	3	185	2	231	1	292	4		
63	27	92	16	139	4	187	3	232	3	293	33		
64	4	93	9	140	3	188	1	233	1	294	3		
65	13	96	3	149	1	189	3	234	4	295	1		
74	5	104	100	154	2	190	1	235	24	355	2		
75	19	105	12	155	26	202	12	236	6	357	2		
76	42	107	2	156	4	203	13	237	24				
77	9	108	59	157	25	204	13	238	2				

Tableau 3

**Les mesures des masses exactes en haute résolution pour le composé I**

m/e	Formule brute	Masses exactes	m <sub>c</sub> -m <sub>g</sub>
		calculées (m <sub>c</sub> ) trouvées (m <sub>g</sub> )	(m.u.m.)
227	C <sub>9</sub> H <sub>11</sub> NPS	227,0898	227,0901
171	C <sub>7</sub> H <sub>9</sub> NPS	171,0271	171,0253
170	C <sub>7</sub> H <sub>9</sub> NPS	170,0193	170,0162
196	C <sub>8</sub> H <sub>13</sub> NP	196,0795	196,0779
153	C <sub>7</sub> H <sub>9</sub> O <sub>2</sub> S	153,0157	153,0152
154	C <sub>7</sub> H <sub>8</sub> NCS	154,0327	154,0342
139	C <sub>7</sub> H <sub>9</sub> OS	139,0218	139,0218
138	C <sub>7</sub> H <sub>9</sub> NP	138,0473	138,0466
138	C <sub>4</sub> H <sub>11</sub> NPS	138,0357	138,0334
123	C <sub>7</sub> H <sub>7</sub> S	123,0269	123,0278
121	C <sub>4</sub> H <sub>9</sub> PS	121,0241	121,0220
119	C <sub>9</sub> H <sub>11</sub>	119,0861	119,0854
108	C <sub>2</sub> H <sub>7</sub> NPS	108,0037	108,0036
104	C <sub>6</sub> H <sub>11</sub> NP	104,0636	104,0638
92	C <sub>2</sub> H <sub>5</sub> PS	91,9850	91,9866
80	H <sub>3</sub> NPS	79,9724	79,9720
77*	C <sub>6</sub> H <sub>5</sub>	77,0391	77,0393
78	C <sub>2</sub> H <sub>7</sub> NP	78,0316	78,0317
63	PS	62,9458	62,9449
48	H <sub>3</sub> NP	48,0003	48,0006
46	HNP	45,9847	45,9846

\* ions qui ne font pas partie du schéma de fragmentation

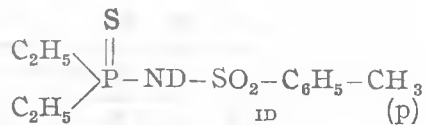
Tableau 4

**Les mesures des masses exactes en haute résolution pour le composé II**

m/e	Formule brute	Masses exactes	m <sub>c</sub> -m <sub>g</sub>
		calculées (m <sub>c</sub> ) trouvées (m <sub>g</sub> )	(m.u.m.)
235	C <sub>8</sub> H <sub>7</sub> BrNPS	234,9220	234,9196
234	C <sub>8</sub> H <sub>6</sub> BrNPS	233,9142	233,9138
219	C <sub>6</sub> H <sub>4</sub> BrSO <sub>2</sub>	218,9140	218,9145
218	C <sub>6</sub> H <sub>5</sub> BrNOS	217,9275	217,9288
203	C <sub>8</sub> H <sub>4</sub> BrSO	202,9166	202,9196
202	C <sub>6</sub> H <sub>6</sub> BrNP	201,9421	201,9419
121	C <sub>4</sub> H <sub>10</sub> PS	121,0241	121,0233
104	C <sub>4</sub> H <sub>11</sub> NP	104,0638	104,0635

La formulation correcte des fragmentations a nécessité des déterminations de transitions métastables et des mesures de haute résolution. Une transition marquée d'un astérisque soit dans le texte, soit dans un schéma de rupture est une transition confirmée par un pic métastable. Chaque fois que cela était nécessaire pour déterminer ou confirmer la formule brute d'un ion, nous avons mesuré sa masse exacte en haut résolution. Les résultats de ces déterminations sont résumés dans les tableaux 3 et 4.

Pour confirmer les structures des ions formulés avec un hydrogène mobile nous avons enregistré le spectre de masse du dérivé déutérié ID.



Les résultats sont réunis dans le tableau 5.

Les figures 1 et 2 résument les conclusions concernant les mécanismes de fragmentation auxquels nous avons abouti.

Il faut ajouter que pour le composé II ont été enregistrés comme transitions métastables seulement les suivantes :

355 → 291 ; 235 → 202 ;  
263 → 234, les autres étant prises par analogie avec le premier composé.

**Discussions.** Les ions présents dans les deux spectres sont ceux provenant d'une part de la fra-

Tableau 5

## Le spectre de masse du composé ID

$\frac{m}{e}$	%	$\frac{m}{e}$	%								
39	6	76	9	105	23	123	7	170	21	229	9
46	19	77	11	106	10	138	39	171	54	291	8
47	6	80	25	107	2	139	67	172	20		
48	14	81	8	108	28	140	7	198	7		
49	4	91	72	109	18	154	30	199	67		
61	7	92	20	119	37	155	22	200	19		
63	19	93	7	120	3	156	3	227	100		
65	35	104	51	121	7	166	13	228	48		

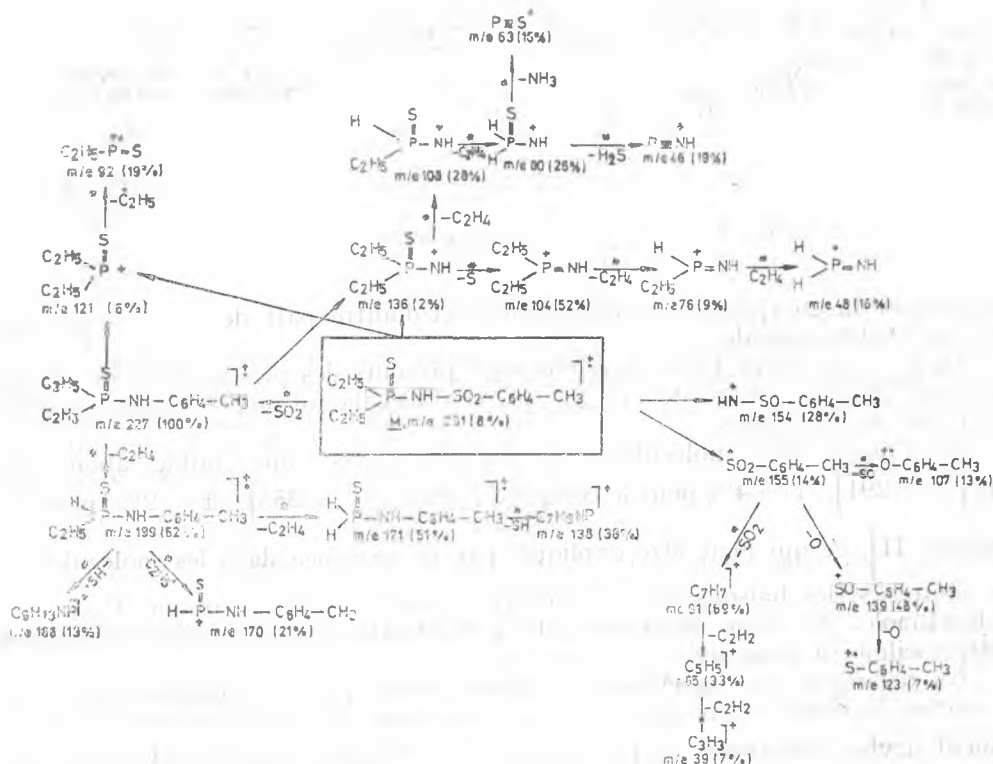


Fig. 1. Le schéma de fragmentation du composé I.

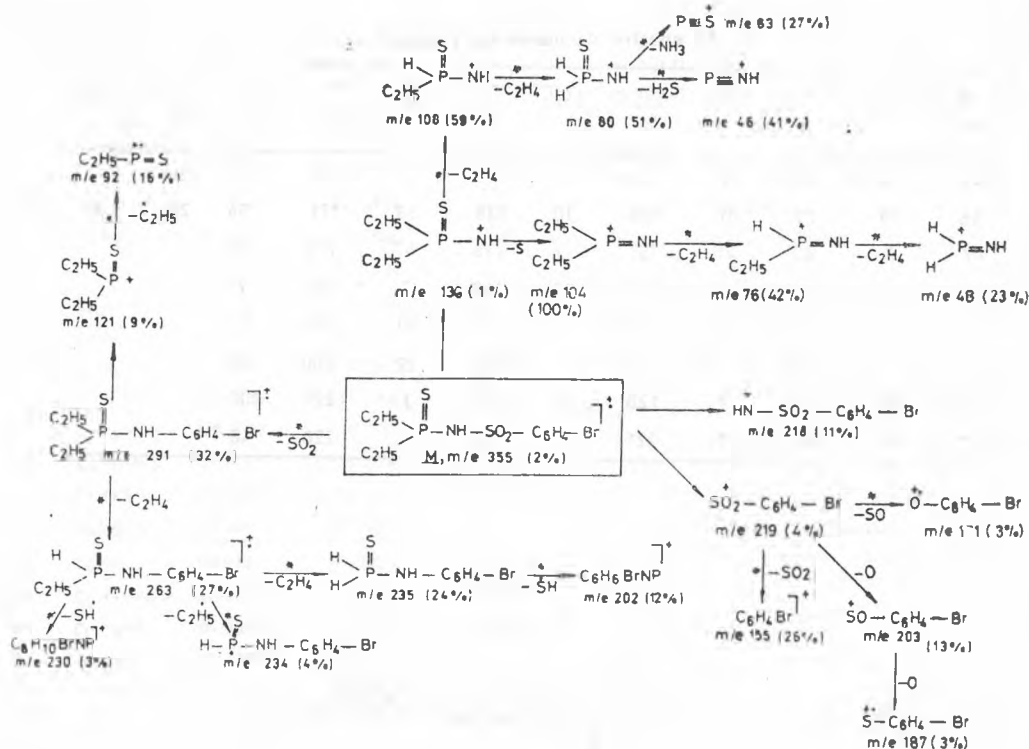


Fig. 2. Le schéma de fragmentation du composé II.

gmentation du groupement thiophosphorylé et d'autre part de celle du groupement arylsulphonamide.

Dans les deux spectres enregistrés sont présents des pics moléculaire, situés à la plus grande valeur de  $m/e$ , ce qui confirme la formule moléculaire et la pureté de ces composés.

Les deux ions moléculaires se trouvent avec une faible abondance  $[M^+ \left( \frac{m}{e} = 291 \right), I = 4\% \text{ pour le composé I et } M^+ \left( \frac{m}{e} = 355 \right), I = 2\% \text{ pour le composé II}]$ , ce qui peut être expliqué par la présence dans les molécules de ces composés des liaisons avec des énergies relativement faibles, comme  $\text{C}_{\text{aryle}} - \text{S}$  57 Kcal/mole,  $\text{N} - \text{S}$  46 Kcal/mole,  $\text{P} - \text{C}$  62 Kcal/mole, des liaisons capables d'être facilement rompues.

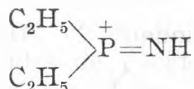
En regardant les deux spectres obtenus, nous pouvons observer que dans le spectre du deuxième composé les pics provenant des ions contenant le groupement arylsulphonamide sont déplacés vers  $\frac{m}{e}$  plus grands de 64 unités par rapport aux pics du premier composé. Ce fait, peut confirmer, dans une cer-

taine manière, la justesse des mécanismes de fragmentation proposés pour les deux composés.

En plus, dans le spectre du deuxième composé, tous les pics correspondant aux ions dans lesquels est présent l'atome de brome, se présentent comme des pics doubles, avec des intensités approximatives égales, différenciés par 2 unités, fait du à la composition isotopique de l'atome de brome.

Plusieurs mémoires ont été consacrés à l'étude des sulfonamides par la spectrométrie de masse [24-27]. Ainsi a été établi que ces composés subissent sans l'impact électronique une transposition moléculaire accompagnée d'élimination d'une molécule neutre de  $\text{SO}_2$ . Cette fragmentation a été retrouvée dans le cas de nos composés par la présence dans les spectres de masse de l'ion à  $\frac{m}{e} = 227$  et de l'ion à  $\frac{m}{e} = 291$  (voir les figures 1 et 2). Cette transposition moléculaire constitue la principale voie de fragmentation de l'ion moléculaire pour le composé I, l'ion issu de celle-la étant l'ion de base du spectre.

Dans le spectre du deuxième composé, l'ion à  $\frac{m}{e} = 291$  n'est pas l'ion de base ( $I = 32\%$ ). Cette différence peut être liée à la nature du substituant situé en position para du cycle benzénique du groupement arylsulphonamide. Le composé I possède en cette position un substituant ayant un effect inductif +I — le groupement  $\text{CH}_3$  — qui défavorise la rupture des liaisons, tandis que dans le composé II, dans la même position il y a un substituant fortement attractif d'électrons — le brome — dont l'effect inductif — I facilite la rupture des liaisons. Par conséquence, pour le composé II l'ion de base est l'ion à  $\frac{m}{e} = 104$  provenant du rest phosphorylé, pour lequel nous avons proposé la structure suivante

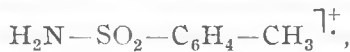


Cet ion est également présent dans le spectre de masse du composé I, mais avec une abondance plus faible, de l'ordre de 52% en intensité relative. La formule brute de celui-ci a été confirmée par la mesure de masse exacte (voir les tableaux 3 et 4). L'abondance élevée de cet ion dans les deux spectres peut être expliquée par sa structure, l'atome de phosphore étant entouré de deux groupes éthyle dont le caractère inductif répulsif tend à „combler” partiellement le déficit électronique de l'atome central.

L'ion à  $\frac{m}{e} = 104$  peut provenir soit de l'ion moléculaire par la rupture de la liaison  $\text{N}-\text{S}$ , soit de l'ion  $\text{M}-\text{SO}_2^{1+}$  par la rupture de la liaison  $\text{N}-\text{C}_{\text{aryle}}$  suivie dans les deux cas de la perte d'un atome de soufre (voir les figures 1 et 2).

L'intensité faible de l'ion à  $\frac{m}{e} = 136$  ( $I = 2\%$ ) n'a pas fait possible la détermination des ions métastables correspondant aux transitions :  $227 \rightarrow 126$  et  $291 \rightarrow 136$  (voir la figure 1), les deux filiations restant toutes les deux plausibles.

À l'ion à  $\frac{m}{e} = 171$  peut être attribuée soit la formule brute  $C_7H_{10}NPS$  (de structure présentée dans la figure 1), ion issu de l'ion de base par l'élimination de deux molécules neutres d'éthylène, soit la formule brute  $C_7H_9NO_2S$  de structure probable

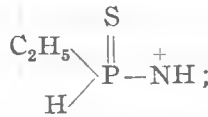


ion résultant de l'ion moléculaire par la rupture de la liaison P—N. La haute résolution effectuée sur ce pic permet de lui attribuer la formule brute  $C_7H_{10}NPS$ . D'autre part la formation de celui-ci a été confirmée par détermination de deux pics métastables (voir la figure 1).

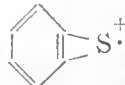
L'abondance élevée de l'ion à  $\frac{m}{e} = 171$  ainsi que de celui correspondant au spectre du composé II, l'ion à  $\frac{m}{e} = 199$ , sont probablement liées à la stabilité de la molécule neutre d'éthylène éliminée. La perte de molécule neutres d'éthylène a été signalée dans la littérature comme étant caractéristique aux dérivés diéthylphosphiniques [28].

À l'ion à  $\frac{m}{e} = 108$  du spectre du composé I, nous avons pu attribuer aussi deux formules brutes :

a)  $C_2H_7NPS$  correspondante à la structure

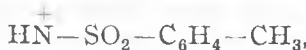


b)  $C_4H_4S$  de structure cyclique

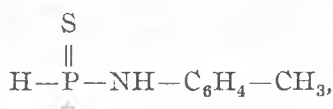


Dans ce cas, le choix entre les deux formules n'a pas été possible à l'aide de mesures de masse en haut résolution, parce que la différence entre la masse calculée et celle trouvée expérimentalement est dans les limites des erreurs expérimentales (voir le tableau 3). L'examen du spectre du composé déuterisé ID montre que le pic à  $\frac{m}{e} = 109$  se trouve avec une intensité plus grande que dans le spectre du composé nondéutérié I. Alors, la structure proposée avec un hydrogène mobile devient la structure la plus probable (voir les tableaux 1 et 5).

Il est à remarquer aussi que l'ion à  $\frac{m}{e} = 170$  du spectre du composé I ne correspond pas à la formule brute  $C_7H_8NO_2S$  avec la structure



mais à la formule brute  $C_7H_9NPS$  avec la structure



l'ion correspondant étant issu par élimination d'un radical éthyle de l'ion à  $\frac{m}{e} = 199$ . Cette affirmation est confirmée par les mesures de masses exactes (voir le tableau 3) et par la présence d'un pic métastable  $199 \xrightarrow{*} 171$  (voir la figure 1). Dans le spectre est présent l'ion à  $\frac{m}{e} = 154$ , qui pourrait provenir de l'ion  $C_7H_8NO_2S$  par élimination d'un atome d'oxygène, la fragmentation caractéristique aux sulphones [26, 25]. Ainsi le choix de la formule brute n'avait pas été possible sans des déterminations supplémentaires, l'ion à la formule brute  $C_7H_8NO_2S$  pouvant bien provenir de l'ion moléculaire par la rupture de la liaison P—N.

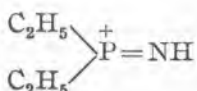
Mentionnons que dans le spectre du composé I nous avons mis en évidence l'ion tropylion à  $\frac{m}{e} = 91$  avec la formule brute  $C_7H_7$ . C'est un ion avec valeur analytique, celui-ci étant très caractéristique aux composés monoalkylés nonramifiés à l'atome de carbone benzylique [29], l'ion qui confirme l'existence de la partie méthylbenzensulphonamide de la molécule.

On ajoute encore que tous les ions formulés à un hydrogène mobile sont retrouvés dans le spectre du composé déuterié comme des ions à  $\frac{m}{e}$  plus grande d'une unité (voir les tableaux 1 et 5).

**Conclusions.** Nous avons enregistré et étudié les spectres de masse de deux représentants des arylsulphonamides de l'acide diéthylthiophosphinique, dont nous avons attribué les principaux pics. Leur comportement est à rapprocher des sulphonamides, d'une part et des dérivés diéthylthiophosphinique, d'autre part.

Les mécanismes de fragmentation induits par impact électronique de deux composés sont identiques, l'abondance différente des ions qui proviennent du même processus pouvant être liée à la nature du substituant situé en position para du cycle benzénique du groupement arylsulphonamide. Le substituant  $-CH_3$  défavorise la rupture des liaisons, tandis que le substituent Br facilite les fragmentations.

Le spectre de masse du composé I est dominé de l'ion issu de l'ion moléculaire par l'élimination d'une molécule neutre de  $SO_2$  et par deux ions provenant de celui-ci par élimination en deux temps de deux molécules neutres d'éthylène. On trouve aussi dans ce spectre comme ion abondant l'ion



Dans le spectre du composé II, cet ion génère le pic de base. Il est accompagné d'autres ions abondants provenant des coupures avec éliminations des molécules neutres comme  $\text{H}_2\text{S}$ ,  $\text{C}_2\text{H}_4$ , ou bien d'un atome de soufre.

#### BIBLIOGRAPHIE

1. L. Almasi, R. Popescu, *Chem. Ber.*, **108**, 856 (1975).
2. L. Almasi, R. Popescu, R. Greco, *Tetrahedron*, **33**, 1327 (1977).
3. L. Almasi, R. Popescu, L. Paskucz, *Rev. Roumaine Chim.*, **24**, 3 (1979).
4. L. Almasi, N. Popovici, I. Zsakó, *Chem. Ber.*, **106**, 1384 (1973).
5. L. Almasi, N. Popovici, A. Hantz, E. Hamburg, *Monatsch. Chem.*, **104**, 1360 (1973).
6. L. Almasi, N. Popovici, E. Hamburg, *Chem. Berg.*, **96**, 3148 (1963).
7. L. Almasi, A. Hantz, E. Hamburg, *Chem. Ber.*, **103**, 2976 (1970).
8. I. Fenesan, V. Mureşan, A. Barabás, M. Bogdan, *Rev. Roumaine Chim.*, **29**, 761 (1984).
9. L. Almasi, V. Mureşan, A. Barabás, *Z. anorg. allg. chem.*, **458**, 62 (1979).
10. A. Barabás, R. Popescu, V. Mureşan, L. Almási, *Org. Magn. Reson.*, **10**, 35 (1977).
11. L. Almási, R. Popescu, *Rev. Roumaine Chim.*, **24**, 741 (1979).
12. D. H. Williams, R. S. Ward, R. G. Cooks, *J. Amer. Chem. Soc.*, **90**, 966 (1968).
13. J. Granoth, J. B. Levy, C. Gimmers Jr., *J. Chem. C. Perkin II*, **1972**, 697.
14. J. M. Miller, *J. Chem. Soc., A*, 828 (1967).
15. K. Diemer, P. Haas, W. Kuchen, *Chem. Ber.*, **111**, 629 (1978).
16. R. A. Spence, V. M. Swan, H. B. Wright, *Austral. J. Chem.*, **22**, 2358 (1968).
17. R. G. Cooks, R. S. Ward, D. H. Williams, *Chem. Commun.*, **1967**, 850.
18. R. Collon, P. N. Porter, *Austral. J. Chem.*, **21**, 2215 (1968).
19. J. Granoth, J. B. Levy, *J. Chem. Soc. B*, **1971**, 2391.
20. J. G. Pritchard, *Org. Mass. Spectrom.*, **3**, 163 (1970).
21. R. G. Cooks, A. F. Gerrard, *J. Chem. Soc. B*, **1968**, 1327.
22. R. S. Edmundson, *Phosphorus and Sulfur*, **9**, 307 (1981).
23. J. E. R. Wils, A. G. Hulst, *Org. Mass. Spectrom.*, **21** (3), 169 (1986).
24. A. Tatematsu, T. Nadai, H. Yoshizumi, K. Naito, *Yakugaku Zasshi*, **90**, 1428 (1970); *Chem. Abstr.*, **74**, 30571.
25. J. Spiteller, R. Kaschnitz, *Monatsh. Chem.*, **94**, 964 (1963).
26. A. Cambon, R. Guédj, D. Robert, J. A. Soyfer, M. Azzaro, *Bull. Soc. Chim. France*, **567** (1970).
27. M. F. Grostic, R. J. Vnuk, F. A. Mac Kellar, *J. Amer. Chem. Soc.*, **88**, 4664 (1966).
28. P. Haake, P. S. Ossip, *Tetrahedron*, **24**, 565 (1968).
29. I. Oprean, „Spectrometria de masă a compușilor organici”, Ed. Dacia, Cluj, 1974, p. 194.

## STUDIEREA REACTIILOR CHIMICE ȘI A OPERAȚIILOR DE ABSORBȚIE ȘI DE EXTRACTIE ÎN APARATE CU SERPENTINA DE PELICULIZARE-BARBOTARE

I. Absorbția dioxidului de carbon în soluții apoase de hidroxid de potasiu

IOAN VODNÁR\* și IOAN DEMETER-VODNÁR\*\*

Intrat în redacție la 1 septembrie 1987

**The Study of the Chemical Reactions and of Operations as Absorption and Extraction.** The paper presents the experimental results obtained during the absorption of carbon dioxide in aqueous solutions of potassium hydroxide, using an apparatus of contacting equipped with a spiral curved tube [1–3] (these apparatuses are usually named Vodnár-type apparatuses). The absorbent was partially transformed in a turbulent liquid film in the internal side of the spiral curved tube, which exhibits an internal area equal to 0.014 m<sup>2</sup>. The absorption took place both by bubbling and in the turbulent liquid layer.

În industria chimică absorbția bioxidului de carbon în diverse absorbanți constituie cazuri particulare importante ale operației unitare de absorbție. Dintre procesele tehnologice aplicate în unitățile chimice din țara noastră, în care apare ca etapă importantă absorbția bioxidului de carbon, amintim următoarele: fabricarea acetilenei prin oxidarea parțială a metanului, fabricarea amoniacului, alcoolului metilic, carbamidei, sodei calcinată etc.

În scopul absorbției s-a utilizat un aparat brevetat de autor [1–3] dotat cu un tub de peliculizare-barbotare sub formă de spirală în interiorul căruia absorbantul s-a transformat parțial într-o peliculă ascendentă. Suprafața interioară a tubului-spirală a fost de 0,014 m<sup>2</sup>. Fenomenul de absorbție a avut loc atât prin barbotare cât și în peliculă ascendentă de absorbant. Experiențele s-au efectuat în flux continuu.

**Partea experimentală.** *Metoda de lucru.* Experiențele au fost făcute într-un aparat de tip Vodnár-3 cu funcționare continuă\*. Concentrația CO<sub>2</sub> în amestecul gazos ( $C_{CO_2}$ ) s-a determinat prin absorbție în soluții apoase de hidroxid de sodiu. Absorbantul s-a alimentat continuu cu o pompă cu un debit constant de 3,6 l/h la toate experiențele, iar compoziții gazoși — oxigenul și bioxidul de carbon — s-au luat din butelii de oțel de această natură. Debitul total de gaz s-a variat între 6 și 35 l/h, iar concentrația bioxidului de carbon s-a mărit pînă la 43% vol.

*Descrierea și funcționarea aparatului și a instalației de laborator.* Aparatul cu care a fost dotată instalația de laborator este prezentată în figura 1. Structura de principiu a aparatului este descrisă în brevetul românesc nr. 75628 din 1981. Față de brevet, aparatul utilizat în aceste experiențe (Aparat Vodnár-3) este dotat în plus cu cîte o conductă pentru alimentarea absorbantului și eliminarea absorbitului. La punerea în funcțiune aparatul se umple cu absorbant pînă la capătul

\* Universitatea din Cluj-Napoca, Facultatea de științe economice, 3400 Cluj-Napoca, România

\*\* Universitatea din Cluj-Napoca, Facultatea de Tehnologie Chimică, 3400 Cluj-Napoca, România

\* Pentru condiții disconținute se utilizează aparatul Vodnár-1 [1], care poate fi dotat și cu un robot de golire în acest caz numindu-se aparat Vodnár-2; toate pot fi comandate de la Fábrica de sticlă din Turda, județul Cluj

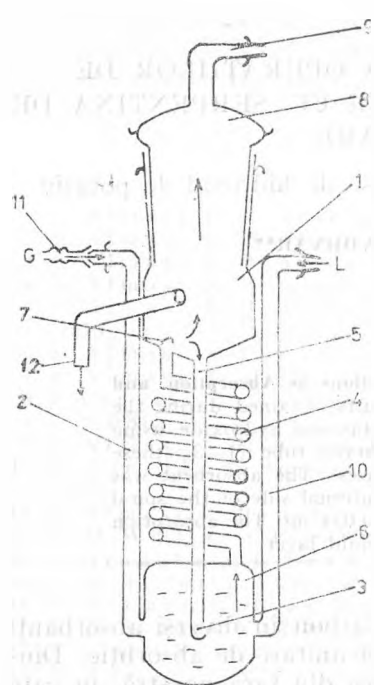


Fig. 1. Aparat cu spirală de peliculizare — barbotare de tip Vodnárt—3, cu funcționare continuă: 1 — cameră de separare a fazelor; 2 — tub pentru introducerea gazului; 3 — deschidere laterală; 4 — tub-spirală; 5 — tub de recirculare; 6 — rezervor (cameră de alimentare); 7 — șicană boltită; 8 — dop gol cu șif; 9 — ștăuț pentru eliminarea gazului rezidual; 10 — tub pentru introducerea absorbantului; 11 — ștăuț cu șif; 12 — ștăuț pentru eliminarea absorbantului.

superior al tubului de recirculare 5, după care se începe introducerea treptată și continuă a gazului prin conducta 2 și a absorbantului prin conducta 10. Componentii ajung în rezervorul 6, unde gazul barbotează prin stratul de absorbant aflat acolo, după care este obligat să pătrundă în tubul 4 în formă de spirală, unde urmează o cursă ascendentă prin care absorbantul aflat în spirală se proiectează parțial (sau chiar total) pe suprafața interioară a acesteia, unde se formează astfel o peliculă turbulentă de absorbant. Astfel absorbția bioxidului de carbon (sau în general a gazului dat) în afara spiralei are loc prin barbotare, iar în spirală prin barbotare și în peliculă turbulentă de lichid. Amestecul gaz-lichid care ieșe din spirală pe la partea ei superioară, ajunge în camera 1 de separare a fazelor, de unde absorbantul se elimină continuu prin conducta (preaplin) 12, iar gazul rămas, prin ștăuțul 9. Între timp, faza lichidă se recirculă mereu prin tubul 5, contribuindu-se astfel

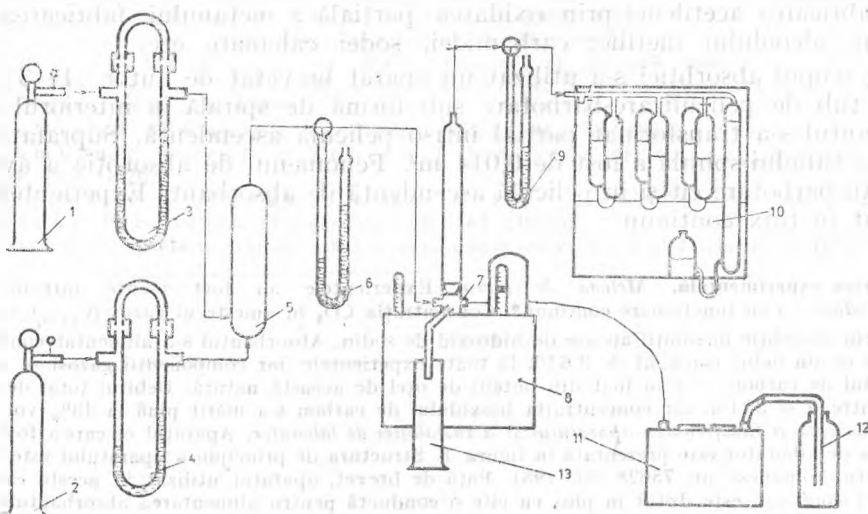


Fig. 2. Schema instalației de laborator folosite: 1 — butelie cu bioxid de carbon; 2 — butelie cu oxigen; 3,4 — reometre; 5 — amestecător de gaze; 6 — manometru pentru măsurarea presiunii inițiale; 7 — aparat de tip Vodnár—3; 8 — ultratermostat; 9 — manometru pentru măsurarea presiunii finale; 10 — aparat Orsat; 11 — pompă peristaltică; 12 — rezervor cu absorbant; 13 — vas de colectare a absorbantului.

la o foarte bună amestecare și contactare a fazelor, ceea ce face ca acest aparat să aibă o eficacitate foarte mare la absorbtile și reacțiile chimice în sistem gaz-lichid, care se execută în laborator sau în industrie. La toate acestea se mai adaugă și avantajul că aparatul nu reacționează sensibil la apariția în sisteme a unor impurități mecanice de dimensiuni mici, aşa cum se întâmplă la spălătoarele de gaze dotate cu frită (sticlă poroasă).

Schemă generală a instalației de laborator folosite este prezentată în Figura 2. Bioxidul de carbon și oxigenul luate din buteliile de oțel 1 și 2 se trec prin reometrele 3 și 4 în scopul măsurării debitelor de gaz, după care ajung în aparatul 5 de amestecare a gazelor. De aici amestecul omogen de gaze se trimite în aparatul 7 de absorbție, după ce în prealabil i se măsoară presiunea cu manometrul 6. Gazul rămas în urma absorbției se elimină din aparat, i se măsoară presiunea finală cu manometrul 9 și i se determină conținutul final de bioxid de carbon cu aparatul 10. Absorbantul se ia din vasul 12 și se alimentează în aparatul de absorbție 7 prin intermediul pompei 11. Absorbutul format se elimină din aparat și se colectează în vasul 13.

**Descrierea și interpretarea rezultatelor.** În prima serie de experiențe s-a urmărit influența pe care o are concentrația de bioxid de carbon asupra coeficientului ( $C_a = \text{g}/\text{m}^2 \cdot \text{h}$ ) și gradului de absorbție ( $q_a = \%$ ). Temperatura s-a menținut la 19°C, debitul de gaz la 24,14 l/h, iar concentrația hidroxidului de potasiu în soluția apoasă utilizată drept absorbant a fost de 1,25% (Fig. 3). Din cele înfățișate de graficul din figura 3 reiese că, odată cu creșterea concentrației de bioxid de carbon al amestecului gazos (oxigen + bioxid de carbon) de la 23,78 la 43,16% vol., coeficientul de absorbție crește de la 737 la 1004 g CO<sub>2</sub>/m<sup>2</sup>·h. În același timp, gradul de absorbție scade de la 91,59 la 65,7%, ceea ce înseamnă că din motive economice concentrațiile de bioxid de carbon mai mari decât 31,5% vol. (valoarea concentrației de CO<sub>2</sub> la punctul de intersecție ale celor două curbe) nu se recomandă, deoarece în aceste condiții gazul rămas după absorbție conține prea mult bioxid de carbon neabsorbit.

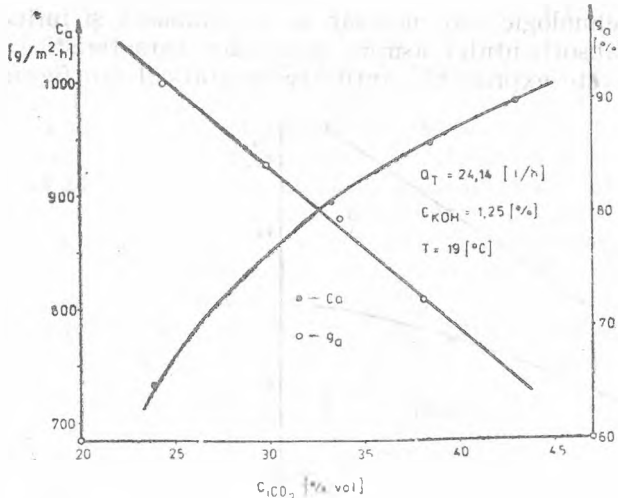


Fig. 3. Variația coeficientului ( $C_a$ ) și gradului de absorbție ( $q_a$ ) în funcție de concentrația bioxidului de carbon în amestecul de gaze.

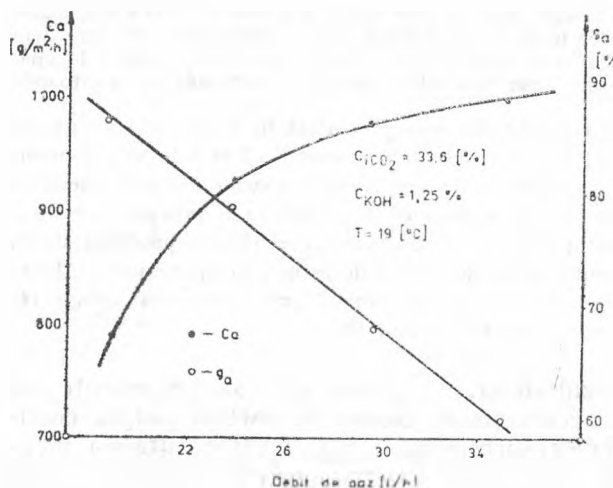


Fig. 4. Variația coeficientului ( $C_a$ ) și a gradului de absorbție în funcție de debitul de gaz

În a două serie de experiențe s-a studiat dependența dintre coeficientul de absorbție și respectiv gradul de absorbție și debitul de gaz (l/h). Rezultatele experimentale sunt ilustrate de graficul din figura 4.

Parametrii menținuți la valori constante sunt: temperatura, 19,0°C; concentrația CO<sub>2</sub> în amestecul gazos, 33,6% vol.; concentrația soluției apoase de hidroxid de potasiu, 1,25%. Se poate vedea că, odată cu creșterea debitului de gaz (l/h) de la 19,5 la 35 l/h, coeficientul de absorbție crește de la 793 la 1001 g CO<sub>2</sub>/m<sup>2</sup>·h, iar gradul de absorbție scade de la 86,3 la 60,7% (scădere valorilor este liniară), ceea ce constituie fenomene previzibile în cadrul chemosorbției.

Sub aspect tehnologic este necesar să se cunoască și influența pe care o are concentrația absorbantului asupra mărimilor caracteristice ale absorbției. Această influență este exprimată cantitativ în graficul din figura 5.

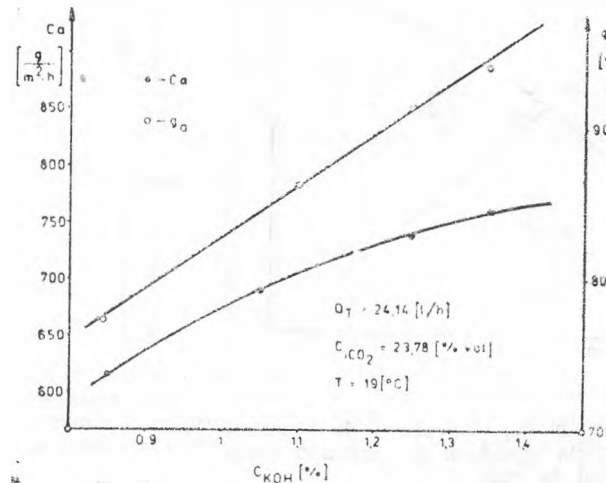


Fig. 5. Variația coeficientului ( $C_a$ ) și gradului de absorbție ( $g_a$ ) în funcție de concentrația în KOH a absorbantului.

Debitul de gaz s-a menținut la valoarea constantă de 24,41 l/h, concentrația de bioxid de carbon în amestecul gazos la 23,78% vol., iar temperatura la 19°C. Din grafic putem afla că în timp ce concentrația soluției apoase de KOH ( $C_{KOH}$ ) utilizată ca absorbant crește de la 0,85 la 1,35%, coeficientul de absorbție crește de la 622 la 757 g/m<sup>2</sup>·h, iar gradul de absorbție în același timp crește de la 77,3 la 94,1%.

În final s-a studiat variația coeficientului de absorbție și gradului de absorbție, în funcție de temperatură. Debitul de gaz s-a menținut constant la 24,14 l/h, concentrația bioxidului de carbon în amestecul gazos la 23,78% vol., iar concentrația absorbantului la 1,25%. Rezultatele experimentale sunt ilustrate de graficul din figura 6.

Se poate vedea că atât coeficientul de absorbție cât și gradul de absorbție cresc odată cu creșterea temperaturii. Și anume, în timp ce temperatura crește de la 19 la 83°C, coeficientul de absorbție crește de la 737,3 la 798,3 g CO<sub>2</sub>/m<sup>2</sup>·h, iar gradul de absorbție crește de la 91,6 la 99,1%.

În scopul de a se evidenția eficacitatea aparatului utilizat, în comparație cu un aparat clasic (fără serpentină de peliculizare-barbotare) cu același volum de umplere de 120 ml, s-au făcut experiențe de absorbție în ambele tipuri de apарат, aplicind aceleași condiții de lucru. Astfel, de exemplu, la 19°C, cu un debit de gaz de 24,14 l/h și cu concentrația bioxidului de carbon în amestecul gazos de 23,78% vol., iar concentrația absorbantului fiind 1,25%, gradul de absorbție în aparatul clasic este de numai 45,95%, iar în aparatul cu serpentină de contactare de tip Vodnár-3, este egal cu 91,59%. Aceasta reprezintă o creștere a gradului de absorbție de 99,32%.

Utilizându-se datele experimentale de la experiența făcută la 83°C, s-a calculat coeficientul de transfer de masă total ( $K_g$ ), pentru care s-a obținut valoarea :

$$K_g = 368 \left[ \frac{\text{moli CO}_2}{\text{m}^2 \cdot \text{h} \cdot \text{atm.}} \right]$$

#### BIBLIOGRAFIE

1. I. Vodnár, *Brevet R.S.R.*, nr. 75628, 1981.
2. J. Vodnár, *Journal of Applied Chemistry*, **20**, 99 (1970), London.
3. I. Vodnár, *Brevet R.S.R.*, nr. înreg. 125720, 1986.

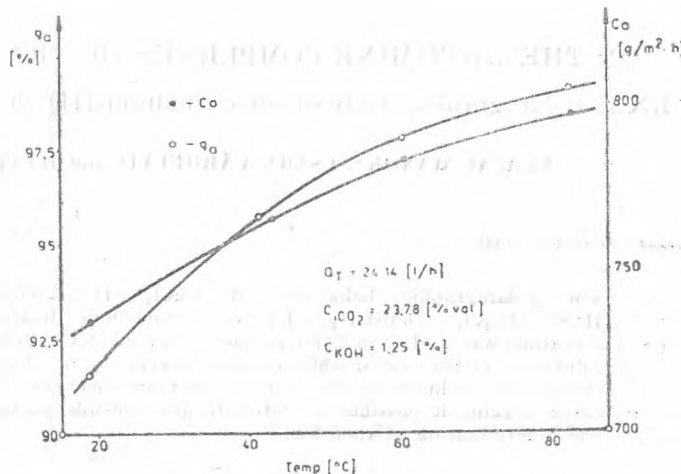


Fig. 6. Variația coeficientului ( $C_a$ ) și gradului de absorbție ( $g_a$ ), în funcție de temperatură.

ON THE DIOXIMINE COMPLEXES OF TRANSITION METALS  
LXX. Polarographic study of some rhodium(III)-chelates with  $\alpha$ -dioximes<sup>1</sup>

FERENC MÁNOK\*, CSABA VÁRHELYI\* and HAJNAL SZAKÁCS\*

Received: September 6, 1987

The polarographic behaviour of  $\text{RhCl}_3$ ,  $\text{H}[\text{Rh}(\text{Octox.H})_2(\text{NO}_2)_2]$  and  $\text{H}[\text{Rh}(\text{DH})_2\text{Cl}_2]$  ( $\text{Octox.H}_2 = 1,2\text{-Cyclo-octanedione dioxime}$ ,  $\text{DH}_2 = \text{Dimethylglyoxime}$ ) was studied in different basic solutions (KCl, Britton-Robinson's buffer solutions). In the case of  $\text{RhCl}_3$  catalytic waves can be observed. The dioximinochelates are reduced on the dropping mercury electrode in multielectronic processes making it possible to elaborate new sensible polarographic methods for the determination of rhodium.

**Introduction.** The simple salts of Rh(III) are reduced at the dropping mercury electrode already about 0 V (vs. SCE). In the presence of some non-complexing anions in the supporting electrolyte catalytic hydrogen waves appear which overlap the rhodium reduction steps. In the presence of complexing agents, e.g. pseudohalides [1], aliphatic mono- and dianines [2], heterocyclic amines, dicarboxylic acids, oxyacids [3], EDTA-type compounds [4–6] the half wave potential of  $[\text{Rh}(\text{H}_2\text{O})_6]^{3+}$  is shifted towards more negative potential values ( $-0.4$ – $-1.3$  V (vs. SCE)). Some amine complexes of the type:  $[\text{Rh}(\text{NH}_3)_5\text{X}]^{2+}$  and  $[\text{Rh}(\text{en})_2\text{X}_2]^+$  were studied by Willis [7] and Baranovskii [8]. Crow [9] compared the  $E_{1/2}$  values of a series of rhodium(III)-amine complexes with the position of the first d-d ligand-field transition band in their electronic spectra. The shifts of the half wave potentials show a good linearity with the increase of sigma donor properties of the ligands. Addison *et al.* [10] and Vleek [11], comparing the polarographic behaviour of some mono- and binuclear Co(III), Rh(III) and Ir(III) complexes have found, that with identical coordination sphere composition, the cobalt(III) derivatives can be reduced most easily due to their greatest electron affinity.

**Results and Discussion.** In the present paper the polarographic behaviour of  $\text{RhCl}_3$ , in comparison with that of two dioximinochelates of rhodium(III):  $\text{H}[\text{Rh}(\text{Octox.H})_2(\text{NO}_2)_2]$  ( $\text{Octox.H}_2 = 1,2\text{-cyclo-octanedione dioxime}$ ) and  $\text{H}[\text{Rh}(\text{DH})_2\text{Cl}_2]$  ( $\text{DH}_2 = \text{dimethylglyoxime}$ ) was studied in a wide pH-range in Britton-Robinson's buffer- and neutral KCl solutions.

We observed that the  $\text{RhCl}_3$  forms one or two polarographic waves in function of the pH-value of the supporting electrolyte. At  $\text{pH} = 2.66$  two reduction steps appear with  $E_{1/2}$  values  $-0.12$ – $-0.13$  V (and  $-0.95$  V (vs. SCE)), respectively. The first well formed wave begins practically already at 0 V and increases linearly with the concentration of Rh(III). The second wave

<sup>1</sup>LXIX. F. Mánok, G. Drneşti, Cs. Várhelyi, A. Benkő, *Stud. Univ. Babes-Bolyai, Chem.* 1987, in press

\* University of Cluj-Napoca, Faculty of Chemical Technology, 3100 Cluj-Napoca, Romania

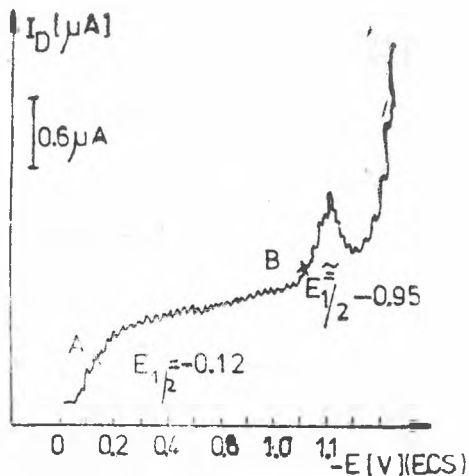


Fig. 1. Polarogram of  $\text{RhCl}_3$  at  $\text{pH} = 2.56$ ;  
 $C_{\text{Rh}} = 3 \times 10^{-4}$  mole/l  $C_{\text{NaClO}_4} = 0.125$  mole/l

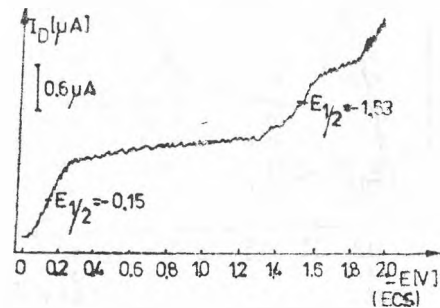
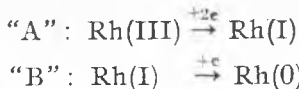


Fig. 2. Polarogram of  $\text{RhCl}_3$  at  $\text{pH} = 2.56$ ;  
 $C_{\text{Rh}} = 4 \times 10^{-4}$  mole/l  $C_{\text{NaClO}_4} = 0.225$  mole/l

has a sharp maximum which cannot be suppressed by addition of gelatine or methylene blue. At higher Rh(III) concentrations the first wave is also superposed by a maximum, but this disappears on gelatine addition. (Fig. 1 and 2.)

The ratio of the heights wave is in agreement with the following electrode processes:



In buffered solution at  $\text{pH} = 3.29$  two waves also appear, the second being 7-fold higher than the first one. We can presume that this wave is a catalytic one, due to the catalytic action of the metallic rhodium formed at the reduction of oxonium ( $\text{H}_3\text{O}^+$ ) ions. The height of this wave, "B", varies simultaneously with the concentration of rhodium and can be used for analytic purposes. A calibration curve for small Rh concentrations is shown in Fig 3. In more basic supporting electrolytes, e.g.  $\text{pH} = 8.96$ , only a single, well formed wave appears with  $E_{1/2} = -0.17$  V (vs. SCE). The polarographic measurements prove that the first Rh(III) wave ("A") is not influenced by the

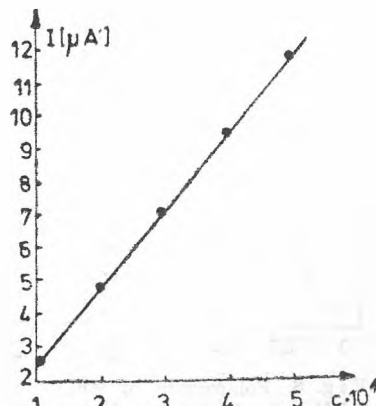


Fig. 3. Calibration curve for  $\text{RhCl}_3$  at  $\text{pH} =$

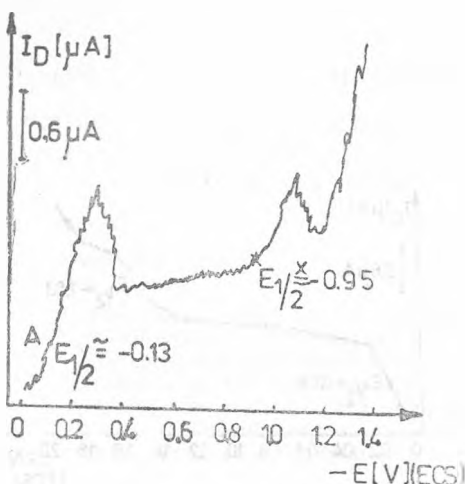


Fig. 4. Polarogram of  $\text{RhCl}_3$  at  
 $\text{pH} = 3.29$ ;  $C_{\text{Rh}} = 2 \times 10^{-4}$  mole/l  
 $C_{\text{NaClO}_4} = 0.125$  mole/l

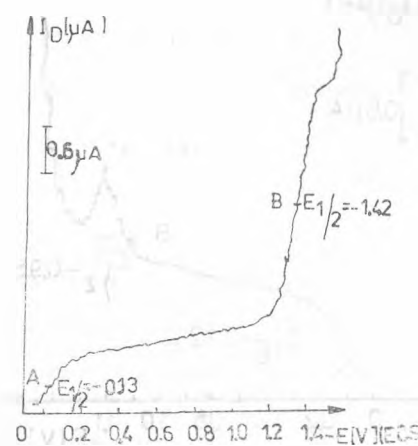


Fig. 5. Polarogram of  $\text{RhCl}_3$  at  
 $\text{pH} = 8.95$ ;  $C_{\text{Rh}} = 3 \times 10^{-4}$  mole/l  
 $C_{\text{NaClO}_4} = 0.125$  mole/l

pH-value of the supporting electrolyte up to  $\text{pH} = 11$ . Over this pH-value the hydrolysis of  $\text{RhCl}_3$  takes place with precipitation of  $\text{Rh}(\text{OH})_3$ .

In non-buffered KCl basic solution also two waves appear.

The polarographic data are presented in Table 1.

The polarograms of  $\text{H}[\text{Rh}(\text{Octox.H})_2(\text{NO}_2)_2]$  and  $\text{H}[\text{Rh}(\text{DH})_2\text{Cl}_2]$  were also taken in KCl and in Britton-Robinson's buffer solutions.

Some typical polarograms are presented in Fig. 7-11. and the numerical data in Table 2.

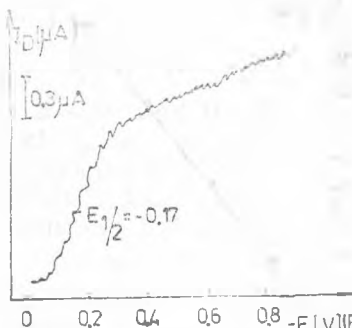


Fig. 6. Polarogram of  $\text{RhCl}_2$  in  
 $0.1 \text{ M KCl}$ ;  $C_{\text{Rh}} = 3 \times 10^{-4}$  mole/l

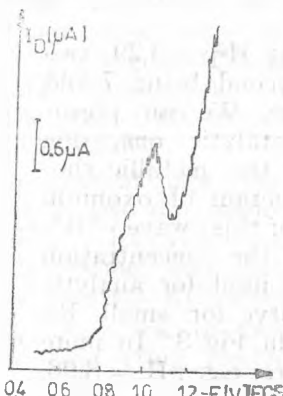


Fig. 7. Polarogram of  
 $\text{H}[\text{Rh}(\text{Octox.H})_2(\text{NO}_2)_2]$  at  
 $\text{pH} = 2.56$ ;  $C_{\text{complex}} = 3 \times 10^{-4}$   
mole/l;  $C_{\text{NaClO}_4} = 0.125$  mole/l

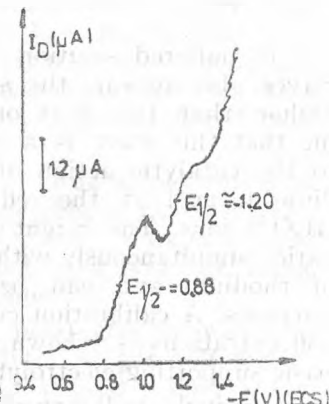


Fig. 8. Polarogram of  
 $\text{H}[\text{Rh}(\text{Octox.H})_2(\text{NO}_2)_2]$  at  
 $\text{pH} = 3.29$ ;  $C_{\text{complex}} = 6 \times 10^{-7}$   
mole/l;  $C_{\text{NaClO}_4} = 0.125$  mole/l

Table 1

Polarographic data on the RhCl<sub>3</sub>

Supporting electrolyte	E <sub>1/2</sub>			I <sub>D</sub> (μA)		I <sub>D</sub> /c × 10 <sup>4</sup>	
	A	B	C	A	B	A	B
0.1 M KCl				0.49		0.49	
				0.94	0.32	0.47	0.32
	0.145	0.153		1.53	0.70	0.51	0.35
				1.84	0.90	0.46	0.30
				2.40	1.12	0.48	0.28
Britton-Robinson's solution pH = 2.56 NaClO <sub>4</sub> 0.125 M				0.30	0.19	0.30	0.19
	0.12	0.94		0.70	0.34	0.35	0.17
				0.93	0.63	0.31	0.21
				1.08	0.64	0.27	0.16
				1.40	0.90	0.28	0.18
Britton-Robinson's solution pH = 3.29 NaClO <sub>4</sub> 0.125 M				0.35	2.40	0.35	2.40
				0.74	4.86	0.37	2.43
	0.12	1.17	1.416	0.96	7.14	0.32	2.38
				1.20	9.68	0.30	2.42
				1.90	11.95	0.38	2.39
Britton-Robinson's solution pH = 8.95 NaClO <sub>4</sub> 0.125				0.15		0.50	
	0.167			1.08		0.54	
				1.44		0.48	
				1.96		0.49	
				2.55		0.51	

Table 2

Polarographic data on the H[Rh(Octox.H) (NO<sub>2</sub>)<sub>2</sub>]

Supporting electrolyte	E <sub>1/2</sub>			I <sub>D</sub> (μA)		I <sub>D</sub> /c × 10 <sup>4</sup>	
	A	B	A	B	A	B	
0.1 M KCl			0.30		0.02		
	0.678		1.80		0.12		
			1.26		0.07		
				2.80		0.93	
				5.60		1.10	
Britton-Robinson's solution pH = 2.56 NaClO <sub>4</sub> 0.125 M			9.45		1.05		
	0.887		10.44		0.87		
			12.00		0.80		
				1.86	4.02	0.62	1.34
				4.80	7.20	0.80	1.20
Britton-Robinson's solution pH = 3.29 NaClO <sub>4</sub> 0.125 M			4.86	13.68	0.54	1.52	
	0.920	1.30	6.00	13.44	0.50	1.12	
			10.20	23.10	0.68	1.54	
				0.26	0.29	0.08	0.09
				5.40	1.80	0.30	0.15
Britton-Robinson's solution pH = 8.95 NaClO <sub>4</sub> 0.125 M			7.38	5.40	0.82	0.60	
			9.20	12.00	0.01	1.00	
			9.90	0.15	0.06	0.01	

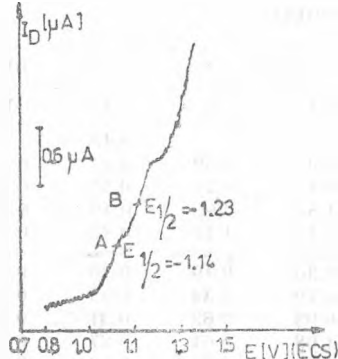


Fig. 9. Polarogram of  
 $\text{H}[\text{Rh}(\text{Octox.H})_2(\text{NO}_2)_2]$  at  $\text{pH}=8.95$   
 $C_{\text{compl}}=6 \times 10^{-7}$  mole/l;  
 $C_{\text{NaClO}_4}=0.125$  mole/l

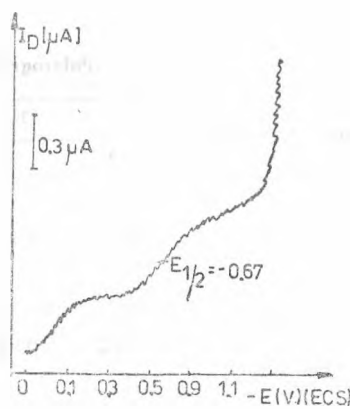


Fig. 10. Polarogram of  
 $\text{H}[\text{Rh}(\text{Octox.H})_2(\text{NO}_2)_2]$  in  
 $0.1 \text{ M KCl}$ ;  $C_{\text{compl}}=1.2 \times 10^{-6}$   
mole/l.

In the case of  $\text{H}[\text{Rh}(\text{Octox.H})_2(\text{NO}_2)_2]$  at  $\text{pH}=2.56$  only a single step appears, similarly with  $\text{RhCl}_3$ , but the  $E_{1/2}$  value is shifted towards more negative potential values. This wave "A" is overlapped by a sharp maximum, which can be suppressed with addition of gelatine. At higher pH-values a second wave is also developed. The height of this wave ("B") is much higher than in the case of  $\text{RhCl}_3$ . This means that simultaneously with the Rh(III) and Rh(I) species, the chelating dioxime ligands (Octoxime, dimethylglyoxime) are also reduced on the dropping mercury electrode to the corresponding 1,2-

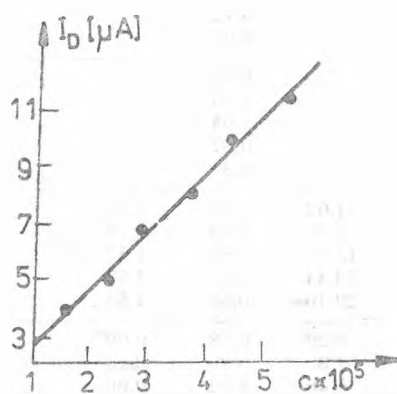


Fig. 11. Calibration curve for  
 $\text{H}[\text{Rh}(\text{Octox.H})_2(\text{NO}_2)_2]$  at  $\text{pH}=3.29$

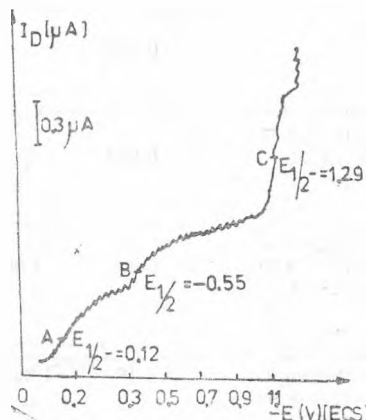


Fig. 12. Polarogram of  $\text{H}[\text{Rh}(\text{Dh})_2\text{Cl}_2]$  in  
 $0.1 \text{ M KCl}$  (comp  $10^{-6}$  mole/l)

diamines (1,2-cyclooctanediamine and 2,3-butane diamine) in an eight electronic electrode process:



The half wave potential value of the first wave is considerably influenced by the pH-value of the supporting electrolyte. The  $E_{1/2}$  value of the "B"-wave is very little sensible to pH alterations. The height of this "B"-wave is proportional to the concentration of Rh(III) in the solution, and is suitable for analytical purposes. Due to the multielectronic reduction of the dioximino-chelates, this method is much more sensible for the determination of rhodium, than the polarographic reduction of the simple rhodium salts.

In non-buffered KCl solution a third wave appears at the initial part of the polarograms ( $E_{1/2} = -0.15$  V (vs. SCE) of the examined chelates Fig. 12.

**Experimental.**  $\text{H}[\text{Rh}(\text{DH})_2\text{Cl}_2]$  was obtained by refluxing 2 mmoles of  $\text{RhCl}_3 \cdot 3\text{H}_2\text{O}$  with 4 mmoles dimethylglyoxime in 25 ml methanol. The synthesis of  $\text{H}[\text{Rh}(\text{Octox.H})_2(\text{NO}_2)_2]$  was described earlier [12]. The polarograms were taken on a Radelkis-Type-OH-120 polarograph by using a conventional polarographic cell with a saturated calomel reference electrode, connected to the cell by means of an agar-agar bridge (1 M  $\text{KNO}_3$ ). The oxygen was eliminated from the solutions with purified methane.

#### REFERENCES

1. G. van Loon, J. A. Page, *Talanta*, **12**, 227 (1965).
2. L. E. Johnston, J. A. Page, *Canad. J. Chem.*, **47**, 4241 (1969).
3. F. Pantani, *J. Electroanal. Chem.*, **5**, 40 (1963).
4. P. W. Alexander, L. E. Hoer Smythe, *J. Electroanal. Chem.*, **80**, 143 (1977).
5. N. A. Ezerskaya, I. N. Kiseleva, *Zhur. analit. Khim.*, **28**, 316, 1149 (1973); **29**, 1385 (1974); **32**, 1772 (1977); *Zavodskaya lab.*, **47**, 18 (1981).
6. M. V. Klyuev, M. L. Kghidekel, V. V. Strelets, *Transition Metal Chem.*, **3**, 380 (1978).
7. J. B. Willis, *J. Amer. Chem. Soc.*, **66**, q067 (1944).
8. I. B. Baranovskii, *Zhur. neorg. Khim.*, **12**, 2860 (1967).
9. R. D. Crow, "Polarography of Metal Complexes", Academic Press, London, 1969.
10. A. W. Addison, R. D. Gillard, *J. Chem. Soc., Dalton Trans.*, **1970**, 2523; **1973**, 1187.
11. A. L. Vlcek, *Electrochim. Acta*, **13**, 1063 (1968); *Progr. Inorg. Chem.*, **3**, 371 (1963).
12. Cs. Várhelyi, F. Mánok, N. Almási, I. Nagy, *Stud. Univ. Babeş-Bolyai, Chem.*, **31**, (1), 32 (1986).

## EFFICIENCY REQUIREMENTS IN TODAY RESEARCH, DESIGN AND DEVELOPMENT OF LARGE SCALE SEPARATION PROCESSES BY RECTIFICATION AND EXTRACTION<sup>1</sup>

FRANCIS A. GOTTHARD\*

Received: September 8, 1987

The arguments related to two opposite approaches in the development of large scale separation processes, by rectification and liquid extraction, one starting from all achievements of theory and available experimental data, the other based on empirism, are discussed briefly. The role of the methodology in this field is pointed out and the use of an existing methodology in the critical selection of fundamental data to be considered in this field is exemplified and recommended to interested users.

Most of the energy required to manufacture chemical products is consumed in separation processes, especially in distillation equipment. Therefore an increasing attention must be concerned to design step, whenever competitiveness of the product and of the process is the ultimate target. It is wellknown that design efficiency depends strongly on the accuracy of the necessary data, mainly phase equilibrium data.

The literature contains various approaches to this problem. Always the accuracy of thermodynamic data makes the point [1]. Very convincing examples of what erroneous thermodynamic data may generate can be found in works published by Zudkevich [2, 3] and Kletz [4].

It is not an easy task to fulfil current accuracy requirements, as well as to provide the user with all information needed to perform his own critical evaluation of data, compulsory if one intend to deal with responsibility, "nothing being guaranteed" [5]. To such a high efficiency in the development of separation processes specialised working teams, very good experimental tools, powerful computers and large data banks are needed. So, handling algorithms for correlation and critical selection becomes possible. Access to selected reference data and a quasicontinuous effort toward general understanding become almost compulsory for future development. There is no doubt that success is directly conditioned by exhaustive knowing and critical use of all what human mind achieved until now. A worldwide exchange of opinions through attending regular meeting is imperatively recommended.

Unfortunately, the people attached to this point of view, when asked for advise or while trying to build up conditions to help applied thermodynamics become effective, meet a lot of cases of misunderstanding or even underestimation of need on critical evaluation of thermodynamical data. Sometimes one can hear: "Chemical technologies were developed in the past, also say half

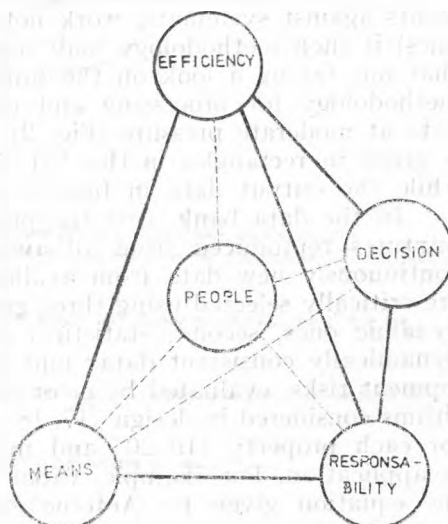
<sup>1</sup> Lecture at the University of Cluj-Napoca in October 1986.

\* Romanian Institute for Research, Design and Development for Oil Refineries — Ploiești, 2000 Ploiești, Romania.

a century ago, without databanks, computers and sophisticated experimental tools". That is true, but not for today when competition is completely different and the scale of the processes has become many times larger. Another opinion which can be heard: "Let's keep this moving. We'll see what'll happen. It'll be some changes but never mind, the product will be there quickly. That's important for commercial expansion and not some of your theoretical plates". Such arguments should be weighed carefully, because the actual experience teaches us the contrary at this very point. Decisions of this kind, without taking into account deep insight in the physical chemistry of all process involved, as possible today, were always paid for by severe penalty in quality or amount of product. The latter call for data results rather in explanations instead of product. The scientists are frequently blamed for consequences of ... overlooking their own advices, especially by management able to avoid responsibility. If prevented by well skilled experts, they call for others, "experts" (in everything), who never strove hard to get reliable data for substantiated decisions. It is easy to recognize the experts in everything, especially (retro-) active in fields where long range efforts are required for the smallest but valuable results. In this very field they take delight in assuming ideal behaviour of all mixtures. It is easy to realize what happen if some of the "unbearable" components make azeotropes discovered too late, in the ... plant.

Limiting the engineering work to shortcut methods also results, as a rule, in bad surprises and to rescue some of the investment cost expensive changes are necessary. After all, even extended research, using all available informations, sponsoring experimental work and theoretical efforts which require also but smaller investment in equipment, are always cheaper, than supporting loss of product and time ("... is money") arising from use of unreliable data and subsequent changes in plant until a competitive product can be delivered.

To find out the way leading to increased efficiency through this network of problems (far to be exhausted above), some of the categories acting in the field and how they are related should be briefly analysed. Restraining the discussion to concepts mentionned above, *Responsibility, People, Means and Decisions*, we shall build up a tetrahedron which have the first three as vertices. The symbol of the decision step is located in the inside of the tetrahedron. The shorter the edge: of this tetrahedron, the closer the hills Efficiency. Ideally the figure can be reduced to one point, but the complexity of the problems involved in investment and cost usually it makes impossible to concentrate all decision in one hand (the people which deals with responsibility with all means). The way how the edges of the tetrahedron of efficiency can be made

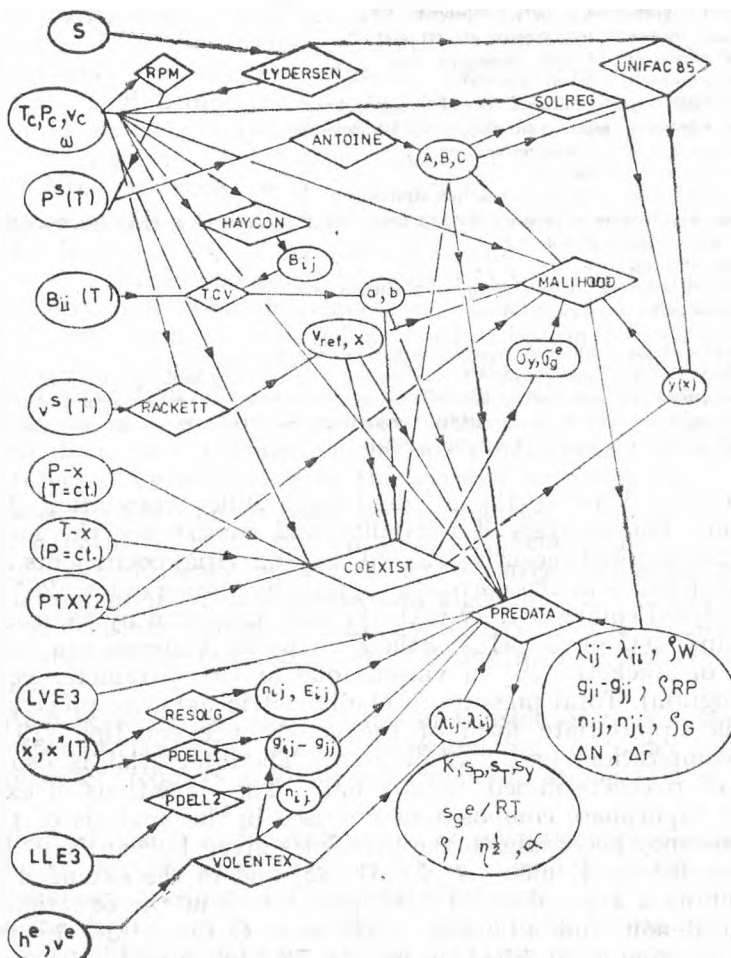


shorter is straightforward: decisions should be suggested by specialists but considered by management; the suggestions should be made with responsibility, which is possible only with adequate means (so  $M$  and  $P$  are closer, thus  $P$  and  $R$  also). Without  $M$ ,  $P$  can't provide management with elements for reasonably  $D$  and  $E$  is also far away, therefore the problem of  $R$  can't be a question of playing a role. The face  $R-P-M$  becomes very small, if management recognizes chemical engineering, chemical thermodynamics, as basic fields of fundamental and applied research, strongly related to mathematics. These must be handled by special working teams, able not only to predict phase equilibria accurately, but also the risks in design and development, admitting as a fact the experimental error.

Another possibility to reduce the size of the tetrahedron is strong cooperation between various specialists engaged in connected fields, as mentioned above, to make the tools more effective even when the evaluation of available data indicates lack of reliability. For that, a common language is required. This is one of the roles of something what may be called "methodology". A definition is not easy to formulate, but perhaps it is a system of most effective and practically verified of paths leading in shortest time to optimized solutions. Methodologies may be designed only in fields where experience meet theoretical deep insight. This leads commonly to including selected informations and algorithms in informational systems where the data bank plays the role of the support for all movement toward  $E$  through  $D$ . For the very reason of extending knowledge in the field, such methodologies are open for new achievements, (the more one knows, the more one is convinced that there is much more to know...) and also for revision taking into account the results of comparisons between prediction and reality. This is the point where methodologies should have sound criteria for selecting data and all kind of information including computational methods.

As a matter of fact, one can ask (and this is often one of the latest arguments against systematic work not only in the field of chemical thermodynamics) if such methodology may really exist. There is no other way to answer that but taking a look on the functional links of one part of a computerized methodology for processing and critical selection of liquid-vapor equilibrium data at moderate pressure (Fig. 2). The summary of the considered data bank is given in rectangles in the left side column, the main programs in rhombs, while the output data in figures appearing as ellipses.

In the data bank, first the properties of the pure components and of the mixtures reproduced from all available collections [6-16] are included, but continuously new data from available literature [45] are considered. All data are critically selected using three groups of criteria: first, with priority thermodynamic ones, second, statistical ones, oriented to selecting between thermodynamically consistent data; and third, empirical criteria related to the development risks, evaluated by error propagation from selected data through algorithms considered in design [17, 18]. The last two groups of criteria are specific for each property [19, 20] and must be adjusted according to actual results in application. For example, vapor pressures are reduced to the parameters in the equation given by Antoine [21] (ANTOINE program) which is used only in temperature ranges of less than 60 K. The predicted values are compared



*List of abbreviations:*

- A, B, C — The constants in the equation given by Antoine (21) vapor pressure dependence on temperature
- a, b — The constants in the equation given by Tsontopoulos (26) for the temperature dependence of second viria coefficients.
- $g^e$  — Gibbe excess energy,  $\text{J.mole}^{-1}$
- $g_{ji} - g_{jj}$  — Interaction energy differences in the equation given by Renon and Prausnitz (NRTL) for  $g^e/RT$  (34)
- $h^e$  — Excess enthalpy,  $\text{J.mole}^{-1}$
- K — Equilibrium „constants” =  $y_i/x_i$
- $E_{ij}$  — Critical exponent in the temperature dependent parameters  $n_{ij}$  of the equation given by Gothard (35)
- LVE3 — Ternary liquid-vapor equilibrium data\*
- LLE3 — Ternary liquid-liquid equilibrium data\*
- $B_{ii}(T)$  — Second virial coefficients for pure components at various temperatures  $\text{ml.mole}^{-1}$ \*
- $B_{ij}(T)$  — Interaction second virial coefficients,  $\text{ml.mole}^{-1}$ \*
- $n_{ij}$  — Parameters in the equation given by Gothard (35) for  $g^e/RT$ .
- $P^s(T)$  — Saturated vapor pressures for pure components at various temperatures\*
- $P_c$  — Critical pressures for pure components, MPa\*

$T_c$	- Critical temperatures of pure components, K*
$v_c$	- Critical volumes for pure components, ml.mole <sup>-1</sup> *
$P-x$	- Total pressure liquid-vapor equilibrium data*
$T-x$	- Boiling points at constant pressure*
$PTXY2$	- Total liquid-vapor equilibrium data in binary systems*
$S$	- Pure substances (name, codification, UNIFAC groups*)
$v^S(T)$	- Orthobaric molar volumes, ml.mole <sup>-1</sup> *
$v^e$	- Excess volumes, ml.mole <sup>-1</sup>
$x', x''(T)$	- Mutual solubility data at various temperatures*
$s_p, s_T, s_y$	- Standard deviations of pressure (kPa), temperature (K) and vapor phase compositions (mole fractions)
$R$	- The gas constant, J.mole <sup>-1</sup> .K
$T$	- Temperature, K
$\rho$	- Statistical selecting criterion given by Panaitescu (37)
$\omega$	- Acentric factor = $\lg(P/P_c) - 1,000$
$\frac{1}{\rho/\tau_1^2}$	- Semiaxes of the confidence ellipses of various parameters
$\alpha$	- Inclination of the larger semiaxe to the abscissa where the first model parameter is represented.
$\Delta N$	- Development risk expressed by deviation between the largest and smallest number of theoretical plates of the rectification column, predicted using various parameter pairs inside the confidence area of a given model
$\Delta r$	- Idem, expressed in terms of the reflux number.

with those obtained using the Riedel-Planck-Millier correlation [22, 23] (by RPM program). For analysis of reliability and consistency the method given by Lehman [24, 25] was recently selected. Second virial coefficients are reduced to parameters  $a$  and  $b$  in the correlation given by Tsionopoulos [26] (TCV program) but analysed comparatively with the data predicted by the method given by Hayden and O'Connell [41]. Orthobaric molar volumes are correlated by the equation of Rackett [28] in various one or two parameter versions [27] (RACKETT program). Total pressure or ebulliometric data are processed by integration of the appropriate form of the coexistence equation [29] to obtain vapor-phase compositions (COEXIST program). The integration is also performed in the case of overdetermined (PTXY) data. The deviations of experimental and predicted vaporphase compositions are used in the analysis of the thermodynamic consistency according to the principles given by van Ness [30] in the form recommended by Kemény *et al.* [31, 32] and in the extended form [20].

Consistent data are reduced to the parameters in the equations given by Wilson [33], Renon and Prausnitz [34] and Gothard [35] by the method based on the maximum likelihood principle [36] as given by Panaitescu [37]. All deviations are checked for significance by the Fischer test. For including the third group of selection criteria, column efficiency and reflux ratios required for standard separations are estimated using the Fenske-Gilliland method [38, 39], starting from the prediction of relative volatilities from the parameters at the endpoints of the semiaxes of the 95% confidence ellipses computed for each model. Mutual solubility data are reduced to the parameters in the equation given by Gothard (RESOLG program). Ternary liquid-liquid equilibrium data are reduced to the parameters in the equations given by Renon and Prausnitz (PDELL1 program) and by Gothard (PDELL2 program). Equilibrium "constants" as functions of temperature, liquid phase composition and pressure are predicted using parameters obtained by reduction of binary or ternary equilibrium data for all models considered and compared with multicomponent data if available (PREDATA program). The deviations are also considered in selecting the model to be in view for predicting multicomponent data.

When no experimental data are available, data are estimated using methods mainly based on the group-contribution principle (e.g. Lydersen method [40] for constants — LYDERSEN program, 1985-version UNIFAC method [47] for liquid-vapor equilibrium data — by the UNIFAC 85 program) or other methods, such as given by Hayden and O'Connell [41] for second virial coefficients (HAVCON-Program). Liquid-vapor equilibrium data may be estimated for regular and related solutions (SOLREG program).

All paths constituting the methodology have been verified on selected reference data, such as those recommended by CODATA [42] or obtained in the framework of the fruitful cooperation with I.D.S., [45], Technical University of Budapest [46], and through Academies of Sciences of socialist countries. Additional reference data are selected as a contribution to CODATA work and considered together with new elements expanding the verified algorithms by exchange and cooperation [43]. The use of the methodology in the development of new separation processes or to improve others as well as the efficiency of using selected data, were outlined in various publications (see a summary in [44]) and promoted by assistance of the authors for the users.

**Conclusions.** In the present state of the knowledge in the field of chemical thermodynamics, in particular on solution theory, there are possibilities that accuracy meet efficiency in development of large scale separation process-design ; when computerized data banks and algorithms are handled by specialized teams and decisions emerge by taking into account the results of research together with statistically evaluated risks starting from experimental error and its propagation.

Cooperation between specialized teams and inside of teams where physico-chemists, mathematicians specialised in programming and other specialists who must work together, requires a common language in application of any methodology.

In the field of design and development of separation processes, it is especially possible to develop methodologies which should be verified in practice. Such a methodology adequate for moderate pressure, may be considered now by the interested users and is available in computerized form with a bank of selected phase equilibrium data as well as all other data required for correlation, selection and prediction of multicomponent data.

#### REFERENCES

1. E. J. van de Kraats, "The Use of Basic Data in the Oil and Petrochemical Industry", *Phase Equil. & Fluid Properties in Chem. Ind., Proceedings of the 2-nd International Conference Berlin (West), 17—21 March 1980*, European Feder. of Chem. Engrs, Publ. Ser. 11, pp. 205—20.
2. D. Zudkevich, "Forensic Thermodynamics — Erroneous Decision on Thermodynamic Data can Cause Plant Failure", *ibid.*, pp. 883—904.
3. D. Zudkevich: "Design Data — Importance of Accuracy", *Encyclopedia of Chemical Process Design*, vol. 19, pp. 431, Ed. Marcel Dekker Inc. New York, January 1982; see also "Effect of Thermodynamic and Phase Equilibrium Data on Design, Operation and Economics of Separation Processes", *Collection of Proposed Lectures*, 1985.
4. T. A. Kletz, "What Went Wrong?", Gulf Publishing Co., Houston, London, Paris, Tokyo, 2-nd Edition, 1986.

5. D. Zudkevich, S. Malanevski, J. Vera, "Guideline for Reporting Data on Vapor-Liquid Equilibrium of Mixtures at Low and Medium Pressures", CODATA TASK GROUP members & experts meeting, Warshaw, 1986.
6. R. C. Reid, J. M. Prausnitz, T. K. Sherwood: "The Properties of Gases and Liquids" (3rd Ed.), McGraw-Hill, New York - Tokyo, 1977.
7. A. Maczynski & coworkers, "Verified Vapor-Liquid Equilibrium Data Collection", Thermodynamical Data for Technology, 1-9, P.A.N., Warszawa, 1978-1985.
8. J. Gmehling, U. Onken & coworkers, "Vapor-Liquid Equilibrium Data Collection", Chemistry Data Series, DECHEMA, 1977-1985.
9. J. H. Dymond, E. B. Smith, "The Viral Coefficients of Gases" (2nd Ed.), Clarendon Press, Oxford, 1979.
10. J. Jimmermans, "Physico-Chemical Constants of Pure Organic Compounds", Elsevier, Amsterdam, 1950.
11. J. Ch. Chu, R. J. Getty, L. F. Brenneke, R. F. Paul, "Distillation Equilibrium Data", Reinhold, New York, 1950.
12. E. Hála, I. Wichterle, J. Polák, T. Boublík, "Vapor-Liquid Equilibrium Data at Normal Pressure", Pergamon Press, London, 1968.
13. T. Boublík, V. Fried, E. Hála: "The Vapour Pressures of Pure Substances", Elsevier, Amsterdam, 1973.
14. V. B. Kogan, V. M. Friedman, "Spravocinik po Ravnovesiu Mejdu Jidkostiu i Parom v Binarnih i Mnogokomponentnih Sistemah", Gosudarst. Nauch. Tehn. Izdat. Him. Lit. Leningrad, 1957.
15. R. R. Dreisbach, "Physical Properties of Chemical Compounds", Ed. Amer. Chem. Soc., Washington D. C., 1955.
16. J. Choliński, A. Szafrański, D. Wyrykowska-Stankiewicz, "Computer Aided Second-Virial Coefficient Data for Organic Individual Compounds and Binary Systems", Thermodynamical Data for Technology, Ed. P.A.N., Warszawa, 1986.
17. F. A. Gothard, Al. Barhală, D. I. Marchidan, *Rev. Chim. (Bucureşti)* **32**, 1, 11-8 (1981).
18. F. A. Gothard, M. Florovici, I. Dumitru, "Informationnaia Sistema I Baza Dan- nikh Dlia Obosnovania Protsessov Razdelenia Putem Rektifikatsii", Communication to the Symposium on Informatics, Moscow, 1982.
19. F. A. Gothard, V. Suărășanu, G. Panaitescu, I. Cheța, I. Dumitru, "Critical Evaluation of Liquid-Vapor Equilibrium Data, Models and Correlation Methods Based on the Maximum Likelihood Principle", Communication to the 1-st CODATA Meeting on Critical Evaluation of Phase Equilibrium Data, Zaborów, Poland, May 1984.
20. F. A. Gothard, "An Extended Test for Thermodynamic Consistency of Liquid-Vapor Equilibrium Data", Communication to the 3-rd CODATA Symposium on Critical Evaluation and Prediction of Phase Equilibria in Multicomponent Systems, Budapest, 1987.
21. C. Antoine, *Cont. rend.*, **107**, 681, 836, 1143 (1888).
22. L. Riedel, *Chem. Ing. Tech.*, **26**, 83, 679 (1954).
23. D. G. Miller, *Ind. Eng. Chem.*, **56**, 3, 46 (1964); *Ind. Eng. Chem. Fundamentals* **2**, 68, 78, 80 (1980).
24. H. Lehmann, H. Freydank, I. Westmeier, *Z. Phys. Chem. (Leipzig)*, **266**, 2, 269-80 (1985).
25. H. Lehmann, H. Freydank, 2-nd International IUPAC Workshop on Vapor-Liquid Equilibria in *l-Alkanol-n-Alkane Mixtures*, Paris 5-7 September, 1985.
26. C. Tsionopoulos, *Amer. Inst. Chem. Engineers J.*, **20**, 253 (1974).
27. F. A. Gothard, „Echilibre lichid-vapor. I. Baze teoretice și metode de calcul”, Ed. Acad., R. S. România, București, 1975.
28. H. G. Rackett, *J. Chem. Eng. Data* **15**, 514 (1970); **16**, 308 (1971).
29. H. C. van Ness, "Classical Thermodynamics of Nonelectrolyte Solutions", Pergamon Press, New York, 1969.
30. H. C. van Ness, S. M. Byer, R. E. Gibbs, *Amer. Inst. Chem. Engineers J.*, **19**, 2, 238 (1971).
31. S. Kemény, J. Manczinger, K. Héberger, *The 3-rd Conference on Applied Chemistry, Unit Operations and Processes*, Veszprém, Hungary, 23-31 August 1977.
32. K. Kollár-Hunek, S. Kemény, E. Thury, J. Manczinger, "Thermodynamic Consistency Test for Binary Vapor-Liquid Equilibrium Data", *The 3-rd Austrian-Italian and Yugosl. Chem. Engng. Conference*, Graz, 1982.

33. G. M. Wilson, *J. Amer. Chem. Soc.*, **86**, 127 (1964).
  34. H. Renon, J. M. Prausnitz, *Amer. Inst. Chem. Engineers J.*, **14**, 135 (1968); *Ind. Eng. Chem. Proc. Des. Dev.*, **8**, 413 (1969).
  35. F. A. Goethard, *Ind. Eng. Chem. Fundamentals*, **20**, 3, 300–3 (1981); **24**, 330–9 (1985); *The 6-th IUPAC Conference on Thermodynamics*, Merseburg, GDR, Poster Session Paper **61**, 1980; *The 2-nd CODATA Symposium on Critical Evaluation and Prediction of Phase Equilibria in Multicomponent Systems*, Paris 11–13 September 1985, Paper 3RP–3.
  36. T. L. Sutton, J. F. McGregor, *Canad. J. Chem. Eng.*, **55**, 602 (1977).
  37. G. Panaitescu, *Rev. Chim. (Bucureşti)*, **33**, 12, 1110–3 (1982); *Internat. Chem. Engng.*, **25**, 688 (1985).
  38. C. S. Robinson, E. R. Gilliland, "Elements of Fractional Distillation", McGraw-Hill, New York, 1950.
  39. Y. K. Molokanov, T. P. Korabina, N. T. Marutina, G. A. Nikiforov, *Internat. Chem. Engng.*, **12**, 2, 209 (1972).
  40. A. L. Lydersen: "Estimation of Critical Properties of Organic Compounds" Univ. Wisconsin Coll. Eng. Exp. Stn. Rep. 3, Madison, 1955.
  41. J. G. Hayden, P. O'Connell, *Ind. Eng. Chem. Proc. Des. Dev.*, **14**, 209 (1975).
  42. A. Bylicki, *personal communication*, 1984.
  43. F. A. Goethard, „Referenz – Phasengleichgewichtsdaten für vergleichsmässige Untersuchungen an Modellen für Nichtelektrolytlösungen”, *Invited Lecture to the 15-th WAT Seminar of Society of Chemists of GDR*, Kühlungabor, 1985.
  44. F. A. Goethard, “Predicting Fluid Phase Equilibria by a Model of the Equilibrium of Interactions in Restrained Molecular Systems”, *Revue Roumaine de Chimie*, **33**, 331 (1988).
  45. Int. DATA Ser., Selected Data on Mixtures, Ser. A, H. Kehiaian, Editor.
  46. Courtesy of Dr. S. Kemény and G. Chikány, 1984–1986.
  47. D. Tiegs, P. Rasmussen, J. Gmehling, A. Fredenslund, SEP 8508 from *Phase Equilibria and Separation Processes*, Lyngby, Denmark, 1985.

# THE GRAVIMETRIC DETERMINATION OF TUNGSTEN AND MOLYBDENUM

MARIANA RUSU\*, ALEXANDRU BOTAR\*\* and GHEORGHE MARCU\*

*Received: October 13, 1987*

The paper presents a process of gravimetric determination of tungsten and molybdenum, as salts of tetra alkylammonium, phosphonium or arsenium of the type  $R_4XCl$  where  $R \geq C_4H_9$  and  $X = N, P, As$ . With that end in view, tungsten and molybdenum are condensed in acid medium to isopolyanions of the type  $W_{10}O_{32}^{-4}$  and  $Mo_6O_{19}^{-2}$ .

It is known that tungsten and molybdenum are gravimetrically determined by precipitation with different chemical reagents, then they are calcinated to  $WO_3$  and  $MoO_3$ , respectively, and weighed as such. These methods are not advantageous because they imply operations as precipitation, washing and calcination, stages that offer the possibility to the cations and anions (within the system) to interfere with the already formed compounds.

The method proposed in the present paper eliminates the disadvantages characteristic of the methods of gravimetric determination of tungsten and molybdenum, by precipitation of the tungstate and molybdate solutions, adjusted to the value of  $pH=2$ . In these circumstances the condensed forms of tungstate and molybdate, respectively, exist under the form of the following isopolyanions:  $W_{10}O_{32}^{-4}$ ,  $Mo_6O_{19}^{-2}$ , respectively. These isopolyanions precipitate with tetra-alkylammonium, phosphonium or arsenium salts under the form of some water insoluble precipitates, easily filtrable and very stable.

**Experimental.** *The Gravimetric Determination of W(VI) as  $[(C_6H_5)_4P]_4W_{10}O_{32}$ .* 300 cm<sup>3</sup> solution 0,04 mol/dm<sup>3</sup> of HCl is added to 100 cm<sup>3</sup> solution 0,4 mol/dm<sup>3</sup> of  $Na_2WO_4 \cdot 2H_2O$  for acidulation and the mixture is boiled under reflux for 20 minutes. The reaction mixture is cooled at 70°C then 100 cm<sup>3</sup> solution of  $[(C_6H_5)_4P]Cl$  with 1,5% concentration is added by dropping and continuous stirring. After a slight cooling at room temperature the precipitate is filtered on a filter crucible G<sub>4</sub>, is washed 3—4 times, each time with 25 cm<sup>3</sup> distilled water, and then is dried at 110°C to constant weight. The gravimetric factor for tungsten is  $f = 0,4959$ . The results of the chemical analysis for  $[(C_6H_5)_4P]_4W_{10}O_{32}$  are given in Table 1, representing the arithmetical mean

The results of the chemical analysis for  $[(C_6H_5)_4P]_4W_{10}O_{32}$

*Table 1*

%	W	C	H	P
Calcd.	49,5808	31,0961	2,1746	3,3412
Found.	49,5562	30,9208	2,0843	3,3508

\* University of Cluj-Napoca, Faculty of Chemical Technology, 3400 Cluj-Napoca, Romania

\*\* Institute of Chemistry, 3400 Cluj-Napoca, Romania

of six determinations and the experimental results obtained in the gravimetric determination of tungsten are shown in Table 2.

The results of gravimetric determination of tungsten

Table 2

g $\text{Na}_2\text{WO}_4 \cdot 2\text{H}_2\text{O}$ 100 ml solution with $c = 0,4 \text{ M}$	g $[(\text{C}_6\text{H}_5)_4\text{P}]_4\text{W}_{10}\text{O}_{32}$	g W
1. 13,1943	15,0896 (15,1695)	7,4814 (7,5066)
2. 13,1943	15,1242	7,4985
3. 13,1943	15,2446	7,5582
4. 13,1943	15,1042	7,4886

The Gravimetric Determination of Molybdenum as  $[(\text{C}_6\text{H}_5)_4\text{P}]_2\text{Mo}_6\text{O}_{19}$ . 300 cm<sup>3</sup> solution 0,04 mol/dm<sup>3</sup> HCl is added to 100 cm<sup>3</sup> solution 0,2 mol/dm<sup>3</sup> of  $\text{Na}_2\text{MoO}_4 \cdot 2\text{H}_2\text{O}$ , in such a way as pH become, 2, then it is heated to boiling. 100 cm<sup>3</sup> solution of  $[(\text{C}_6\text{H}_5)_4\text{P}]_2\text{Cl}$  with a 1.5% concentration is added slowly by dropping and continuous stirring to the heated solution. The yellow precipitate that occurs immediately is filtered on a filter crucible G<sub>4</sub>, it is washed 3—4 times, each time with 25 cm<sup>3</sup> distilled water, it is dried to 110°C and then it is weighed. The gravimetric factor for molybdenum is  $f = 0.3695$ . The elementary chemical analysis for  $[(\text{C}_6\text{H}_5)_4\text{P}]_2\text{Mo}_6\text{O}_{19}$  is given

The results of the chemical analysis for  $[(\text{C}_6\text{H}_5)_4\text{P}]_2\text{Mo}_6\text{O}_{19}$ 

Table 3

%	Mo	C	H	P
Calcd.	36,9291	36,9876	2,6071	3,9741
Found.	36,8982	36,8804	2,5862	3,8834

in Table 3, the experimental data representing the value of six determinations. Experimental result obtained by the gravimetric determination of molybdenum are shown in Table 4.

The results of gravimetric determination of molybdenum

Table 4

g $\text{Na}_2\text{MoO}_4 \cdot 2\text{H}_2\text{O}$ 100 ml solution with $c = 0,4 \text{ M}$	g $[(\text{C}_6\text{H}_5)_4\text{P}]_2\text{Mo}_6\text{O}_{19}$	g Mo
1. 9,6779	26,1248 (26,2066)	9,6475 (9,6778)
2. 9,6779	25,9882	9,5948
3. 9,6779	26,2304	9,6842
4. 9,6779	25,9582	9,5837

The values resulted from calculation are given in parentheses.

**Conclusions.** The tetraalkyl ammonium, phosphonium or arsonium salts of  $W_{10}O_{32}^{-4}$  and  $Mo_6O_{19}^{-2}$  isopoly anions are insoluble in water, easily filtrable and very stable precipitates.

The methods of determination proposed in this paper rule out the inconveniences characteristic of the methods of gravimetric determination of tungsten and molybdenum known up to the present, by eliminating a series of chemical operations as well as the interference of heterogeneous ions in the system.

#### REFERENCES

1. A. I. Vogel, "Quantitative Inorganic Analysis", 3-ed., London, 1961, p. 575, Ed.
2. L. Erdély, "Theorie und Praxis der Gravimetrischen Analyse", Akadémiai Kiadó, Budapest, 1964, Vol. II, p. 530-559.
3. C. Gh. Macaroviči, „Analiza Chimică Cantitativă Anorganică”, Ed. Academiei RSR, Bucureşti, 1979, p. 230, 349, 366, 372, 381.

P	H	C	W	A
base	2,971	3,6936	3,6391	3,6391
ACB, E	3,2982	3,6804	3,6385	3,6385
Carbo				
Funda				
Q-Mo	$a(C_6H_5)_3P_2Mo_6O_19$	$a(H_2Mo_6O_19)$		
7516,12749,0		2,61548, 2,61508		2,61533, 2,61530
7516,12749,0		2,61548, 2,61508		2,61533, 2,61530
5,9545,0		2,61548, 2,61508		2,61533, 2,61530
3,282,0		2,61548, 2,61508		2,61533, 2,61530

## LINEARIZATION OF POTENTIOMETRIC TITRATION CURVES

## IV. Redox Titrations

JÁNOS ZSAKÓ\* and FERENC MAKKAY\*

*Received: October 26, 1987*

The equation of redox titration curves is derived by taking into account the equilibrium constant of the redox reaction. The validity of the simplified equations used by Gran in the elaboration of his linearization procedure is tested on theoretical titration curves. Analysis of the Liteanu-Mioşcu procedure shows the nonlinear character of the curves obtained, but reveals the usefulness of this procedure in determining the equivalent point of the titration.

**Introduction.** In potentiometric titrations the equivalent point (*EP*) generally is determined by plotting *E* or pH versus volume of reagent added and the inflexion point of the curve is considered to coincide with the *EP*. Since these two points are not always identical [1], linearization procedures have been proposed allowing the determination of the *EP* as the intersect of two straight lines. All these procedures are based on simplifying presumptions, which under certain conditions, might affect the accuracy of the method. In the present paper two linearization procedures are discussed, viz. those proposed by Gran [2] and by Liteanu and Mioşcu [3], in order to clear up their limitations in redox titrations. A similar analysis of precipitation and of neutralization titrations was performed earlier [4].

Gran considers [2] that  $V_0$  ml of solution, having the concentration *a* and containing substance A in its reduced state, is titrated with a solution of B in its oxidized state, having the concentration *b*. In solution the following reactions occur:



and the potential of the redox electrode obeys the well known formula:

$$E = E_0 + \frac{RT}{n_A F} \ln \frac{[A_{\text{ox}}]}{[A_{\text{red}}]} \quad (2)$$

If *V* ml of solution of B has been added, the concentration of  $A_{\text{ox}}$  is calculated according to Gran, by means of the relation

$$[A_{\text{ox}}] = \frac{n_B}{n_A} b \frac{V}{V_0 + V} \quad (3)$$

i.e. by presuming reaction (1) to be total.

---

\* University of Cluj-Napoca, Faculty of Chemical Technology, 3400 Cluj-Napoca, Romania

From Eqs. (2) and (3) the following relation is derived :

$$\frac{dV}{dE} = \frac{n_A F}{RT} \cdot \frac{V_e}{V} (V_e - V) \quad (4)$$

where  $V_e$  stands for the volume of solution B, necessary to reach the EP. In the vicinity of the EP, Eq. (4) is proposed to be approximated by the relation :

$$\frac{dV}{dE} = \frac{n_A F}{RT} (V_e - V) \quad (5)$$

When the EP has been exceeded, the potential of the redox electrode may be given as

$$E = E'_0 + \frac{RT}{n_B F} \ln \frac{[B_{ox}]}{[B_{red}]} \quad (6)$$

In the same approximation, that reactions (1) are total, from Eq. (6) the following relation can be derived :

$$\frac{dV}{dE} = \frac{n_B F}{RT} (V - V_e) \quad (7)$$

According to Eqs. (4) and (7), before the EP the plot of  $dV/dE$  vs.  $V$  is a parabolic curve, with a linear portion in the vicinity of the EP. After the EP a straight line results.

Gran proposes to plot  $(1/V)(dV/dE)$  vs.  $V$  before the EP, since it is linear accordingly to Eq. (4) and  $dV/dE$  vs.  $V$ , after the EP. The intersection of the two straight lines is considered to correspond to the EP.

In order to avoid the tiresome graphical derivation of the titration curves, Gran proposes to use  $\Delta V/\Delta E$  instead of  $dV/dE$ . This difference ratio is plotted versus a corrected volume  $V_c$ , at which  $dV/dE = \Delta V/\Delta E$ . It is given as

$$V_c = V_1 + c \frac{1}{2} \Delta V \quad (8)$$

where  $\Delta V = V_2 - V_1$  and as stated by Gran,  $c$  is a unique function of the ratio  $r = \Delta V/(V_e - V)$ , and has the values tabulated in [2].

The Liteanu-Mioșcu procedure [3] is based on Gran's statement concerning the uniqueness of the relation between  $c$  and  $r$ . These authors propose to take  $r \approx 1$  and consequently to perform a plot of  $\frac{|V - V_i|}{|E - E_i|}$  vs.  $V$ , where  $V_i$  and  $E_i$  stand for  $V$  and  $E$  at the inflection point of the titration curve, i.e.  $V_i \approx V_e$ .

**Results and Discussions.** Since reactions (1) lead to an equilibrium, even if they are practically total, in the vicinity of the EP Gran's approximation is not rigorously valid. Therefore, we made an attempt to derive the accurate function  $\frac{dV}{dE} = f(V)$ , in order to test Gran's method on theoretical titration curves.

This function can be easily obtained if  $n_A = n_B = n$ , i.e. for a reaction



By taking the activity coefficients to be equal to unity, the equilibrium constant of reaction (9) can be written as

$$K = \frac{[A_{ox}][B_{red}]}{[A_{red}][B_{ox}]} \quad (10)$$

During the titration the following material balance relations are valid

$$\frac{aV_0}{V_0 + V} = [A_{ox}] + [A_{red}] \quad (11)$$

$$\frac{bV}{V_0 + V} = [B_{ox}] + [B_{red}] \quad (12)$$

$$[A_{ox}] = [B_{red}] \quad (13)$$

$$V_e = \frac{aV_0}{b} \quad (14)$$

The system of Eqs. (10)–(13) allows us to express both  $[A_{ox}]$  and  $[A_{red}]$  as function of  $K$ ,  $a$ ,  $b$ ,  $V_0$  and  $V$ . By substituting these expressions into Eq. (2) and by taking into account Eq. (14), eventually one obtains the equation of the titration curve:

$$E = E_0 + \frac{RT}{nF} \ln \left[ K \frac{V - V_e}{2V_e} + \frac{1}{2V_e} \sqrt{K^2(V_e - V)^2 + 4KV_eV} \right] \quad (15)$$

For the EP Eq. (15) transforms into

$$E_e = E_0 + \frac{RT}{nF} \ln \sqrt{K} \quad (16)$$

Derivation of Eq. (15) with respect to  $V$  leads to the function

$$y = \frac{RT}{nF} \cdot \frac{dV}{dE} = \frac{(V_e - V) \sqrt{K^2(V_e - V)^2 + 4KV_eV} - K(V_e - V)^2 - 4V_eV}{2V_e(K - 1)} \quad (17)$$

which gives for very large  $K$  values

$$\lim_{K \rightarrow \infty} y = \begin{cases} \frac{V}{V_e} (V_e - V), & \text{for } \sqrt{(V_e - V)^2} = V_e - V \\ V - V_e, & \text{for } \sqrt{(V_e - V)^2} = V - V_e \end{cases} \quad (18)$$

Obviously, the two limits are identical with Eqs. (4) and (7), respectively, derived by Gran for total reactions, and both of them giving  $y = 0$  for  $V = V_e$ . On the other hand, Eq. (17) yields for  $V = V_e$ , the following value:

$$y_e = \frac{2V_e}{\sqrt{K} + 1} \quad (19)$$

which generally is not vanishing, only if  $K$  is large enough.

In order to test the limitations of Gran's procedure,  $y$  values have been calculated for several hypothetical titration curves by using Eq. (17) and by

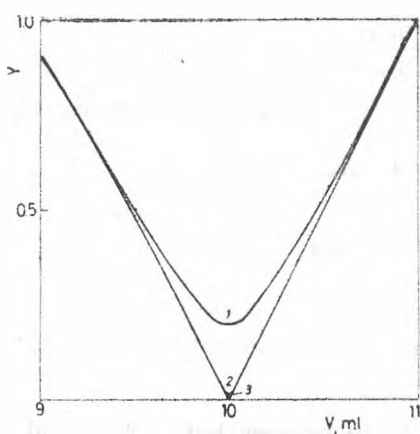


Fig. 1. Theoretical  $y$  vs.  $V$  curves for the vicinity of the EP.

$V_0 = 100 \text{ ml}$ ,  $a = 10^{-2} \text{ M}$ ,  $b = 10^{-1} \text{ M}$ .  
1 —  $K = 10^4$ ; 2 —  $K = 10^6$ ; 3 —  $K \geq 10^8$

taking  $V_0 = 100 \text{ ml}$ ,  $a = 10^{-2} \text{ M}$ ,  $b = 10^{-1} \text{ M}$ , leading to  $V_e = 10 \text{ ml}$ . Some examples of  $y$  vs.  $V$  curves are given in Fig. 1 for the vicinity of the EP. As seen, if  $K > 10^6$ , the shape of the curve is practically not affected by the value of  $K$ . Gran's linearizations, performed on theoretical curves are visualized in Fig. 2, also for the vicinity of the EP. One can see, that if  $K \geq 10^6$  two common straight lines are obtained, intersecting each other at  $y = 0$  and  $V = V_e$ , i.e. Gran's linearization works perfectly. For  $K = 10^4$  already important deviations from the linearity appear and a discontinuity at the EP. Consequently, Gran's procedure cannot be applied if  $K$  is less than about  $10^5$ — $10^6$ .

The theoretical titration curves constructed were used to verify Gran's statement concerning the constancy of the coefficient  $c$  in Eq. (18) for a given ratio  $r = \Delta V/(V_e - V)$ . For this purpose the ratio  $r = 1$  has been chosen, since this ratio is used in the Liteanu-Mioșcu linearization. Results are presented in Tab. 1. As seen, this coefficient is not constant at all, it depends

Coefficient  $c$  in Eq. (18) as derived from theoretical titration curves Table 1  
for the ratio  $V/(V_e - V) = 1$ .  $a = 10^{-2} \text{ M}$ ,  $b = 10^{-1} \text{ M}$ ,  $V_0 = 100 \text{ ml}$

$V, \text{ ml}$	K				
	$10^4$	$10^6$	$10^8$	$10^{10}$	$10^{12}$
2	1.615	1.745	1.798	1.857	1.860
4	1.543	1.703	1.780	1.820	1.851
6	1.475	1.670	1.765	1.815	1.845
8	1.360	1.620	1.740	1.800	1.840
9	1.240	1.560	1.720	1.800	1.840
9.2	1.175	1.550	1.700	1.800	1.825
9.4	1.133	1.533	1.700	1.757	1.833
9.6	1.050	1.500	1.650	1.750	1.825
9.8	0.900	1.400	1.600	1.700	1.800

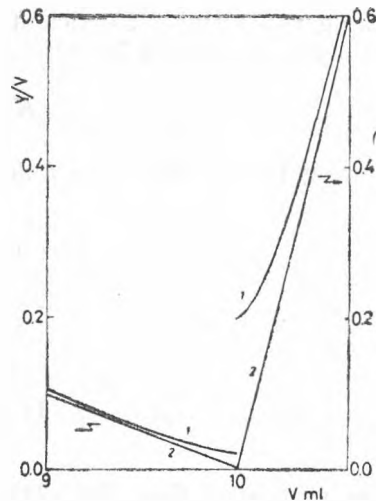


Fig. 2. Gran's linearization performed on theoretical curves.

$V_0 = 100 \text{ ml}$ ,  $a = 10^{-2} \text{ M}$ ,  $b = 10^{-1} \text{ M}$ .  
1 —  $K = 10^4$ ; 2 —  $K \geq 10^6$

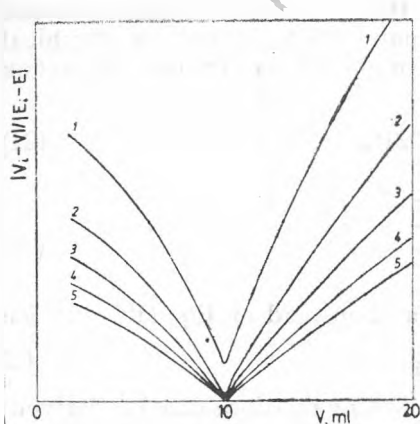


Fig. 3. Linearization of theoretical titration curves according to the procedure proposed by Liteanu and Mioșcu.  
 $V_e = 100 \text{ ml}$ ,  $a = 10^{-2} \text{ M}$ ,  $b = 10^{-1} \text{ M}$ .  
 1 —  $K = 10^4$ ; 2 —  $K = 10^6$ ; 3 —  $K = 10^8$ ;  
 4 —  $K = 10^{10}$ ; 5 —  $K = 10^{12}$

Table 2

Theoretical and calculated by means of the Liteanu—Mioșcu procedure  $\Delta E_{\pm 1\%}$  and  $\Delta E_{\pm 0.1\%}$  values in units  $RT/nF$ .

$K$	$\Delta E_{\pm 1\%}$		$\Delta E_{\pm 0.1\%}$	
	theor.	calc.	theor.	calc.
$10^4$	0.97	0.99	0.10	0.11
$10^6$	4.63	4.23	0.96	0.66
$10^8$	9.22	8.26	4.63	1.66
$10^{10}$	13.83	12.70	9.21	3.13
$10^{12}$	18.43	17.32	13.82	5.00

on  $K$  and varies even during the titration. The latter effect diminishes very much with increasing  $K$  value.

Anyhow, by taking into account that  $c$  is not constant, the Liteanu—Mioșcu linearization cannot be expected to give straight lines. Several "linearized" theoretical titration curves are presented in Fig. 3. As seen, instead of straight lines, curves of parabolic shape are obtained, which is not surprising, since by presuming that  $V_i = V_e$ , the magnitude plotted vs.  $V$  in the Liteanu—Mioșcu procedure can be given as

$$\frac{|V_i - V|}{|E_i - E|} = \frac{nF}{RT} \frac{|V_e - V|}{\left| \ln \sqrt{K} - \ln \left[ K \frac{V - V_e}{2V_e} + \frac{1}{2V_e} \sqrt{K^2(V_e - V)^2 + KV_e} \right] \right|} \quad (20)$$

by taking into account Eqs. (15) and (16). Obviously, the right hand side of Eq. (20) is not linear in  $V$  at all. Consequently, the linearization proposed, and especially the applying of linear regression methods, cannot give trustful information.

In order to illustrate the correctness of the above statement  $\Delta E_{\pm 1\%}$  and  $\Delta E_{\pm 0.1\%}$  values have been calculated by using the Liteanu—Mioșcu procedure. For this purpose the  $(|V_i - V|)/(|E_i - E|)$  data calculated for the vicinity of the EP, viz. for the intervals  $9 \leq V < 10$  and  $10 < V \leq 11$ , were processed by means of linear regression and  $\Delta E_{\pm 1\%}$  and  $\Delta E_{\pm 0.1\%}$  values were calculated by using the equations of both straight lines. In Tab. 2 these values are given as calculated and are compared with the theoretical ones computed by means of Eq. (15). Obviously, the potential jump  $\Delta E_{\pm 1\%}$  is relatively well approximated by the linear regression methods, generally the errors do not exceed 10%, but the calculated  $\Delta E_{\pm 0.1\%}$  values are very far from the real ones, especially if  $K$  is large, i.e. even in the case of redox reactions used for analytical purposes. Consequently, the calculation of potential jumps by means of statistical methods can give reliable results only if the  $|V_i - V|/|E_i - E|$  vs.  $V$  curves are approximated by means of second order polynomials.

In the case of asymmetric titrations, i.e. if  $n_a \neq n_b$ , the equation of the titration curve cannot be given in an explicit analytical form, but its graphical construction can be easily carried out. As an example, let us consider the redox reaction



Its equilibrium constant can be written as

$$K = \frac{[A_{\text{red}}][B_{\text{ox}}]^2}{[A_{\text{ox}}][B_{\text{red}}]^2} \quad (22)$$

Eqs. (11) and (12) maintain their validity and instead of Eq. (13) one has

$$[B_{\text{ox}}] = 2[A_{\text{red}}] \quad (23)$$

By using Eqs. (11), (12), (21) and (22) the following relations can be derived:

$$V = \frac{2[A_{\text{red}}](V + V_0)}{b} \left[ 1 + \sqrt{\frac{A_{\text{red}}(V + V_0)}{K[aV_0 - [A_{\text{red}}](V + V_0)]}} \right] \quad (24)$$

and

$$\frac{[A_{\text{ox}}]}{[A_{\text{red}}]} = \frac{aV_0}{[A_{\text{red}}](V + V_0)} \quad (25)$$

These relations enable us to calculate  $V$  corresponding to different  $[A_{\text{red}}]$  ( $V + V_0$ ) values by means of Eq. (24) and the corresponding  $E$  value by using Eqs. (25) and (2). Several titration curves constructed by means of this procedure are visualized in Fig. 4.

Obviously, if  $K = 10^6$ , the redox reaction cannot be used for analytical purposes, since the potential jump near to the EP is too small, but for  $K = 10^9$  it is already large enough.

From the titration curves, presented in Fig. 4,  $\Delta V/\Delta E$  values have been derived. Their graphical plot vs.  $V_c$  (as given by Eq. (8) and by using  $c$  values tabulated by Gran [2]) is given in Fig. 5. for the vicinity of the EP. From these curves it is obvious that for the EP ( $V_c = 20 \text{ ml}$ ),  $\Delta V/\Delta E$  is practically zero only if  $K$  is large enough and for lower  $K$  values the minimum of the curves does not appear at  $V = V_e$ . Practically, the position of the minimum coincides with the inflection point of the titration curves. The  $V_i$  values derived from the theoretical titration curves are given in Tab. 3. One can conclude, therefore, that Gran's procedure gives the EP only if the redox reaction is practically total, i.e. if  $K \geq 10^{12}$ . For lower  $K$  values it yields rather  $V_i$  than  $V_e$ .

The linearization of the titration curves given in Fig. 4 according to the procedure proposed by Liteanu and Mioșcu, is shown in Fig. 6 for the vicinity of the EP. The more linear portions corresponding to  $1 \leq V \leq 19$  and  $21 < V < 40$ , respectively, were used to establish the equation of the curves by linear regression. The volume, corresponding to the intersection of the straight lines is given also in Tab. 3 as  $V_{e(LM)}$ . As seen, this procedure does not give the real EP for low  $K$  values, but volumes even exceeding  $V_i$ .

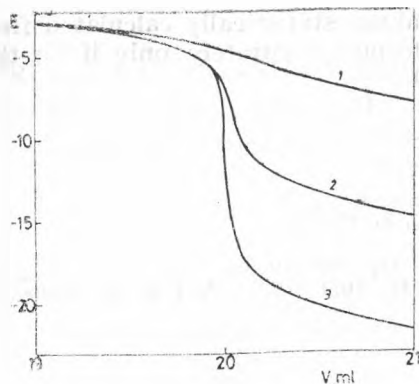


Fig. 4. Theoretical titration curves implying the redox reaction (21), constructed by using relations (24) and (25).  $E$  expressed in units  $RT/n_A F$ .  
 $V_0 = 100 \text{ ml}$ ,  $V_e = 20 \text{ ml}$ . 1 —  $K = 10^6$ ;  
2 —  $K = 10^9$ ; 3 —  $K = 10^{12}$ .

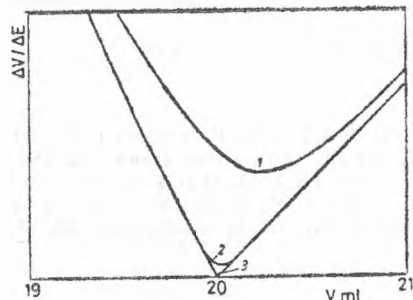


Fig. 5.  $\Delta V/\Delta E$  vs.  $V_e$  curves for asymmetric titrations in the vicinity of the EP. Reaction (21).

$V_0 = 100 \text{ ml}$ ,  $V_e = 20 \text{ ml}$ .  
1 —  $K = 10^6$ ; 2 —  $K = 10^9$ ; 3 —  $K = 10^{12}$ .

Table 3

Inflexion volumes ( $V_i$ ) in the asymmetric titrations based on reaction (21) and  $V_e$  values obtained by the Liteanu-Mioșeu procedure

$K$	$V_i$ , ml	$V_e(LM)$ , ml
$10^6$	20.231	20.328
$10^9$	20.031	20.121
$10^{12}$	20.008	19.998

Table 4

Potential jumps, expressed in units  $RT/n_A F$ , calculated by means of Liteanu-Mioșeu procedure and theoretical ones, derived from the titration curves given in Fig. 4

$K$	$\Delta E \pm 1\%$		$\Delta E \pm 0.1\%$	
	calc.	theor.	calc.	theor.
$10^6$	1.571	1.332	0.177	0.138
$10^9$	7.323	6.930	1.449	1.336
$10^{12}$	14.909	13.812	4.844	7.006

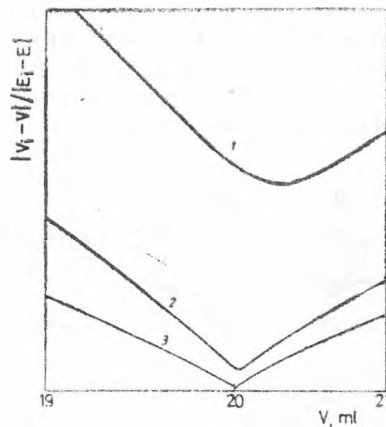


Fig. 6. Liteanu—Mioșeu linearization of asymmetric titration curves in the vicinity of the EP.

$V_0 = 100 \text{ ml}$ ,  $V_e = 20 \text{ ml}$ .  
1 —  $K = 10^6$ ; 2 —  $K = 10^9$ ; 3 —  $K = 10^{12}$ .

The  $|V_i - V| / |E_i - E|$  values calculated for  $18 \leq V < 20$  and  $20 < V \leq 22$  have been processed by means of linear regression and potential jumps  $\Delta E \pm 1\%$  and  $\Delta E \pm 0.1\%$  values have been calculated. These calculated values are compared with the theoretical ones, derived directly from the titration curves given in Fig. 4. As seen from Tab. 4, the results obtained by both procedures are rather different from each other. Consequently, the characterization of the sensitivity

of potentiometric redox titration by  $\Delta E_{\pm e}$  values, statistically calculated from  $|V_i - V|/|E_i - E|$  and  $V$  pairs, can be performed accurately only if for this purpose second order polynomials are used.

## REFERENCES

1. F. L. Hahn, M. Frommer, *Z. phys. Chem.*, **127**, 37 (1927).
2. G. Gran, *Acta chem. scand.*, **4**, 559 (1950).
3. C. Liteanu, M. Mișcu, *Rev. Roumaine Chim.*, **13**, 1185 (1968).
4. J. Zsakó, F. Makkay, *Rev. Roumaine Chim.*, **17**, 1071 (1972); *Zhur. Analit. Khim.*, **29**, 1894 (1974); *Chem. Analityczna*, **25**, 95 (1980).

## STRUCTURAL CONSIDERATIONS AND THEIR CORRELATION WITH POSSIBLE CONDUCTION MECHANISMS IN ORGANIC FREE RADICALS OF THE HIGHLY HALOGENATED PHENOTHAZINES SERIES

I. A. SILBERG\* and I. MARIAN\*

Received: October 22, 1987

The molecular and crystal structure of the very stable nitrogen free radicals octahalophenothiazinyls are correlated with the electrical conduction mechanisms explaining the semiconductor behaviour of these compounds.

The electrono-structural characteristics and the high stability of organic free radicals of the superior halogenated phenothiazines series suggested the correlation of these features with some conduction mechanisms, particularly at high temperatures. Detailed knowledge about the conduction type and mechanisms in the case of these compounds is obviously indispensable for the production of functional devices based on such materials.

**1. Structural data concerning the molecule and lattice of the free radical octachlorophenothiazinyl.** The most thoroughly investigated term of the series of octahalophenothiazinyls (Fig. 1) is the octachloroderivative ( $x_1 = \dots = x_8 = \text{Cl}$ ) obtained by the thermal decomposition of undecachlorophenothiazine [1, 2], under isothermal conditions at  $170 \pm 10^\circ\text{C}$ .

However, the growth of single crystal is difficult, so that a complete structural analysis by Fourier diagrams could not be carried out; consequently structural data were indirectly obtained by Debye-Scherrer diagrams.

The latter indicated that octachlorophenothiazinyl displays a crystalline structure similar to that of the base compound, without radicalic character (having a N—H group), namely octachlorophenothiazine [1, 2]. Single crystals could be obtained from octachlorophenothiazine, so that it became possible to determine the elementary cell dimensions:  $12.7 (\pm 0.2)$ ;  $8.5 (\pm 0.1)$  and  $3.8 (\pm 0.1)$  Å (Weissenberg goniometer technique).

By corroborating these data with models depicting the association of octachlorophenothiazine molecules (by H bonds) and taking into account the possibility of the free radical octachlorophenothiazine to form dimers by N—N bonding, we put forward a plausible hypothesis about the disposition of free radical molecules in the crystalline lattice [2].

According to this structure, the free radicals adopt a geometry ensuring maximum overlap of the orbitals accounting for most of the unpaired spin,

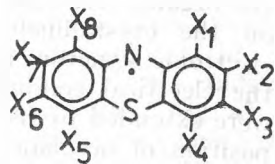


Fig. 1. Molecular structure of octahalophenothiazinyls.

\* University of Cluj-Napoca, Faculty of Chemical Technology, 3400 Cluj-Napoca, Romania

orbitals with a relatively high degree of localization at N (see RES studies in solutions [2, 3]).

A dimer lattice is thus actually formed, but with very weak intermolecular interaction between the two free radical moieties, due to the steric hindrance generated by the halogen atoms, and to the very marked delocalization of unpaired electron on the phenothiazine nucleus [3, 4].

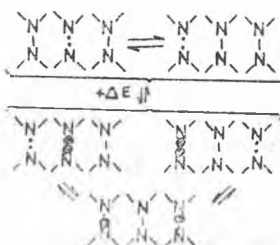


Fig. 2. Spin -- and charge delocalization on the crystalline lattice of octachlorophenothiazinyll.

In this way the radicalic character "moves" along the lattice, a fact which provides a good explanation for the exceptional stability of the radical (heating it up to 380°C, and cooling it without sensible modification of spin density being observed). Thus along with unpaired spin delocalization on the atoms within the molecules — a rather well-known stabilization mechanism among the organic free radicals — we witness, at the same time, a spin delocalization on the crystalline lattice of octachlorophenothiazinyll. This mobility of the electronic structure represented one of the premises prompting us to investigate the electrical conductivity of the free radical under scrutiny. The researches were extended to also cover the bromo derivatives obtained by thermal decomposition of octahalophenazathionium perchlorogenides [6] which present similar chemical properties, despite physical and electronical differences induced by the presence of molecular asymmetries due to a partial substitution of chlorine by bromine.

**2. Electrical conductance. Mechanisms.** The determinations were made on pellets obtained by compression at about 25 atm, in inert atmosphere (to avoid redox interactions) and started at the sensibility threshold of the apparatus ( $10^{-10} \Omega^{-1} \text{cm}^{-1}$ ) ; they were carried out up to 297°C, temperature where the decrease of mechanic resistance by melting may appear. All of the studied compounds display a more or less pronounced tendency to change the slope of  $\log \sigma$  vs.  $10^3 T^{-1}$  linear dependences (Fig. 3). Thus in the higher temperatures domain the slope is steeper than the one in the inferior temperatures domain. The general outline of the diagrams, in the case of our compounds, determine us to assimilate them with strongly doped semiconductors or with ionic conducting combinations. This assumption is supported by the possibility of existence, in octahalophenothiazinyll samples, of impurities consisting of the closest to the free radical redox forms, i.e. reduced phenothiazines and oxidized phena-

dence that under ambiental temperature conditions, despite the variations in the sample preparation way (isothermal decomposition, use of temperature gradient, or chemical treatment of undecachlorophenothiazine) [5] RES determinations show a constant density of spin (about 30%) that is, one unpaired electron to three octachlorophenothiazinyll moieties, or a dissociated pair to two dimerized ones, can be interpreted [2] only as a result of a thermal equilibrium between the bonded and unbonded dimer states (Fig. 2, top line).

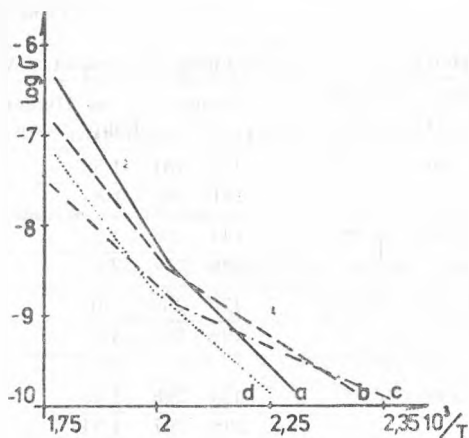


Fig. 3. Temperature dependence of electrical conductivity in octahalophenothiazinyls: a. octachloro-; b. 1-bromo-heptachloro-; c. 2-bromo-heptachloro-; d. 1, 2, 4, 6-tetrabromo-tetrachloro-.

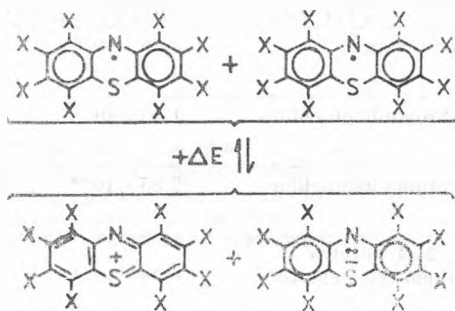


Fig. 4. The formation of octahalophenothiazinium cation-octahalophenothiazinium anion by the disproportionation of two molecules of octahalophenothiazinyl free radicals.

zathionium cations, or even the quinones (phenothiazone-3) which may be identified in traces, by IR spectra (characteristic frequencies of C=O groups).

The specific molecular and crystal structure of octahalophenothiazinyls, suggest a particular conduction mechanism.

The migration process of unpaired spin, and the extended aromatic electronic delocalization, similar to that in anthracene (see the structure of octachlorophenothiazinium cation) determine the disproportionation of a free radical pair into a phenothiazinium cation-phenothiazinium anion pair (Fig. 4), a process expected to be of low activating energies. The occurrence of this process may migrate along the lattice in a way similar to the one described for the propagation of the radicalic character (Fig. 2, down) but bringing with it however the qualitatively new feature of different displacement in electric field, of the opposite charges. In this way, with a moderate energy consumption it can pass from the equilibrium state radical-dimer existent at the room temperature — which explains the delocalization (the "migration") of unpaired spin — to a new state in which, along with the dimer dissociation there is also the redox disproportionation process, the radical and ionic states migrating simultaneously. In Table 1 it can be noted that the activating energies of conductivity, calculated from the diagrams of electric conductivity at the variable temperature, are in the 1.5–2.1 eV range (for higher temperatures) and 1.0–1.5 eV (for lower temperatures). It must be noted that the microcrystal structures of octachlorophenothiazinyl free radicals, evidences a specific dichroism, which influences the visible spectra of a radical layer deposited by vacuum vaporization.

This conduction model, does not require a fixation, in the lattice reference system, of the charge density wave (CDW) and even of the lattice distortion.

Table 1

Free radical phenothiazinyl	Electrical conductivity		Activ.energ. of conduct. (eV)		
	At 297 °C $\Omega^{-1}\text{cm}^{-1}$	At the sensibility threshold t °C $\Omega^{-1}\text{cm}^{-1}$	Range °C	Lower temp	Higher temp
Octachloro	$4.39 \cdot 10^{-7}$	126	$2.86 \cdot 10^{-10}$	126—181	1.5
				181—297	1.8
1-bromo-heptachloro	$1.60 \cdot 10^{-7}$	144	$2.00 \cdot 10^{-10}$	144—196	1.3
				196—297	2.1
2-bromo-heptachloro	$2.85 \cdot 10^{-8}$	170	$4.50 \cdot 10^{-10}$	170—206	1.0
				206—297	1.6
1, 2, 4, 6-tetra- bromo-tetra-chloro	$6.60 \cdot 10^{-8}$	144	$5.00 \cdot 10^{-10}$	144—208	1.15
				208—297	1.54

Thus a collective charge transfer appears, as in the case of a great effective charge with a great effective mass. The charge density wave and the periodic lattice distortion are considered together like a condensed state in a Fröhlich model [7].

If the above described model could be assimilated with the Fröhlich mechanism, then this fact could lead to an increase of conductivity even at finite temperatures.

#### REFERENCES

1. C. Bodea, I. A. Silberg, *Nature*, **198**, 883 (1963).
2. C. Bodea, I. A. Silberg, *Rev. Roumaine Chim.*, **9**, 505 (1964).
3. C. Bodea, I. A. Silberg, *Rev. Roumaine Chim.*, **10**, 887, (1965).
4. J. M. Hoste, F. Tonnard, *J. Chim. Phys.*, **63**, 678 (1966).
5. I. A. Silberg, *Brev. RSR*, 64 164 (1977).
6. I. A. Silberg, *Thesis*, Institute of Chemistry Cluj-Napoca, (1970).
7. H. Fröhlich, *Proc. Roy. Soc. London ser. A*, **223**, 296 (1954).

## NEUE KOBALT(III)-AMIN-KOMPLEXBASEN MIT HEPTOXIM

GHEORGHE MARCU\*, CSABA VÁRHELYI\*, JÓZSEF FÜLÖP\* und DANA ITUL\*

Eingegangen am 26 October 1987

**New Cobalt(III)-Amine Complex Bases with Heptoxime.** A number of 20 new complex salts of the types:  $[\text{Co}(\text{Heptox.H})_2(\text{NH}_3)_2] \cdot \text{X}$  and  $[\text{Co}(\text{Heptox.H})_2(\gamma\text{-picoline})_2]\text{X}$  ( $\text{Heptox.H}_2$  — 1,2-cycloheptanedione dioxime) were obtained and characterized by IR and UV spectra and by derivatographic measurements. Some characteristics of these compounds were compared with those of the analogous dimethylglyoxime derivatives.

**Einleitung.** Die alycyclischen  $\alpha$ -Dioxime zeigen aus analytischem Standpunkt eine Reihe Vorteile gegenüber den aliphatischen und aromatischen Dioximen. Wegen der erheblichen Löslichkeit der niedrigeren Homologen (mit  $C_5$ ,  $C_6$  und  $C_7$ ) in Wasser, verunreinigen sie die  $\text{Ni}(\text{Diox.H})_2$ ,  $\text{Pd}(\text{Diox.H})_2$  und  $\text{Pt}(\text{Diox.H})_2$  Niederschläge bei den gravimetrischen Analysenverfahren nicht. Von den alycyclischen  $\alpha$ -Dioximen mit 5 ... 12 Kohlenstoffatomen im Ring, wurden nur die leichter zugänglichen 1,2-Cyclopantan ..., Cyclohexan ... — und Cycloheptandiondioxim aus analytischem und koordinationschemischem Standpunkt untersucht. Die Herstellung der höheren Homologen ist zu teuer und die Löslichkeit im Wasser dieser Chelatbildner ist viel geringer als diejenige der Derivate mit  $C_5$  ...  $C_7$  im hydroaromatischen Ring.

In früheren Arbeiten [1—8] wurden die Bildung und die Stabilität der  $\text{Cu}(\text{II})$ ,  $\text{Co}(\text{II})$ ,  $\text{Ni}(\text{II})$ ,  $\text{Fe}(\text{II})$ -Chelate des 1,2-Cyclohexandiondioxims, bzw. 1,2-Cycloheptandiondioxims (Heptoxims) potentiometrisch, polarographisch und spektrophotometrisch untersucht.

Das Heptoxim, so wie die anderen  $\alpha$ -Dioxime, ist eine sehr schwache zweibasische Säure deren Dissoziationskonstanten folgende Werte haben:  $pK_1 = 10,60—10,80$  und  $pK_2 = 11,80—12,10$  [9].

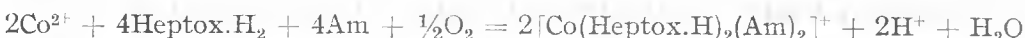
In schwachsaurer und neutralem Medium verhält sich dieses Reagenz wie ein monodeprotonierter, zweizähniger Chelatbildner. Die durch Komplexbildung entstehenden fünfgliedrigen Chelatringe sind sehr beständig. In stark sauren Lösungen erlitt das Heptoxim eine partielle Deoximierungsreaktion. Dieser Prozess kann auf polarographischem Wege leicht verfolgt werden [10].

In stark basischem Medium ist das Heptoxim in doppeltdeprotonierter Form ( $\text{Heptox}^{2-}$ ) vorhanden.

**Ergebnisse und Diskussion.** Wir haben beobachtet, daß gemischte Komplexsäuren und — basen des Kobalts(III) mit diesem alycyclischen Dioxim

\* Universität Cluj-Napoca, Facultät für Chemische Technologie, 3100 Cluj-Napoca. Rumänien

durch Oxydation einer Mischung von Kobalt(II)-Salzen, Heptoxim und ein-, bzw. zweizähnigen neutralen und sauren Liganden leicht entstehen:



(X = Cl, Br, I, NCS, NCSe, CN, N<sub>3</sub>, usw., Am = primäre und tertiäre Amine, Phosphine, Arsine).

Zur Oxydation der Mischungen können Luftsauerstoff, Perhydrol, Cl<sub>2</sub>, Br<sub>2</sub>, usw. verwendet werden.

Einige Chelate dieser Klasse können auch aus [Co(NH<sub>3</sub>)<sub>5</sub>Cl]Cl<sub>2</sub>, Na<sub>3</sub>[Co(NO<sub>2</sub>)<sub>6</sub>]Na<sub>3</sub>[Co(CO<sub>3</sub>)<sub>3</sub>] durch Substitutionsreaktionen hergestellt werden. Das Heptoxim kann das CN<sup>-</sup> im K<sub>3</sub>[Co(CN)<sub>6</sub>] nicht ersetzen. Analoge Substitutionsreaktionen mit Chrom(III)-derivaten, wie [Cr(NH<sub>3</sub>)<sub>6</sub>]Cl<sub>3</sub>, [Cr(en)<sub>2</sub>Cl<sub>2</sub>]Cl, K<sub>3</sub>[Cr(NCS)<sub>6</sub>], K[Cr(NH<sub>3</sub>)<sub>2</sub>(NCS)<sub>4</sub>], usw. in wässrigen Lösungen und in verdünntem Alkohol blieben ohne Erfolg.

In dieser Arbeit beschreiben wir zwei neue Chelatkationen des Kobalts: [Co(Heptox.H)<sub>2</sub>(NH<sub>3</sub>)<sub>2</sub>]<sup>+</sup> und [Co(Heptox.H)<sub>2</sub>(γ-Pikolin)<sub>2</sub>]<sup>+</sup>.

Diese Chelate wurden aus den Komponenten durch die klassische Oxydationsreaktion mit Luftsauerstoff in wässrig-alkoholischer Lösung erhalten. Von den leichtlöslichen Acetaten: [Co(Heptox.H)<sub>2</sub>](NH<sub>3</sub>)<sub>2</sub>] acetat und [Co(Heptox.H)<sub>2</sub>(γ-Pikolin)<sub>2</sub>] acetat ausgehend, wurde eine Reihe von binären Komplexsalzen durch doppelte Umsetzungsreaktionen erhalten. Zu diesem Zweck verwendeten wir Alkalosalze der Halogene und Pseudohalogene, Pikrinsäure und verschiedene monobasische Komplexsäuren des Kobalts(III) und des Chroms(III).

Die Co[Heptox.H]<sub>2</sub>(NH<sub>3</sub>)<sub>2</sub>X-Salze sind in Wasser leichter lösliche als die analogen Pyridinabkömmlinge. Die geringste Löslichkeit in Wasser haben die Pikrate und die Salze des H[Cr(NCS)<sub>4</sub>(Amin)<sub>2</sub>]. Letzten Salze lösen sich leicht im Aceton und in Dimethylformamid.

Die hergestellten Komplexsalze sind in Tabelle 1 und 2 charakterisiert.

In den UR-Spektren der [Co(Heptox.H)<sub>2</sub>(NH<sub>3</sub>)<sub>2</sub>]I und [Co(Heptox.H)<sub>2</sub>(γ-Pikolin)<sub>2</sub>]I wurden die für das koordinierte Heptoxim charakteristischen Banden identifiziert. Im Vergleich mit dem Spektrum des freien Heptoxims sind die ν<sub>C=N</sub>, ν<sub>N-OH</sub> und ν<sub>O-H</sub> Frequenzen verschoben. Diese Verschiebung bestätigt die Bildung von sehr starken Co—N (Oxim)-Bindungen.

Wie es in früheren Arbeiten gezeigt wurde [11, 12], besitzt die M(Heptox.H)<sub>2</sub> (M = Ni, Pd)-Gruppe eine koplanare Struktur, welche von zwei intramolekularen O—H...O-Wasserstoffbrückenbindungen stabilisiert ist. Diese ν<sub>O-H</sub> und δ<sub>O-H...O</sub> Frequenzen treten annähernd bei gleichen Wellenzahlen, wie diejenigen der analogen Dimethylglyoxim-derivaten (M(DH)<sub>2</sub>) auf. Diese Erscheinung spricht für gleiche O—H...O-Brückenbindungsstärken in den M(Heptox.H)<sub>2</sub>, M(DH)<sub>2</sub>, M[Co(Heptox.H)<sub>2</sub>(Am)<sub>2</sub>]X und [Co(DH)<sub>2</sub>(Am)<sub>2</sub>]X-Komplexen.

Im Falle der Heptoxim-Derivate sind die als ν<sub>as</sub>C—H, ν<sub>s</sub>C—H und die δ<sub>CH<sub>3</sub></sub> und δ<sub>CH<sub>2</sub></sub>-Banden viel stärker als bei den Komplexen mit Dimethylglyoxim. Die Valenz- und Deformationsschwingungsfrequenzen der Oxim- und CH<sub>2</sub>-Gruppen sind von der Natur der einzähnigen Liganden nicht beeinflusst. Die Co—N

Tabelle 1.  
Neue Komplexsalze des Typs  $[\text{Co}(\text{Heptox.H})_2(\text{NH}_3)_2]\text{X}$

No.	Formel	Mol. Gew. ber.	Ausbeu- te(%)	Charakteristik		Analyse	
				Ber.		Ber.	Gef.
1. A. Br		483,3	25	Gelbe, rechtanguläre Platten	Co N	12,19 17,40	11,80 16,98
2. A. I		530,3	45	Gelbbraune, kurze Prismen	Co N	11,11 15,85	11,25 15,40
3. A. $\text{ClO}_4$		502,8	50	Gelbe, irreguläre Prismen	Co	11,72	11,60
4. A. $[\text{Co}(\text{NH}_3)_2(\text{NO}_2)_4]$		680,5	60	Gelbbraune rhomb. Prismen	Co N	17,32 24,70	17,50 25,10
5. A. Pikrat		631,5	90	Gelbe mikrokrist. Masse	Co N	9,33 19,97	9,11 19,51
6. A. $[\text{Co}(\text{DH})_2(\text{NO}_2)_2]$		784,5	60	Gelbe, hexagonale Platten	Co N	15,02 21,40	14,70 21,89
7. A. $[\text{Co}(\text{DH})_2(\text{CN})_2]$		744,5	65	Gelbe mikrokrist. Masse	Co N	15,83 22,58	15,20 23,10
8. A. $[\text{Co}(\text{DH})_2(\text{NCS})_2]$		808,5	50	Braune Prismen	Co N	14,58 20,79	14,15 21,24
9. A. $[\text{Cr}(\text{NH}_3)_2(\text{NCS})_4]$		721,7	90	Rotbraune mikrokrist. Masse	N	23,29	23,10
10. A. $[\text{Cr}(\text{NCS})_4(\text{Anilin})_2]$		873,9	90	Rotbraune mikrokrist. Masse	N	19,23	19,02

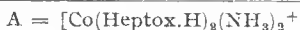


Tabelle 2.  
Neue Komplexsalze des Typs  $[\text{Co}(\text{Heptox.H})_2(\gamma\text{-Pikolin})_2]\text{X}$

No.	Formel	Mol. Gew. ber.	Ausbeu- te(%)	Charakteristik		Analyse	
				Ber.		Ber.	Gef.
11. B. Br		635,4	30	Glänzende, braune unregelmässige Platten	Co N	9,27 13,23	9,18 13,47
12. B. I		682,4	70	Kleine, braune Nadelchen	Co N	8,63 12,32	8,46 12,19
13. B. NCSe		660,5	60	grün-braune, unregel- mäss. Prismen	Co N	8,92 14,84	8,45 14,99
14. B. $\text{ClO}_4$		654,8	80	dunkelgelbe, kleine dünne Nadeln	Co N	9,00 12,83	8,95 13,10
15. B. $\text{IO}_4$		746,7	80	dunkelbraune Prismen	Co	7,89	7,86
16. B. Pikrat		783,6	95	Gelbbraune, kleine Nadelchen	Co C H	7,52 49,04 5,01	7,28 48,58 5,21
17. B. $[\text{Co}(\text{NH}_3)_2(\text{NO}_2)_4]$		832,6	70	Gelbbraune unregel- mäss. Kristallen	Co N	14,06 20,19	13,82 19,66
18. B. $[\text{Co}(\text{DH})_2(\text{NO}_2)_2]$		936,7	60	Gelbe, kleine Prismen	Co N	12,59 17,95	12,26 17,65
19. B. $[\text{Co}(\text{DH})_2(\text{N}_3)_2]$		928,7	50	Schimmernde, braune Prismen	Co N	12,69 24,14	12,40 23,60
20. B. $[\text{Cr}(\text{NH}_3)_2(\text{NCS})_4]$		873,9	90	rotbraune mikrokrist. Masse	N	19,23	19,11



Tabelle 3

IR Spektraldata einiger Komplexe des Typs  $[\text{Co}(\text{Diox.H})_2(\text{Amin})_2]\text{I}$ 

Schwingungsfrequenz	I	II	III	IV
$\nu_{\text{N}-\text{H}}$	—	—	3220 s 3100 m	3230 s 3120 m
$\nu_{\text{C}-\text{H}}$	2940 s 2860 ss	— —	2940 s 2855 ss	— —
$\delta_{\text{O}-\text{H}, \text{O}}$	1740 — 1780 sch	1720 sch	1750 — 1780 sch	1730 sch
$\delta_{\text{NH}_3}$	—	—	1630 m	1620 ,
$\nu_{\text{C}_{\text{Ar}}-\text{C}_{\text{Ar}}}$	1610 ss	1620 ss	1610 —	—
$\nu_{\text{C}=\text{N}}$	1505 ss	1558 ss	1560 ss	1550 ss
$\delta_{\text{CH}_{\text{3k}}}$	1469 ss	1465 ss	1463 ss	1450 s
$\delta_{\text{CH}_{\text{2w}}}$	1340 ss	1378 s	1345 ss	1370 m
$\delta_{\text{NH}_3}$	—	—	1350 m	1340 m
$\nu_{\text{N}-\text{O}}$	1250 ss 1075 s	1240 ss 1092 ss	1250 ss 1080 s	1230 ss 1090 ss
$\gamma_{\text{CH}_{\text{2r}}}$	1150 m	—	1150 m	—
$\gamma_{\text{O}-\text{H}}$	960 s	980 s	960 s	980 ss
$\gamma_{\text{NH}_3}$	—	—	850 sch	850 m
$\gamma_{\text{CH}_3}$	915 s 780 ss	920 m 776 ss	915 s 770 ss	920 m 775 ss
$\gamma_{\text{C}-\text{H}}$	740 s 705 s	745 m 705 s	740 s	740 ss
$\nu_{\text{C}_{\text{Ar}}-\text{C}_{\text{Ar}}}$	—	—	—	—

I.  $[\text{Co}(\text{Heptox.H})_2(\gamma\text{-Pikolin})_2]\text{I}$ III.  $[\text{Co}(\text{Heptox.H})_2(\text{NH}_3)_2]\text{I}$ II.  $[\text{Co}(\text{DH})_2(\gamma\text{-Pikolin})_2]\text{I}$ IV.  $[\text{Co}(\text{DH})_2(\text{NH}_3)_2]\text{I}$ 

( $\text{NH}_3$ )-Bindungen haben also starken kovalenten Charakter (Verschiebung der  $\nu_{\text{N}-\text{H}}$ -Frequenzen um 200—250  $\text{cm}^{-1}$ , gegen das freie nicht koordinierte  $\text{NH}_3$ ). Die wichtigsten Spektraldata sind in der Tabelle 3 zusammengestellt.

Die Elektronenspektren von  $[\text{Co}(\text{Heptox.H})_2(\text{NH}_3)_2]\text{I}$  und  $[\text{Co}(\text{Heptox.H})_2(\gamma\text{-Pikolin})_2]\text{I}$  wurden in Methanol aufgenommen.

Die Bande zwischen 20—30 KK kann einer Ladungsüberführung Amin-Co zugeschrieben werden. Die anderen Banden haben wahrscheinlich einen komplexen Charakter. Die Überlagerung von reinen Ligand (Amin, Heptoxim) Übergängen und von  $\text{Co} \rightarrow \rightarrow$  Ligand Ladungsübergängen macht die Deutung der Spektren schwierig.

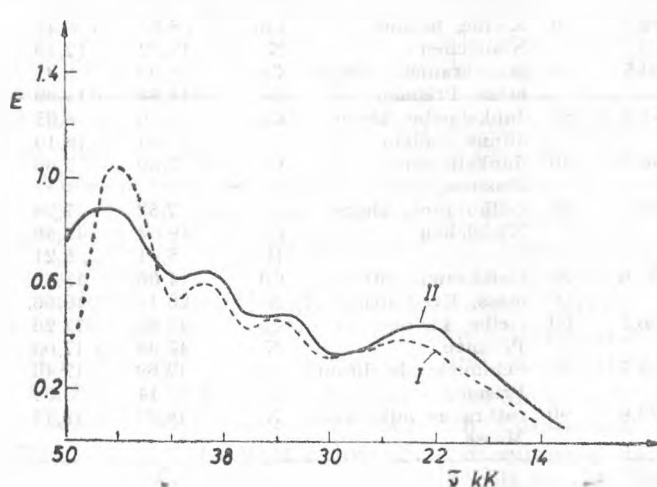
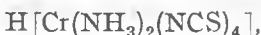
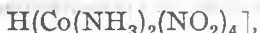


Abb. 1. Elektronische Spektren von  
 "I"  $[\text{Co}(\text{Heptox.H})_2(\text{NH}_3)_2]\text{I}$   
 "II"  $[\text{Co}(\text{Heptox.H})_2(\gamma\text{-Pikolin})_2]\text{I}$

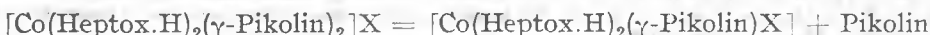
Der Inflexionspunkt, bzw. das breite Band um 39–41 kK können dem  $\text{Co}(\text{Heptox.H})_2$ -Skelett zugeordnet werden.

Das thermische Verhalten einiger Komplexe vom Typ  $[\text{Co}(\text{Heptox.H})_2(\gamma\text{-Pikolin})_2]\text{X}$  wurde derivatographisch untersucht.

Die thermische Zersetzung der Derivate mit Komplexsäuren:



usw. ist ein sehr komplizierter, langsamer Prozess ohne gutdefinierten Abbauzwischenprodukten. Die Derivate mit  $\text{ClO}_4^-$ ,  $\text{IO}_4^-$ ,  $\text{IO}_3^-$ , usw. zerfallen sich explosionsartig. Ist das Anion ein Halogen oder Pseudohalogen ( $\text{NCS}^-$ ,  $\text{NCSe}^-$ ), findet in der ersten Phase der Pyrolyse eine partielle Dezaminierungsreaktion statt:



Diese Reaktion verläuft in stöchiometrischen Verhältnissen zwischen 160–230 °C in Abhängigkeit von der Natur des Anions X.

Die Aminabspaltung ist ein endothermer Prozess (Endothermische Minima auf den DTA-Kurven). Bei höheren Temperaturen zerfällt das intermediäre Produkt unter Freiwerden von Amin,  $\text{N}_2$ ,  $\text{NO}_2$ ,  $\text{CO}$ ,  $\text{CO}_2$  und Oxim in nichtstöchiometrischen Verhältnissen (Endo- und exotherme Maxima auf den DTA-Kurven zwischen 250–650 °C).

In diesem Temperaturbereiche treten neben den Eliminierungsreaktionen an der Luft auch Oxydationsprozesse auf. Das Endprodukt bei 850 °C ist  $\text{Co}_3\text{O}_4$  ( $\text{X} = \text{I}, \text{NCS}, \text{NCSe}, \text{NO}_3$ ), bzw. ein nichtstöchiometrisches Gemisch von  $\text{Co}_3\text{O}_4 + \text{CoX}_2$  ( $\text{X} = \text{Cl}, \text{Br}$ ). Das endothermische Maximum bei 900–920 °C zeigt die Bildung von  $\text{CoO}$  aus  $\text{Co}_3\text{O}_4$ .

Einige typische Derivatogramme für  $[\text{Co}(\text{Heptox.H})_2(\gamma\text{-Pikolin})_2]\text{X}$  sind in Abb. 2 wiedergegeben.

Im Vergleich mit dem thermischen Verhalten der analogen Komplexe des Typs:  $[\text{Co}(\text{Diox.H})_2(\text{Amin})_2]\text{X}$  mit identischen Amin und X-Komponenten nimmt die thermische Beständigkeit in folgender Reihe ab:



**Experimenteller Teil:**  $[\text{Co}(\text{Heptox.H})_2(\text{NH}_3)_2]\text{Cl}$  — Lösung. Erstes Verfahren: 20 mMol  $[\text{Co}(\text{NH}_3)\text{Cl}]_{\text{Cl}_2}$  (5 g) und 40 mMol Heptoxim (7,2 g) in 150 ml Wasser, werden auf dem Wasserbade 3–4 Stunden lang erwärmt. Das Chloropentammin löst sich langsam auf wobei eine dunkelbraune Lösung entsteht. Nach Abkühlung wird die Lösung filtriert und zur doppelten Umsetzungsreaktion verwendet.

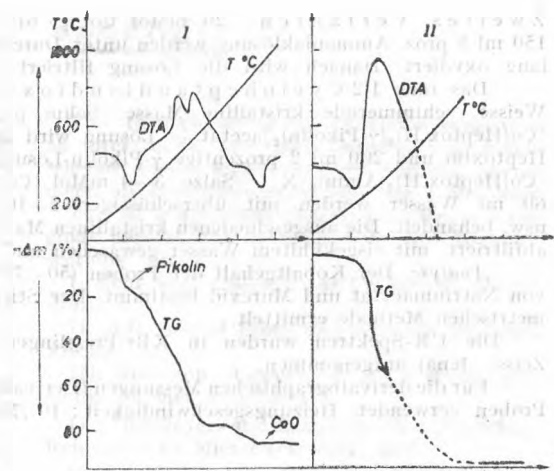


Abb. 2. Derivatogramm von  $[\text{Co}(\text{Heptox.H})_2(\gamma\text{-Pikolin})_2]\text{I}$  Derivatogramm von  $[\text{Cd Heptox}(\gamma\text{-Pikolin})_2]$   
(I)  $\text{ClO}_4^-$  (II)

**Zweites Verfahren:** 20 mMol  $\text{CoCl}_2 \cdot 6\text{H}_2\text{O}$  (4,8 g) und 40 mMol Heptoxim (7,2 g) in 150 ml 5 proz. Ammoniaklösung werden unter Durchleiten eines kräftigen Luftstromes 3–4 Stunden lang oxydiert. Danach wird die Lösung filtriert und zu Fällungsreaktionen verwendet.

Das rohe 1,2-Cycloheptanediimid wird aus heißem Wasser umkristallisiert. Weisse, schimmernde kristalline Masse. Schm. p. 224 C (unter Zers.).

$[\text{Co}(\text{Heptox.H})_2(\gamma\text{-Pikolin})_2]\text{acetat}$  — Lösung wird aus 20 mMol  $\text{Co}(\text{CH}_3-\text{COO})_2 \cdot 4\text{H}_2\text{O}$ , 40 mMol Heptoxim und 200 ml 2 prozentige  $\gamma$ -Pikolin-Lösung erhalten.

$[\text{Co}(\text{Heptox.H})_2(\text{Amin})_2]\text{X}$  — Salze. 3–4 mMol  $[\text{Co}(\text{Heptox.H})_2(\text{Amin})_2]$ -Chlorid (Acetat) in 50–60 ml Wasser werden mit überschüssiger 2–10 prozentiger  $\text{KBr}$ ,  $\text{KI}$ ,  $\text{NaClO}_4$ , Komplexsäure, usw. behandelt. Die ausgeschiedenen kristallinen Massen werden nach 30–60 Minuten Stehenlassen abfiltriert, mit eisgekühltem Wasser gewaschen und an der Luft getrocknet.

**Analyse.** Der Kobaltgehalt der Proben (50–75 mg) wurde komplexometrisch in Anwesenheit von Natriumacetat und Murexid bestimmt. Der Stickstoffgehalt wurde nach der üblichen gasvolumetrischen Methode ermittelt.

Die UR-Spektren wurden in KBr-Presslingen mit einem UR-20-Spektrophotometer (Carl Zeiss-Jena) aufgenommen.

Für die derivatographischen Messungen (Derivatograph — MOM-Budapest) wurden je 100 mg Proben verwendet. Heizungsgeschwindigkeit: 10°/Min.

#### LITERATUR

1. O. Wallach, *Liebigs Ann. Chem.*, **414**, 318 (1918).
2. A. Harr, R. C. Voter, C. V. Banks, *J. Org. Chem.*, **14**, 836 (1949).
3. C. V. Banks, D. V. Barnum, *J. Amer. Chem. Soc.*, **80**, 3579, 4767 (1958).
4. Cs. Várhelyi, Z. Finta, J. Zsakó, *Z. anorg. Chem.*, **371**, 326 (1970).
5. R. Ripan, Cs. Várhelyi, L. Szotyori, *Z. anorg. Chem.*, **357**, 149 (1968).
6. F. Mánok, Cs. Várhelyi, I. Mikulás, *Stud. Univ. Babes-Bolyai, Chem.*, **15**, (1), 113 (1970); **15**, (2), 139 (1970).
7. C. Macarovicci, J. Horák, Cs. Várhelyi, *Rev. Roumaine Chim.*, **25**, 805 (1980).
8. J. Zsakó, J. Horák, Cs. Várhelyi, A. Benkő, *Monatsh. Chem.*, **112**, 945 (1981).
9. J. Zsakó, J. Horák, Z. Finta, Cs. Várhelyi, I. Mitrache, *Mikrochim. Acta (Wien)*, **1979**, I, 405.
10. F. Mánok, E. Kőszegi, Cs. Várhelyi, *Acta Chim. Acad. Sci. Hung.*, **116**, 51 (1984).
11. Gh. Marcu, Cs. Várhelyi, M. Somay, D. Avramescu, *Rev. Roumaine Chim.*, **26**, 575, (1981).

## RECENZII

**Surface and Colloid Science in Computer Technology** (K. L. Mittal, Ed.), Plenum Press, New York and London, 1987, pp. I–XI + 1—44.

Surface and colloid science plays an essential role in characterizing the physico-chemical properties of the materials employed in microelectronics/computer technology.

Among colloidal phenomena, the dispersion behavior of ceramic powders (making the substrate on which the semiconductor chip is placed) and of magnetic particles (used for making magnetic tapes and disks) holds particular importance. Whence the fundamental understanding of stability behavior in both aqueous and nonaqueous media, and the necessity of devising ways to control dispersion characteristics of such materials.

Taking into account the numerous applications of thin films in microelectronics — irrespective of their function —, the thin film adhesion to the underlying substrate is of cardinal importance and, consequently, the study of interfacial interactions between varied materials is of great actuality. Sometimes failures can be traced owing to lack of compatibility or suboptimum interfaces of the materials involved.

Also, surface and colloid phenomena play a key-role in elucidating the mechanisms of ink-paper interactions — a vital point in the obtainment of high quality printing.

Recently, considerable interest has been shown in the use of some new monolayer and Langmuir-Blodgett film materials as electron-beam resists in microlithography, and in obtaining magnetic materials of adjustable thickness for microelectronics.

The here reviewed book is the first to have revealed the importance and the strength of penetration of surface and colloid science in microelectronics/computer technology. The book itself consists of papers contributed in the *Symposium on Surface and Colloid Science in Computer Technology*, held as part of the *5-th International Conference on Surface and Colloid Science*, and the *59-th Colloid and Surface Science Symposium* sponsored by the Division of Colloid and Surface Chemistry of the American Chemical Society, and the International Association of Colloid and Interface Scientists at Clarkson University, Potsdam, New York, between June 24–28, 1985.

The 'thematique' of the collection consists in an inter- multi- and trans-disciplinary approach, relevant to the importance of interfacial phenomena in microelectronics/computer technology.

The 27 contributed papers (reviews and original papers) are distributed in five thematic sections (parts) :

I. Acid-Base Concepts and Colloidal Dispersions;

II. Adhesion of Films and Coatings Including Resists;

III. Adhesion Aspects of Thin Films and Metal-Polymer Interfaces;

IV. Monolayers and Langmuir-Blodgett Films: Relevance to Microelectronics; and,

V. Interfacial Aspects in Printing.

Part I includes six papers, underlying the importance of acid-base interactions in the dispersion behavior of inorganic powders for the colloidal stability in aqueous and nonaqueous media, in the colloidal behavior of ceramic and magnetic particles. The present stage of researches on and development of ceramic materials is shown, as also is stressed their importance in technology — with structural, electronic and optic applications.

The six papers in Part II are devoted to the role of interfaces in the integrated circuit photoresist processing-based electronic device fabrication. Results of researches on polymeric film adhesion are presented, with emphasis on the role of silanes in polymer-polymer enhanced adhesion.

The thin film adhesion and metal-polymer interfaces are tackled in the seven papers of Part III; novelties in this field being presented, such as: ion-, electron-beam or photon irradiation-induced film/substrate interface adhesion enhancement, on chemically nonreacting substrates. Film substrate adhesion can also be improved by "additional sub-monolayer" chemically active species, able to widen the range of composites with stable interfaces, or high adhesion plasma polymerized film/substrate materials.

The five papers of Part IV review diverse industrial applications of organized assemblies and point out the role of monolayers and Langmuir-Blodgett films in microelectronics, microlithography, and the use of magnetic monolayers in computer technology.

The final, Part V includes three works on the major role of ink-paper interactions and of polymer-paper adhesion in printing.

This work is concluded with a brief account on the contributors' biography (occupation and concerns — past and present —, publishing activity etc.), which no doubt is meant to readily acquaint the reader with specialists in the field and enable cooperative work between worldwide schools of surface and colloid science, and a 'Subject Index' giving direct access to selected topics — a point that should not be neglected in any book in the field of science.

The book is therefore useful both to higher year students in chemistry — to enable them make an insight into the interfacial aspects of materials in the wonderful world of computers — and to professionals in the diverse fields of science and technology — for whom the volume may institute in a source to prompt new ideas and directions of research in this as rewarding field of chemistry as exciting it is.

The profound understanding of interfacial

interactions emergent in surface and colloidal systems may entail an upward leap in knowledge, with either immediate and remote application in science and technology.

It is worthwhile to also mention the Editor's painstaking endeavours in the last thirteen years both to unravel the wonders of surface and colloid chemistry, of adhesion, polymers etc. by personal research work, and to disseminate knowledge in the science domain of his concerns, by either chairing a number of very successful international symposia and by editing, in addition to this volume, other 24 volumes, and publishing more than 50 original papers in this field, let alone the many invited talks on the multifarious facets of surface science, particularly adhesion on the invitation of various societies and organizations in many countries all over the world.

MARIA TOMOAIȚA-COTIȘEL



INTreprinderea POLIGRAFICĂ CLUJ, Municipiul Cluj-Napoca c-da nr. 125/1988

În cel de al XXXIII-lea an (1988) *Studia Universitatis Babeș-Bolyai* apare în specialitățile :

matematică  
fizică  
chimie  
geologie-geografie  
biologie  
filosofie  
științe economice  
științe juridice  
istorie  
filologie

In the XXXIII-rd year (1988) of its publication, *Studia Universitatis Babeș-Bolyai* is issued as follows :

mathematics  
physics  
chemistry  
geology-geography  
biology  
philosophy  
economic sciences  
juridical sciences  
history  
philology

Dans sa XXXIII-e année (1988), *Studia Universitatis Babeș-Bolyai* paraît dans les spécialités :

mathématiques  
physique  
chimie  
géologie-géographie  
biologie  
philosophie  
sciences-économiques  
sciences juridiques  
histoire  
philologie